DESIGN AND MANUFACTURE OF A HEAD & NECK PHANTOM FOR THE ASSESSMENT OF IMRT DELIVERY WITH GEL DOSIMETRY

Meyer, J., Harding, P., Mills, J.A., Bonnett, D.E., Wolff, T., Haas, O.C.L. and Burnham, K.J.

Published version deposited in CURVE April 2014

Original citation:
Meyer, J., Harding, P., Mills, J.A., Bonnett, D.E., Wolff, T., Haas, O.C.L. and Burnham, K.J. (2001) Design and manufacture of a head and neck phantom for the assessment of IMRT delivery with gel dosimetry, in Proceedings of DOSGEL 2001, Queensland University of Technology: Australia, pg148-150

Copyright © and Moral Rights are retained by the author(s) and/ or other copyright owners. A copy can be downloaded for personal non-commercial research or study, without prior permission or charge. This item cannot be reproduced or quoted extensively from without first obtaining permission in writing from the copyright holder(s). The content must not be changed in any way or sold commercially in any format or medium without the formal permission of the copyright holders.

CURVE is the Institutional Repository for Coventry University

http://curve.coventry.ac.uk/open

Proceedings of

DOSGEL 2001

2nd International Conference on Radiotherapy Gel Dosimetry

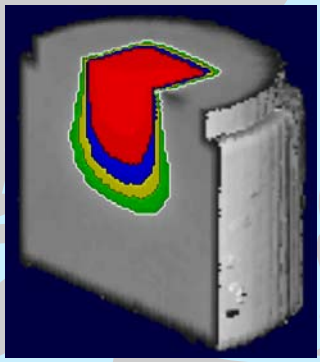

18 - 21 November 2001

Queensland University of Technology
Brisbane, Australia

Proceedings of DOSGEL 2001 - 2nd International Conference on Radiotherapy Gel Dosimetry
November 18 – 21, 2001
Published by Queensland University of Technology
Brisbane
Queensland
Australia

ISBN: 1 74107 018 X

Copyright: Queensland University of Technology

Available from:

Centre for Medical, Health and Environmental Physics
School of Physical and Chemical Sciences
Queensland University of Technology
GPO Box 2434
Brisbane Q 4001
Australia

Editors note:

Information provided in this publication is for instructional use only. The reader is cautioned to verify all information and procedures independently before use. The Editors and Scientific Committee assume no responsibility for the validity of measurements or claims made by individuals or for any damage or harm incurred as a result of the use of this information.

Proceedings of DOSGEL 2001

2nd International Conference on Radiotherapy Gel Dosimetry

November 18 – 21, 2001

Edited by

Clive Baldock and Yves De Deene

Published by
Queensland University of Technology

Gel dosimetry is proving to be a useful tool in clinical radiation therapy. In the future, gel dosimetry may become a standard technique in conformal therapy, brachytherapy, cardiovascular brachytherapy and for quality assurance of radiotherapy treatment planning systems.

These Proceedings contain papers on various aspects of gel dosimetry which were presented at DOSGEL 2001 from 18 – 21 November 2001 and which aimed to bring together individuals with an interest in three-dimensional radiotherapy gel dosimetry.

DOSGEL 2001 was the second international conference on the subject of gel dosimetry, building on the success of DOSGEL '99 held in July 1999 at the University of Kentucky, Lexington, USA. The intended audience of DOSGEL 2001 was individuals currently undertaking gel dosimetry, as well as those interested in establishing gel dosimetry in their own institutes.

DOSGEL 2001 was held at Queensland University of Technology and supported by the Centre for Medical, Health and Environmental Physics. DOSGEL 2001 was endorsed by the International Organization for Medical Physics (IOMP), the Australasian College of Physical Scientists and Engineers in Medicine (ACPSEM), the American Association of Physicists in Medicine (AAPM), the Canadian Organization of Medical Physicists (COMP) and the Institute of Physics and Engineering in Medicine (IPEM).

A number of papers which were submitted and appeared in the Preliminary Proceedings were subsequently not presented by their authors at DOSGEL 2001. These papers do not appear in these Proceedings.

The review paper by Gore and Schulz arising out of an impromptu talk at DOSGEL 2001 by John Gore was included in these Proceedings at the request of the Scientific Committee.

Clive Baldock PhD and Yves De Deene PhD
November 2001

Conference Chairman

Clive Baldock

Proceedings Editors

Clive Baldock
Yves De Deene

International Scientific Committee

Alan Appleby, USA
Chantal Audet, USA
Sven Back, Sweden
Clive Baldock, Australia
David Bonnett, UK
Yves De Deene, Australia / Belgium
Simon Doran, UK
Grazia Gambarini, Italy
John Gore, USA
Geoffrey Ibbott, USA
Keven Jordan, Canada
Stephen Keevil, UK
Tomas Kron, Canada
Martin Lepage, USA / Australia
Daniel Low, USA
Mark Oldham, USA
Lars Olsson, Sweden
L John Schreiner, Canada
Ken Shortt, Austria / Canada

Sponsors of DOSGEL 2001

Principal Sponsor

MGS Research Inc

Main Sponsor

Varian
NOMOS

Sponsor

CMS

3D Dose Mapping

for Conformal RTP & IMRT

1. BANG gels:

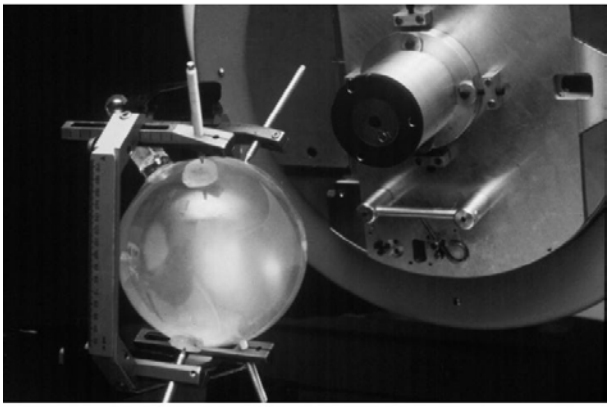

=>

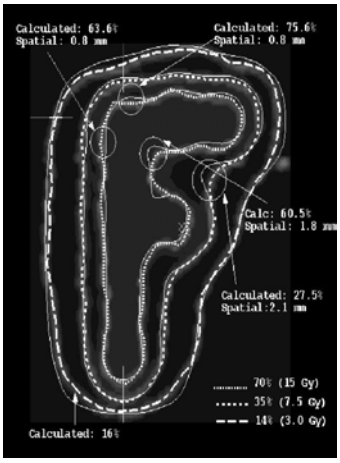

2. OCT-OPUS™ 3D Gel Scanners:

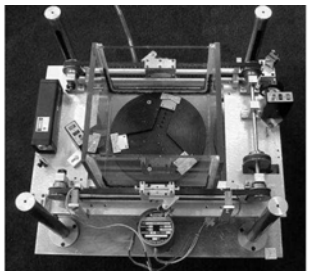

+

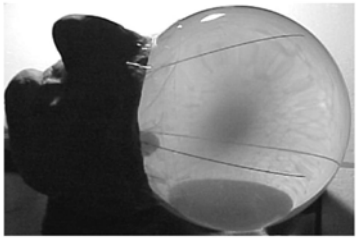

=>

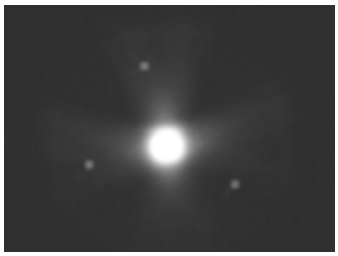

MGS Research Inc.

E-mail: mgsinc1@mindspring.com
PHONE OR FAX in the USA: 1-877-BANG GEL

TABLE OF CONTENTS

Introduction *iii*
Organisation *iv*
Sponsorship *v*
Table of Contents *vii*

Review Papers 1

RADIATION THERAPY REQUIREMENTS: WHAT DO WE EXPECT FROM GEL DOSIMETRY 2
T Kron

FUNDAMENTALS OF FRICKE DOSIMETRY 10
K Shortt

FUNDAMENTALS OF FRICKE GEL DOSIMETRY 15
L J Schreiner

FACTORS INFLUENCING THE POLYMERIZATION PROCESSES IN POLYMER GEL DOSIMETERS 23
A K Whittaker

FUNDAMENTALS OF POLYMER GEL DOSIMETRY 31
M Lepage

APPLICATIONS OF POLYMER GEL DOSIMETRY 40
D E Bonnett

FUNDAMENTALS OF MRI MEASUREMENTS IN GEL DOSIMETRY 49
Y De Deene

FUNDAMENTALS OF OPTICAL MEASUREMENTS IN GEL DOSIMETRY 66
K Jordan

THE ORIGINS OF GEL DOSIMETRY WITH MRI 73
J C Gore and R J Schulz

Proffered Papers 76

INVESTIGATION INTO THE RADIOCHROMIC (FXG) GEL DOSEMETER: STABILITY AND UNCERTAINTY IN OPTICAL MEASUREMENTS 77
M A Bero, W B Gilboy and S J Doran

PVA-FX GEL FOR THREE DIMENSIONAL DOSE DISTRIBUTION MEASUREMENT: A PRELIMINARY STUDY ON DOSE RESPONSE 80
S Brindha, K M Ayyangar, B Shen and C B Saw

SPECTROPHOTOMETRY AND MAGNETIC RESONANCE IMAGING OF FRICKE GELS CONTAINING POLYVINYL ALCOHOL 83
K Nkongchu, K Shortt, G Santyr, J Wallace and A Cross

MANUFACTURING PVA-FRICKE GELS 86
K C Chu and K J Jordan

MANUFACTURING METHOD AND ABSORBED DOSE MEASUREMENTS OF FERROUS SULPHATE POLYVINYL ALCOHOL GEL 89
B Hill, S Å J Bäck, M Lepage, J Simpson and C Baldock

GEL DOSIMETRY IN NEUTRON CAPTURE THERAPY 92
G Gambarini

REFRIGERATION TEMPERATURE GRADIENTS GENERATE DOSE RESPONSE ARTIFACTS IN FRICKE GELATIN DOSIMETERS 95
K J Jordan, D J MacDonald, T M Pajak and J J Battista

DEVELOPMENT OF "NORMOXIC" POLYMER GELS FOR MRI DOSIMETRY 98
P M Fong, D C Keil, M D Does and J C Gore

A POLYMER GEL PREPARED UNDER NORMAL LEVELS OF OXYGENATION: BASIC STUDIES 101
H Gustavsson, S Å J Bäck and L E Olsson

EPOXY BASED GELS: A NEW CLASS OF GEL DOSIMETERS 104
Y S Park and L J Schreiner

CHEMICAL ASPECTS IN THE FORMATION AND PROCESSING OF ACRYLAMIDE GELS 107
A G Jenner, A W Beavis, S Sia, G P Liney, A W Hall and J W Goodby

BASIC INVESTIGATIONS OF AN AQUEOUS POLYACRYLAMIDE DOSIMETER WITHOUT GELATIN 110
Y S Park, L J Schreiner

DEVELOPMENT AND OPTIMIZATION OF A 2-HYDROXYETHYLACRYLATE MRI POLYMER GEL DOSIMETER 113
H Gustavsson, S Å J Bäck, M Lepage, L Rintoul and C Baldock

DYNAMIC MATHEMATICAL MODELING OF A POLYACRYLAMIDE GEL DOSIMETER 116
Q Zhang, K B McAuley, G Salomons and L J Schreiner

DETERMINATION OF DOSE DISTRIBUTION IN A BLOOD IRRADIATOR USING POLYMER GEL DOSIMETRY 119
A R Farajollahi and D E Bonnett

VERIFICATION OF A PROSTATE IMRT TREATMENT PLAN USING BANG-GEL DOSIMETRY 121
S Brindha, K M Ayyangar, B Shen and C B Saw

RELATIVE EFFECTIVENESS OF POLYACRYLAMIDE GEL DOSIMETERS APPLIED TO PROTON BEAMS 124
A Jirasek and C Duzenli

INVESTIGATIONS OF A POLYACRYLAMIDE GEL DOSIMETER WITH HIGH RESOLUTION MRI FOR DOSIMETRY OF A HIGH DOSE RATE BETA SOURCE FOR INTRAVASCULAR BRACHYTHERAPY 127
M N Amin, M A Horsfield, M Dunn, P J Harding and D E Bonnett

VERIFICATION OF A CLINICALLY APPLIED DOSE DISTRIBUTION IN RADIOSURGERY USING BANG GEL DOSIMETRY 130
S G Scheib, S Gianolini and E Lazaridis

COMPARISONS BETWEEN MONOMER/POLYMER GEL DOSIMETRY AND DOSE COMPUTATIONS FOR AN IMRT TREATMENT OF A THORAX PHANTOM 133
K Vergote, Y De Deene, F Claus, W De Gersem, B Van Duyse and C De Wagter

MAGNETIZATION TRANSFER IMAGING FOR POLYMER GEL DOSIMETRY 136
M Lepage, K McMahon, G J Galloway, Y De Deene, S A Bäck and C Baldock

ARTEFACTS IN MONOMER/POLYMER GEL DOSIMETRY OF HDR ^{192}IR SOURCES: SUSCEPTIBILITY ARTEFACTS IN THE VICINITY OF THE GUIDING CATHETER 139
Y De Deene and C De Wagter

ARTEFACTS IN MONOMER/POLYMER GEL DOSIMETRY OF HDR ^{192}IR SOURCES: OXYGEN PERFUSION THROUGH THE GUIDING CATHETER 142
Y De Deene and C De Wagter

ARTEFACTS IN MONOMER/POLYMER GEL DOSIMETRY OF HDR ^{192}IR SOURCES: MONOMER DIFFUSION DURING IRRADIATION 145
Y De Deene and C De Wagter

DESIGN AND MANUFACTURE OF A HEAD & NECK PHANTOM FOR THE ASSESSMENT OF IMRT DELIVERY WITH GEL DOSIMETRY 148
J Meyer, P Harding, J A Mills, D E Bonnett, T Wolff, O C L Haas and K J Burnham

CHARACTERIZATION OF A PORTABLE SYSTEM FOR DOSE IMAGING IN FRICKE-XYLENOL-ORANGE-GELS 151
G Gambarini, M Mariani, L Pirola, E Pompilio, P Prestini, M Sella and S Tomatis

TECHNICAL DEVELOPMENT OF A HIGH-RESOLUTION CCD-BASED SCANNER FOR 3-D GEL DOSIMETRY: (I) SCANNER CONSTRUCTION 154
S J Doran, K K Koerkamp, M A Bero, P Jenneson, E J Morton and W B Gilboy

TECHNICAL DEVELOPMENT OF A HIGH-RESOLUTION CCD-BASED SCANNER FOR 3-D GEL DOSIMETRY: (II) INITIAL RESULTS 157
S J Doran, K K Koerkamp, M A Bero, P Jenneson, E J Morton and W B Gilboy

TECHNICAL DEVELOPMENT OF A HIGH-RESOLUTION CCD-BASED SCANNER FOR 3-D GEL DOSIMETRY CONSTRUCTION: (III) PROBLEMS ENCOUNTERED 160
S J Doran, K K Koerkamp

SIMULATION OF THE EFFECT OF SAMPLE/CONTAINER INTERFACES FOR 3-D GEL DOSIMETRY USING OPTICAL COMPUTED TOMOGRAPHY 163
S J Doran

OPTICAL CONE BEAM TOMOGRAPHY WITH LOW PRESSURE SODIUM LIGHT 166
K J Jordan, T M Pajak, C Piontek and J J Battista

OPTICAL SCATTER MEASUREMENTS IN BANG™ AND FX GEL 169
M Oldham, J Siewerdsen, C Rowbottom and D Jaffray

OPTIMIZING THE DOSE RESOLUTION IN POLYMER GEL DOSIMETRY 172
M Lepage, S Å J Bäck, P M Jayasekera and C Baldock

ULTRASOUND – A NEW METHOD FOR EVALUATION OF POLYMER GEL DOSIMETERS 175
M L Mather, A Whittaker and C Baldock

THEORETICAL CONSIDERATIONS OF SCAN PARAMETERS APPROPRIATE FOR X-RAY CT IMAGING OF POLYMER GEL DOSIMETERS 178
J Trapp, G Michael and C Baldock

OPTICAL CT SCANNING: FROM 2D TO 3D WHILE MEETING THE RTAP CRITERIA 181
M Oldham, J Siewerdsen and D Jaffray

DOSIMETER GELS AND Xe-129 NMR 183
J M Joers, P M Fong, J C Gore

A STUDY OF REPRODUCIBILITY AND POSSIBLE SOURCES OF ERROR IN GEL DOSIMETRY 186
A R Farajollahi and D E Bonnett

3D MRI DOISMETRY BASED ON IMAGE INTENSITY 189
S Akhlaghpour, M H Zahmatkash, H Pourbeigi

UNCERTAINTY CALCULATIONS DETERMINED FROM CALIBRATION DATA FOR CT IMAGING OF POLYMER GEL DOSIMETERS 192
J Trapp, G Michael and C Baldock

PRELIMINARY MEASUREMENTS OF DEPTH DOSES IN POLYMER GEL DOSIMETERS USING RAMAN MICROSCOPY 195
C Baldock, L Rintoul and M Lepage

INDEX 198

REVIEW PAPERS

DESIGN AND MANUFACTURE OF A HEAD & NECK PHANTOM FOR THE ASSESSMENT OF IMRT DELIVERY WITH GEL DOSIMETRY

J Meyer[$], P Harding[†], J Mills[‡], D Bonnett[♀], T Wolff[F], O C L Haas[$] and K J Burnham[$]
[$]Coventry University, Coventry; [†]Leicester Royal Infirmary, Leicester, UK
[‡]University Hospitals Coventry & Warwickshire, Coventry, UK
[♀]Kent Cancer Centre, Maidstone, UK; [F]Clatterbridge Oncology Centre, Liverpool, UK

Introduction

The complexity of intensity-modulated radiation therapy (IMRT) treatments has increased considerably in comparison to conventional radiotherapy (RT). This bears the risk of more potential sources of error and, therefore, appropriate measures have to be taken to ensure that the dose delivered corresponds to the dose that has been prescribed. For conventional RT, the routine quality assurance (QA) within a radiotherapy department may be sufficient to ensure accurate beam delivery [1]. For IMRT, the verification of the delivery of each fraction of a course of radiotherapy treatment requires careful verification [2]. Before routine IMRT treatment can be provided, it is also necessary to assess the selected beam intensity modulation method, such as multi leaf collimators (MLC) or compensators, to test both the geometric and dosimetric accuracy of the delivery method. Point measurements in a three-dimensional (3D) space can be obtained by placing one-dimensional dosimeters, such as TLDs or an ion chamber [3], within the 3D space. More spatial information can be obtained by placing films in consecutive layers in a 3D phantom, which can be a difficult and time-consuming task [4]. A more elegant alternative is the use of radiosensitive gels [5,6], e.g. BANG™ gel, which enables measuring the radiation dose at any given spatial point. It has been demonstrated by e.g. De Deene *et al.* [7] that polymer gel is adequate for verification of 3D conformal radiotherapy.

It has been reported [2] that IMRT is potentially beneficial for both prostate and head and neck cancers due to the concave shape of the tumours,. The more challenging location is the latter due to air cavities in the head and neck area and the fact that there are more organs at risk such as the parotid glands, optic chiasm, spinal cord and the brainstem. The objective of this work was to design a simplistic head & neck phantom, which, nevertheless, incorporates the main features of the anatomy such as the oral cavities, the trachea, the spinal cord and the vertebrae. The novelty in the design is that the entire phantom consists of a number of chambers, which can each be filled with different liquids or gel. Existing phantoms are usually filled with water (or a water equivalent substance) in which a container with the gel is placed [7,8]. The new design also enables the assessment of the dose to critical organs. The phantom was designed to be reusable so that different tumour sites within the head and neck region can be outlined and investigated.

This paper proposes and provides the design and manufacture of a head and neck phantom for 3D gel dosimetry. The aim of the phantom is to enable the validation and inter-departmental comparison of 3DCRT and IMRT delivery methods by means of gel dosimetry.

Materials and Methods

The actual design of the phantom is based on CT slices through the head & neck region, which were obtained from the Digital Anatomy Lab [9]. 3D design drawings and subsequently technical drawings [10] were generated using the Mastercam™ [11] computer aided design (CAD) software package. Based on the technical drawings, wooden formers were manufactured for production of the physical phantom. The formers also enable copies of the phantom to be produced. Barex™ was utilised for the shell material, since it is oxygen impermeable. Oxygen is a free radical, which inhibits polymerisation, giving rise to inaccurate dose measurements, and must therefore be avoided [4]. Plastic containers, such as e.g. Perspex or polystyrene, possess the disadvantage that they allow the transfer of oxygen through the vessel wall [12] and are, therefore, not suited if measurements are to be taken near the edge of the phantom. Lids were glued on either end of the tubes and chambers, in order to contain the gel and seal the phantom airtight. A partition between the head and neck region was attached in order to keep the chambers at a reasonable size. Finally, valves were attached to each chamber to allow filling and draining of liquids

Resemblance of the Anatomy

A 3D design view from Mastercam™ alongside a head is shown in Figure 1. This shows the final design of the head and neck phantom. For comparison, a side view of the phantom and a sagital plane through a head from the Digital Anatomy Lab [9] is shown side by side in Figure 2. The dash-dot lines indicate slices through different planes. The prefix 'S' denotes slice, corresponding to the phantom, and the prefix 'CT' corresponds to the transverse CT slice number [9].

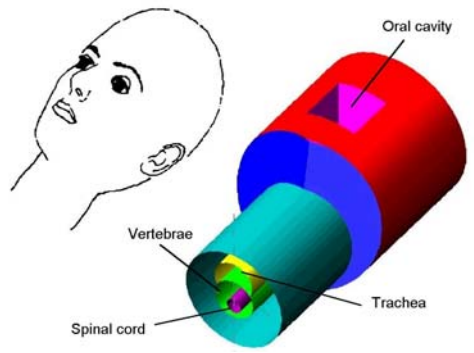

Fig. 1. Comparison of the design drawing of the head & neck phantom (right) and sketch of a head (left).

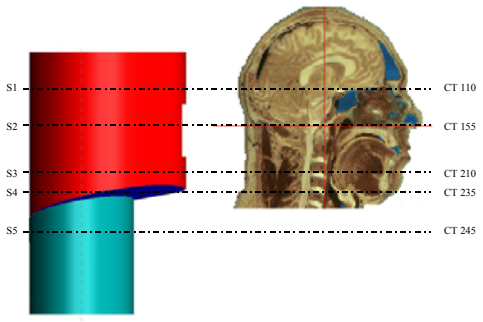

Fig. 2 Side view of phantom (left) and sagital plane through head (right).

The corresponding slices are shown in Figure 3. The materials, which are envisaged to fill the appropriate cavities, are indicated. The volume denoted bone, corresponding to the vertebrae, can be filled with bone equivalent calcium solution or calcium/gel mixture. For stability, the tubes representing the spinal cord, the vertebrae and the trachea extend through the entire phantom, although in reality they only stretch slightly into the head region. This anatomical difference is, however, not considered an issue as the tube/cavity can be filled with an identical gel mixture. A photograph of the fully assembled phantom is shown in Figure 4.

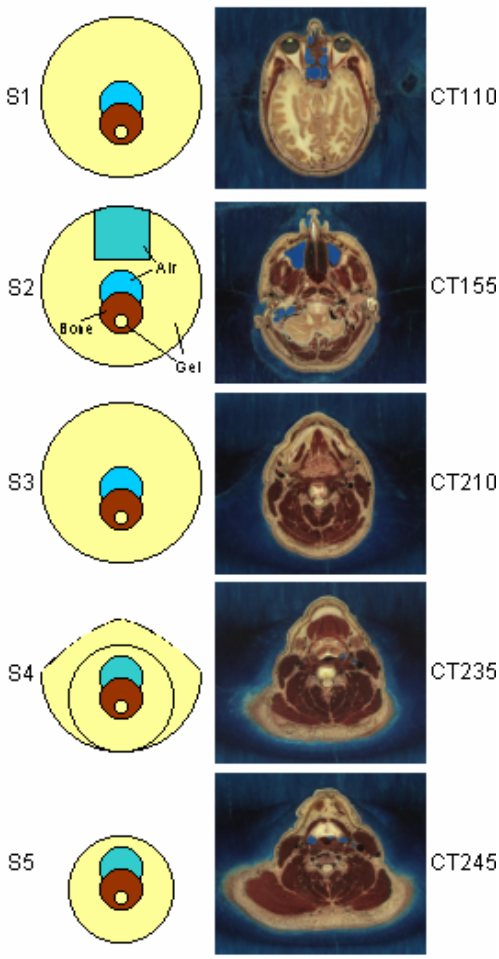

Fig. 3. Transversal slices through the phantom, denoted with 'S' and CT slices, denoted 'CT'. a) S1 vs. CT 110; b) S2 vs. CT 155; c) S3 vs. CT 210; d) S4 vs. CT 235; e) S5 vs. CT 245.

Fig. 4. Photograph of the assembled head and neck phantom.

Concluding Remarks

The design and manufacture of a phantom has been presented, with which it is possible to assess IMRT delivery throughout the head and neck region. The design is functional, i.e. several chambers allow the phantom to be filled with different contents. Although simplistic shapes and forms have been used, the main anatomical features are incorporated.

Acknowledgements

The phantom is the basis for ongoing collaborative work between the CTAC, Coventry University/University Hospitals Coventry & Warwickshire NHS Trust, the Leicester Royal Infirmary NHS Trust and the Clatterbridge Oncology Centre NHS Trust, Liverpool. A detailed plan of work has been set which includes the inverse planning of a challenging head and neck tumour, the delivery of this plan by means of different IMRT delivery techniques and the assessment by means of gel dosimetry. Results of this comparison will also be presented.

References

1. Kehoe T., Rugg L. J., From Technical Quality Assurance of Radiotherapy to a Comprehensive Quality of Service Management System, *Radiotherapy and Oncology*, **51**, pp. 281-290, 1999
2. Nutting C., Dearnaley D. P., Webb S, Intensity Modulated Radiation Therapy: a Clinical Review, *The British Journal of Radiology*, **73**, pp. 459-469, 2000
3. Perrin B. A., Jordan T. J., Hounsell A. R., The Design and Evaluation of a Phantom for the Audit of the Treatment Chain for Prostate Radiotherapy, *Radiotherapy and Oncology*, **60**, pp. 37-43, 2001
4. McJury M., Oldham M., Cosgrove V. P., Murphy P. S., Doran S., Leach M. O., Webb S., Review Article: Radiation Dosimetry Using Polymer Gels: Methods and Applications, *The British Journal of Radiology,* **73**, pp. 919-929, 2000
5. De Deene Y., De Wagter C., Van Duyse B., Derycke S., De Neve W., Achten E., Three-Dimensional Dosimetry Using Polymer Gel and Magnetic Resonance Imaging Applied to the Verification of Conformal Radiation Therapy in Head-and-Neck Cancer, *Radiotherapy and Oncology*, **48**, pp. 283-291, 1998
6. Farajollahi A. R., Bonnett D. E., Ratcliffe A. J., Aukett R. J., Mills J. A., An Investigation into the Use of Polymer Gel Dosimetry in Low Dose Rate Brachytherapy, *The British Journal of Radiology*, **72**, pp. 1085-1092, 1999
7. De Deene Y., De Wagter C. Van Duyse B., Derycke S. Mersseman B., De Gersem W., Voet T., Achten E., De Neve W., Validation of MR-Based Polymer Gel Dosimetry as a Preclinical Three-Dimensional Verification Tool in Conformal Radiotherapy, *Magn. Reson. Med.,* **43** (1), pp. 116-125, 2000
8. Haas O., Experimental Verification of Intensity Modulated Radiation Therapy, *Radiotherapy Treatment Planning: New System Approaches*, Section 6.4, Springer Verlag London, Advances in Industrial Control Monograph, ISBN 1-85233-063-5, 1999
9. The Digital Anatomy Lab [online], University of Brisbane, Australia, available from http://www.dal.qut.edu.au, [accessed 28.11.00]
10. Meyer J., Accommodating Practical Constraints for Intensity-Modulated Radiation Therapy by Means of Compensators, *PHD Thesis*, Coventry University, submitted in June 2001
11. Mastercam™ Software (Version 7.1), Mastercam™, CAD/ CAM Systems. CNC Software Inc., 344 Merrow Road, Tolland, CT 06084, USA
12. Maryanski M. J., Schulz R. J., Ibott G. S., Gatenby J. C., Xie J., Horton D., et al., Magnetic Resonance Imaging of Radiation Dose Distributions Using a Polymer-Gel Dosimeter, *Physics Medicine Biology*, 39, pp. 1437-1455, 1994

CHARACTERIZATION OF A PORTABLE SYSTEM FOR DOSE IMAGING IN FRICKE-XYLENOL-ORANGE-GELS

G. Gambarini[$,†], M. Mariani[&], L. Pirola[$], E. Pompilio[$], P. Prestini[$], M. Sella[&], S. Tomatis[‡]
[$]Physics Department of the University of Milano, Italy; [†]INFN (National Institute of Nuclear Physics), Milano, Italy; [&]Nuclear Engineering Department of the Polytechnic of Milano, Italy; [‡]National Cancer Institute, Milano, Italy

Introduction

A method for gel imaging with portable instrumentation has been proposed [1,2] based on imaging, with a CCD camera, of visible light transmission from layers of fricke-xylenol-orange-infused gel. The requirement of portable instrumentation for dose imaging was a consequence of the fact that ion diffusion is not negligible in irradiated ferrous-gel, and in some irradiation conditions, like as the case of nuclear reactors or accelerators, the time required to reach the laboratory for analysis can be to long. Polymer gels do not present the trouble of image diffusion, and they are a good solution for most circumstances. However, Fricke gel has proved to give reliable results also when gel matrix is suitably changed in order to obtain the necessary isotopic composition. In fact, in thermal and epithermal neutron dosimetry a proper study of the images detected from gels having convenient isotopic compositions allows to separate the doses due to the various secondary components generated by neutron reactions [3-5]. This separation is very important, because the relative biological effectiveness (RBE) of the different secondary radiations is different. From a practical point of view, the preparation of a lot of gels, as required in neutron dosimetry, is simpler in the case of ferrous gels, because they are not toxic. The dose-imaging method is based on the detection of grey-level (GL) images of the transmitted light around 580 nm, taking advantage from the fact that the complexes formed by xylenol-orange (XO) with ferric ions give visible light absorption at this wavelength [6] . In order to detect such images, the gel is prepared in form of layers, piled up for making a phantom; before and after exposure, each layer is placed on a plane light source and imaged. Few minutes are needed for detecting all images. The instrument is just composed of the light source and the CCD camera, with suitable optical filter, connected to a PC. This kind of layered-Fricke-Xylenol-Orange gels imaged with a CCD camera has been named FriXy-gel. When the method was proposed, very few considerations have been made about the amount of XO to be added to the solution. The gel composition was: ferrous sulphate solution [1 mM $Fe(NH_4)_2(SO_4)_2{\cdot}6H_2O$], sulphuric acid [50 mM H_2SO_4] and Xylenol -Orange [0.11 mM $C_{31}H_{27}N_2Na_5O_{13}S$, Fluka Chemie]in the amount of 50% of the final weight; Agarose SeaPlaque [$C_{12}H_{14}O_5(OH)_4$, Fluka Chemie] in the amount of 1% of the final weight; highly purified water [H_2O] in the amount of 49% of the final weight. Recently, some investigations have been performed in order to optimize the XO content, on the basis of the results regarding the range of linearity and the sensitivity of the dosimeters. The range of linearity as obtained by optical measurements is not necessarily the same as that of linearity of ferrous ion oxidation, but it can be a consequence of saturation in GL detection from the analysis instrument.

Xylenol Orange influence on sensitivity and linearity

As known [7], XO has the effect of decreasing gel sensitivity; as a consequence of this, the range of linearity increases with increasing XO concentration. In consideration of the fact that the effects of saturation of ferrous ion oxidation and of GL variation coexist, some measurements have been performed in order to investigate if the last effects can be predominant and in which conditions. Light transmission at 580 nm has been analyzed for different XO concentrations both with a spectrophotometer and with the CCD camera (in the last case, for two different optical paths).

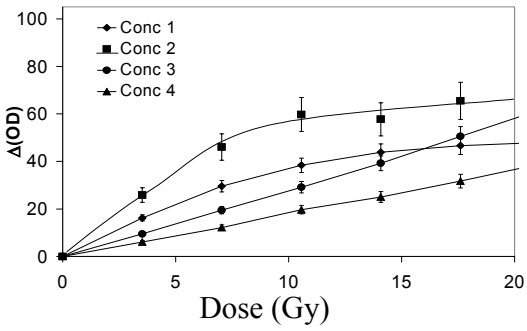

Fig.1 Results of spectrophotometric analysis of gels for different XO concentrations: 1) 0.055 mM 2) 0.11 mM, 3) 0.165 mM, 4) 0.5 mM (10 mm optical path)

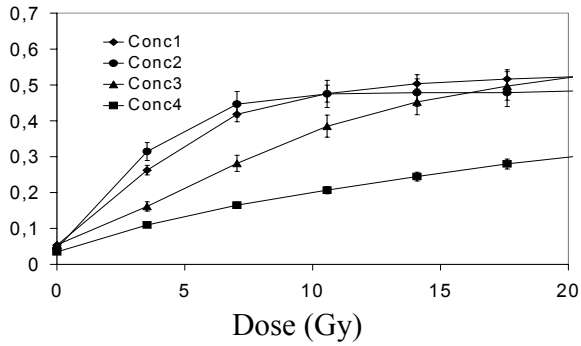

Fig.2 Results of CCD analysis of gels for different XO concentrations: 1) 0.055 mM, 2) 0.11 mM, 3) 0.165 mM, 4) 0.5 mM (10 mm optical path)

The results obtained with the spectrophotometer (10 mm optical path), reported in Fig.1, clearly show that the dosimeter sensitivity, given by the slope in the linearity region, decreases with increasing XO concentration, while the linearity range increases. The same samples (10 mm optical path) have then been placed on the light source and transmission images have been detected with the CCD camera. The linearity ranges have resulted to be shorter in this analysis modality, as it is evident from the results reported in Fig.2. A comparison of images of gels with the same XO concentration but with two different optical paths (10 mm and 3 mm) has shown that for shorter optical paths the linearity range is longer. This effect could be expected because, with increasing gel thickness, images become darker. In Fig 3 the results obtained by analyzing the gel containing 0.165 mM XO with: a) spectrophotometer (10 mm optical path) and b) CCD camera (10 mm or 3 mm optical path) are reported. The concentration of 0.165 mM has been considered to be more convenient of that previously utilized (0.11 mM) when a larger linearity range is convenient, while the first one is suitable for low dose measurements.

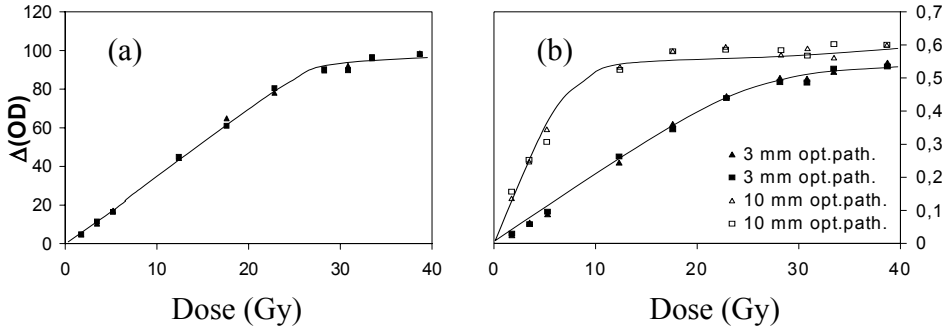

Fig.3 Optical density variation vs. dose as results from measurements with a) spectrophotometer (10 mm optical path) and b) CCD camera with 10 mm optical path (upper) or 3 mm optical path (lower).

Study of Diffusion

The diffusion coefficient of ferric ions has been measured for the two selected XO concentrations. Because of the property of XO of slowing down diffusion, the gel with higher XO concentration is expected to present less diffusion. To this aim, gel layers of circular shape, 3 mm thick and 50 mm diameter, have been irradiated with ^{60}Co γ-rays, in two different geometries: (a) under a cylindrical lead collimator (1 cm of diameter) and (b) screened by a lead block with one side in correspondence of a diameter. Examples of the detected images and of the corresponding central profiles are reported in Fig. 4. Images were detected successively at various times after irradiation, up to 18 hours. In the case (b), that is for plane shield, the diffusion coefficient has been evaluated, following Pedersen [8], and the obtained values are:

$D = 1.37 \pm 0.03$ mm^2/h for 0.11 mM XO

$D = 1.07 \pm 0.03$ mm^2/h for 0.165 mM XO.

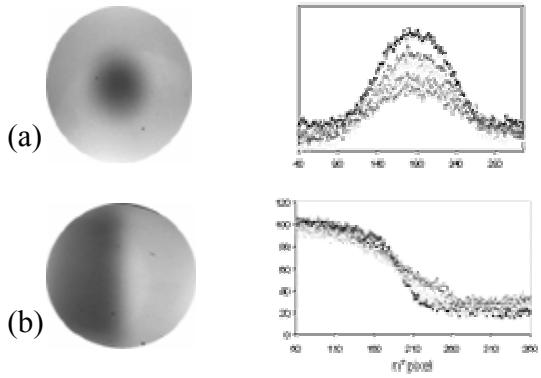

Fig.4 Images and profiles for diffusion study

Factors affecting reliability of dose imaging and profiling

The absorbed dose is measured from GL images, detected before and after irradiation. For good reliability of results, the illumination requirements should be both stability in time and uniformity in space. Such characteristics are scarcely obtainable. Instability in time of light level can be amended by means of a reference Grey-Level strip that is always imaged with each gel sample. In such a way, all images are converted by computer algorithms to a standard illumination level. The scarce uniformity of illuminators is always a hard problem, but this deficiency is made up by the pixel by pixel ratio of gel images before and after exposure. In fact, the transmitted light I_t, detected by the CCD camera, is:

$$I_t = I_o e^{-cx}$$

where I_o is the incident light, not uniform in space, x is the absorber depth and c is characteristic of the material and changes with irradiation dose. It is immediate to see that, in pixel-to-pixel ratio, I_o results to be eliminated and the lack of uniformity of illumination is amended. To show the effectiveness of this matter, in Fig 5 three profiles of a gel layer are reported. The first two are the GL profiles cut, in the same position, in the GL images before and after

irradiation. The effect of illumination non-uniformity is well evident. The last, is the Δ(DO) profile obtained after pixel to pixel ratio. Here the consequence of light non-uniformity results to be disappeared.

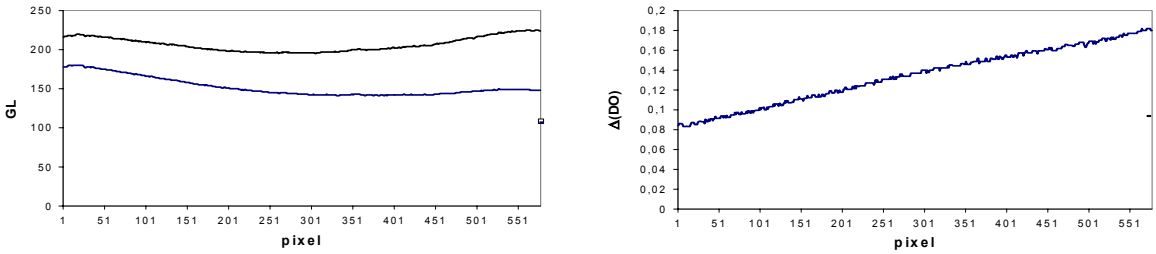

Fig.5. a) GL profiles in not-irradiated (upper) and irradiated (lower) gel. b) Δ(DO) after pixel to

Another cause of error in the dose images is the non-uniformity of gel layer thickness; in fact, a higher thickness should give the erroneous effect of a higher dose. Great attention in gel preparation is necessary to obtain satisfactory uniformity. In order to test the goodness of the FriXy-Gel technique, a set of gel layers was surrounded by polystyrene (density 1.04 g/cm^3) to make a phantom of cubic shape with 20 cm side. Dose profiles have been detected and compared with the calibration data measured with ionization chamber. In Fig. 6 gel and calibration profiles are shown. The results obtained with this technique are satisfactory, and show that the method is valid. Obviously, the quality of images and then of the extracted profiles is strongly dependent on quality of the employed CCD camera.

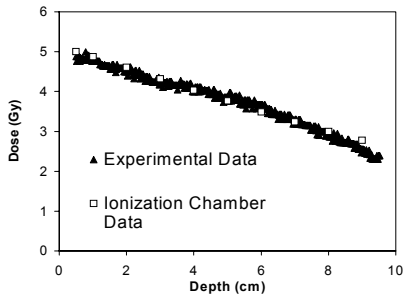

Fig. 6

Acknowledgments

The work was partially supported by INFN (Italy). Authors are grateful to Dr. G.Ranghetti and Dr. P.Giammello of ROYALITE PLASTICS s.r.l., Div. Caleppio, for having supplied polystyrene plates for making phantoms.

References

1. G. Gambarini, G. Gomarasca, A. Pecci, L. Pirola, R. Marchesini, S.Tomatis. Three-dimensional determination of absorbed dose by spectrophotometric analysis of ferrous-sulphate agarose gel. *Nucl. Instr. and Meth.* A 422, 643-648 , 1999;
2. G. Gambarini, U. Danesi, P. Marchesi, P. Palazzi, A. Pecci. Imaging and profiling of various dose contributions in BNCT performed with Fricke-gel. *Proceedings of the 1st International Workshop on Radiation Therapy Gel Dosimetry. Lexington (Kentucky) July 21-23, 1999, pp. 172-174*
3. G. Gambarini, S. Agosteo, P. Marchesi, E. Nava, P. Palazzi, A. Pecci, G. Rosi, R.Tinti. Discrimination of Various Contributions to the Absorbed Dose in BNCT: Fricke-Gel Imaging and Intercomaprison with other Experimental Results and Simulations. *Appl. Radiat. Isot.* 53, 765-772 (2000)
4. G.Gambarini, S.Agosteo, P.Marchesi, E.Nava, P.Palazzi, A.Pecci, G.Rosi, R.Tinti. Dose Imaging and Profiling for Boron Neutron Capture Therapy Planning. *IEEE Transactions on Nuclear Science* , Vol 48, N.3, June 2001 (in press)
5. G. Gambarini, S. Agosteo, P. Marchesi, E. Nava, P. Palazzi, A. Pecci, R. Rosa, G. Rosi and R. Tinti. Three-dimensional measurements of absorbed dose in BNCT by Frickee-gel imaging. **IAEA**-TECDOC-1223, 152-164 (2001)
6. A. Appleby, A. Leghrouz. Imaging of radiation dose by visible color development in ferrous- agarose-xylenol orange gels. *Med. Phys.* 18, 309-312, 1991
7. M. Zahmatkesh, B. Healy, K. Nitschke, P. Murry and C. Baldock - A study of the factors affecting sensitivity of ferrous gel dosimeters. *Proceedings of the 1st International Workshop on Radiation Therapy Gel Dosimetry*. Lexington (Kentucky) July 21-23, 1999, pp. 160-162
8. T.V. Pedersen, D.R. Olsen, A. Skretting. Measurement of ferric diffusion coefficient in agarose and gelatine gels by utilization of the evolution of a radiation induced edge as reflected in relaxation rate images. *Phys. Med. Biol.* 42, 1575-1585, 1997

TECHNICAL DEVELOPMENT OF A HIGH-RESOLUTION CCD-BASED SCANNER FOR 3-D GEL DOSIMETRY: (I) SCANNER CONSTRUCTION

Simon J Doran[1], Koen Klein Koerkamp[2], Mamdouh A Bero[1]
Paul Jenneson[1], Edward J Morton[1] and Walter B Gilboy[1]
[1]Department of Physics, University of Surrey, Guildford, Surrey, UK
[2]Department of Physics, University of Twente, Enschede, The Netherlands

Introduction

For approximately the first decade after its inception, three-dimensional gel dosimetry used a readout method based on Magnetic Resonance Imaging (MRI). However, following the seminal paper of Gore *et al*. in 1996 [1], it became apparent that 3-D dosimetry using the optical equivalent of X-ray computed tomography (CT) offered the potential of scanning at a fraction of the cost of MRI. In principle, it is now possible to construct a scanner cheaply enough so that every radiotherapy department can afford one for regular quality assurance purposes. The challenge for optical methods is now to prove that they are as accurate, robust and fast as MRI.

The technology of optical computed tomography (OCT) has been developed along three distinct routes. Laser-based approaches, typified by the scanners of Gore *et al.* [1] and Kelly *et al.* [2] correspond to first generation (or "pencil-beam") X-ray CT. One point of a projection is obtained per acquisition and then the laser-detector assembly is translated with respect to the gel sample. After all the points in a 1-D projection have been acquired, the sample is rotated and subsequent projections are acquired. A single-slice projection image with resolution 1.5 mm^2 can be acquired in approximately 15 minutes [3]. By contrast, with a CCD-based approach, as previously demonstrated by Bero *et al*. [4] and Wolodzko *et al.*[5], every acquisition is a 2-D projection image. As we show in an accompanying paper, our new CCD-scanner can acquire a high-resolution 3-D dataset in approximately 30 minutes. A third approach has been pursued by Gambarini *et al.* [6], who have created gel phantoms consisting of many separate slices, each of which can be imaged separately using a CCD camera. This allows relatively rapid data acquisition with no need for complex image reconstruction, but the drawback is a relatively low resolution in the "slice" dimension.

Construction of the scanner

Figure 1 shows a schematic diagram of the new scanner, which is a development of the one described in [4]. Light from a mercury lamp is collimated with a purpose-built lens arrangement to form a large-area parallel beam of light. This is normally incident on the walls of the scanning tank, which contains the sample, immersed in a matching liquid and mounted on a turntable, controlled by a stepper motor. A real projection image of the sample, is

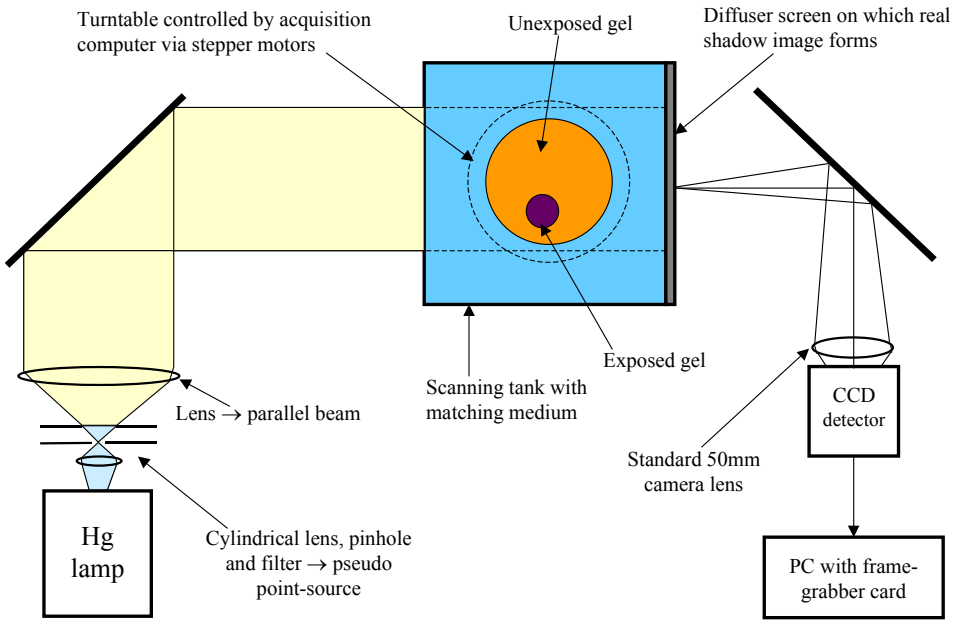

Fig. 1. Schematic diagram of the new optical tomography scanner

formed on

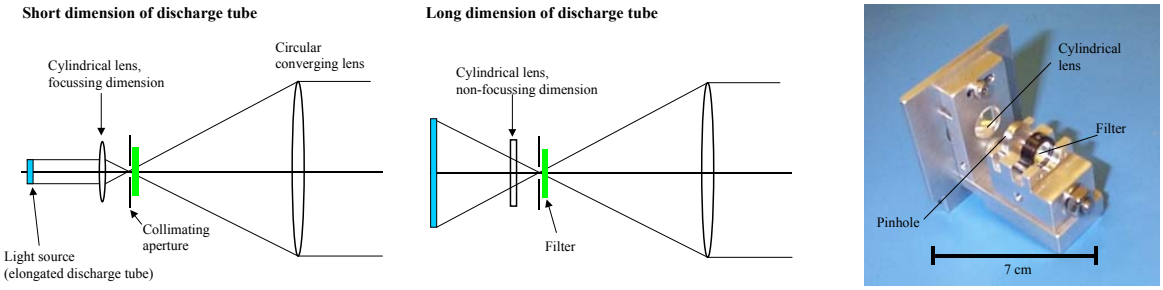

Fig. 2. Enlarged diagram of the lens and filter arrangement used to produce a parallel beam; photograph of the assembly for the cylindrical lens and filter.

a diffuser screen. This image is focussed by a standard 50 mm photographic lens onto a PCB-mounted, off-the-shelf CCD detector chip (~£130, RS Components Ltd., Corby, UK, catalogue number 208-0200). The overall length of the apparatus is reduced by including mirrors to deflect the light path through a suitable angle. The output of the CCD board, in an industry standard video format (CCIR) is captured by a 10-bit PC framegrabber card (Pulsar ~£2000 (discontinued), Matrox Electronic Systems Ltd., Dorval, QC, Canada). The user-interface, acquisition and stepper motor control are handled by an in-house program written in Visual Basic, which is also used to control a similar set of apparatus for use in X-ray microtomography. Projections are acquired over a rotation angle of 180° and the complete dataset is processed using IDL (Research Systems Inc., Boulder, CO, USA) with purpose written code to allow for the various corrections described in the accompanying paper.

A number of components of the scanner will now be described in further detail:

Light source and collimation: The spectral dose-response of the ferrous xylenol gelatin (FXG) gel system that we use was previously presented in [4]. A mercury lamp was chosen as a light source, as opposed to the fluorescent illuminator used in [5] because the output light intensity is concentrated in well defined lines (the strongest in the visible region being at 436, 546 and 580 nm). By using appropriate filters, these different lines can be selected, in particular on either side of the isobestic point, which is situated at around 470 nm. This allows a high degree of control of the image contrast in the projections. Obtaining a parallel beam of large area poses a number of problems associated both with the homogeneity of the beam and its intensity. After discarding a number of approaches based on the expansion of a laser beam, we have adopted the method shown in Fig. 2. Light from an elongated discharge tube is focussed through a pinhole aperture by a cylindrical lens. This gives a "pseudo point source", which can be placed at the focus of a converging lens to yield a parallel beam. With a true parallel beam configuration, the diameter of the converging lens (in our case 10 cm) determines the maximum diameter of the parallel beam of light and, hence, the maximum field-of-view of the optical scanner. However, two simple methods of overcoming this limitation suggest themselves. Firstly, one may adjust the position of the lens such that the beam is diverging, rather than parallel. At the cost of acquiring extra projections, one may then use a cone-beam rather than a parallel beam reconstruction algorithm. Note, however, that one must modify the standard equations from X-ray CT to account for the resulting non-normal incidence of light rays at the front wall of the scanning tank. A simpler alternative is to arrange for the beam to diverge only by a very small angle (such that no modification to the reconstruction algorithm is necessary), but to expand the beam to the desired diameter over a long optical path (several metres), using an appropriate arrangement of mirrors. With our current scanner, the limiting factors are the output intensity of the mercury lamp and detection threshold of the CCD and so fields-of-view greater than 10 cm have not been investigated.

Scanning tank and turntable: A tank consisting of a water-filled hollow perspex cube is attached, via a watertight seal, to a stepper motor-driven rotation table (Time and Precision, Basingstoke, UK, model TR48) with a precision of 0.05°. This is interfaced to the acquisition PC using a stepper motor controller (Parker Hannifin Corporation, Rohnert Park, CA, USA, model 6K4), allowing fully automated positioning of the sample.

Signal detection: After passing through the sample, the light falls on a diffuser screen, made from a sheet of engineering tracing film, to create a projection image. In our case, the light beam is still essentially parallel when it impinges on the back wall of the scanning tank. Without the diffuser screen, the imaging field of view would be limited by the diameter of the collecting lens of the camera. The framegrabber card has a digital resolution of 10-bits, i.e., 1024 separate grey levels are possible. This presents an advantage over the 8-bit systems used by previous

authors. The nominal bandwidth of the card is one frame per 50 ms. In practice, a number of frames were averaged to reduce noise in the measured projections. However, since the time for the stepper motor to move the rotation table to its new position is of the order of about 1 s, the "exposure time" is not the only factor to consider. Even for 20 signal averages, the exposure time still represents only about 50% of the total imaging time. Including both factors, the total time to acquire one projection is approximately 5 s, leading to an imaging time of just over 30 minutes for 402 (~128π) projections.

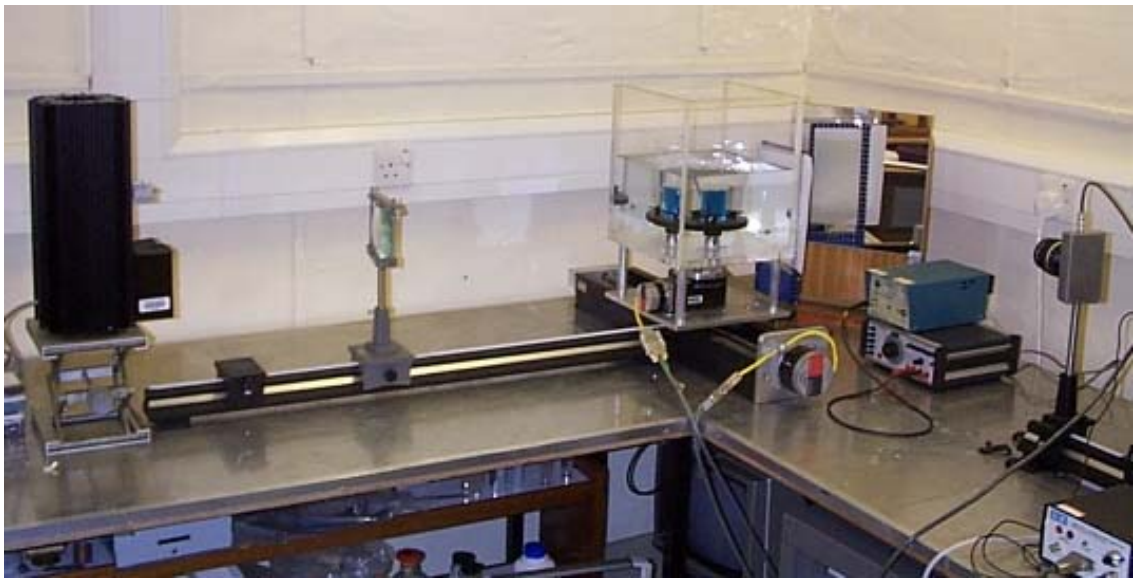

Fig. 3. Photograph of the acquisition portion of the CCD optical tomography scanner

Conclusions

In this paper, we have described the construction of a high-resolution scanner for 3-D gel dosimetry. The 3-D images may be obtained on timescales that are similar to 2-D acquisitions using the laser based optical method. With an acquisition data matrix size of up to (768 × 536 pixels) over a field-of-view whose minimum size is limited only by the minimum focal length of the camera lens, it is clear that the new scanner has the potential to obtain extremely high resolution 3-D dose maps. This makes the system ideal for studying brachytherapy sources.

References

1. J. C. Gore, M. Ranade, M. J. Maryañski and R. J. Schulz. Radiation dose distributions in three dimensions from tomographic optical density scanning of polymer gels: I. Development of an optical scanner. *Phys. Med. Biol.*, 41, 2695-2704, 1996
2. R. G. Kelly, K. J. Jordan and J. J. Battista. Optical CT reconstruction of 3D dose distributions using the ferrous-benzoic-xylenol (FBX) gel dosimeter. *Med. Phys.*, 25, 1741-1750, 1998
3. M. J. Maryanski. *MGS Inc. web site*, http://www.connix.com/~mgsinc/New_prod.html, 2001
4. M. A. Bero, P. M. Jenneson, W. B. Gilboy, P. M. Glover and S. J. Doran. Faster optical tomography with parallel-beam white light for three-dimensional dosimetry. 1st Int. Workshop on Radiation Therapy Gel Dosimetry, Lexington, Kentucky, 1999, pp 136-138
5. J. G. Wolodzko, C. Marsden and A. Appleby. CCD imaging for optical tomography of gel radiation dosimeters. *Medical Physics*, 26, 2508-2513, 1999
6. G. Gambarini, U. Danesi, R. Foroni, G. Gomarasca, R. Marchesini, P. Palazzi, P. Pecci and L. Pirola. Radiation dose imaging in Fricke-xylenol-orange agarose gel by visible light transmittance analysis performed with portable instrumentation. DOSGEL '99 First International Workshop on Radiation Therapy Gel Dosimetry, Lexington, KY, 1999, pp 130-132

TECHNICAL DEVELOPMENT OF A HIGH-RESOLUTION CCD-BASED SCANNER FOR 3-D GEL DOSIMETRY: (II) INITIAL RESULTS

Simon J Doran[1], Koen Klein Koerkamp[2], Mamdouh A Bero[1], Paul Jenneson[1], Edward J Morton[1] and Walter B Gilboy[1]
[1]Department of Physics, University of Surrey, Guildford, Surrey, UK
[2]Department of Physics, University of Twente, Enschede, The Netherlands

Introduction

Three-dimensional gel dosimetry based on Magnetic Resonance Imaging (MRI) has been extremely successful over the last decade. However, the issue of scanner availability may slow the general uptake of the technique by hospital medical physics departments. The possibility of constructing a low-cost scanner, dedicated to gel dosimetry, based on optical computed tomography (OCT) rather than MRI, was introduced by Gore *et al*. in 1996 [1]. As described in an accompanying paper, we have constructed such a scanner, based on a charge-coupled device (CCD) detector. The total cost of the scanner was less than £5000 including the acquisition computer. In this paper, we describe initial results obtained using the system and comment on the potential for further development.

Results

We present the results of two different experiments. In each case, the gel used was a ferrous xylenol gelatin mixture made using the procedures described in [2]. The concentrations of the active reagents were: Fe^{2+} 0.5 mM, H_2SO_4 25 mM and xylenol orange 0.1 mM in Experiment 1 and 0.05 mM in Experiment 2. The samples were irradiated with a newly-installed, experimental X-ray tube, capable of delivering a highly collimated, intense beam (dose rate to air up to 0.2 Gy s^{-1}). Calibration of the system had not been completed at the time of these experiments, so we report only the nominal accelerating voltage, beam current and exposure time. The dose values reported in our images represent nominal figures only and are based on the measured dose-response of the gel to ^{60}Co γ-rays ((0.083 ± 0.003) cm^{-1} Gy^{-1}, $r^2 = 0.996$).

Experiment 1: A cylindrical gel sample was irradiated four times in an axial direction. In each case, the X-ray tube voltage was 100 kV and the beam current was 20 mA. The irradiation times were 20, 15, 10 and 5 minutes. Visual inspection under white light showed four clear beam paths present in the sample, purple against an orange background. 402 projections were acquired, each of 512 × 100 pixels, and a 100-slice dataset was reconstructed at a variety of in-plane resolutions. In all cases, our slice thickness was 140 μm. The time per projection was approximately 5 s, leading to an imaging time of a little over half and hour.

Fig. 1(a) shows the result of using filtered back-projection to reconstruct the data on a 128 × 128 pixel matrix. In this case, the use of 402 (i.e., ~128π) projections ensures that the nominal pixel resolution matches the image resolution that we "genuinely" have at the *edge* of the field-of-view, in this case 560 μm. Were we to reconstruct the image on a large grid, we could resolve features far closer together than this at the centre. Fig. 1(b) shows the same dataset, but with the reconstruction windowed in a more extreme fashion to highlight the residual

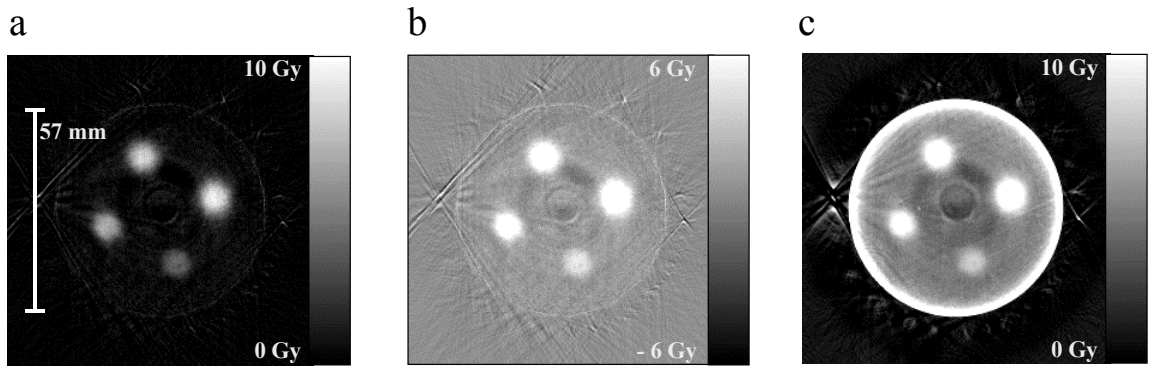

Fig. 1. Results of Experiment 1, as described in the main text: (a) normal windowing level; (b) windowing level adjusted to display residual image artifacts; (c) result obtained without employing correction for reflection and refraction at the container walls.

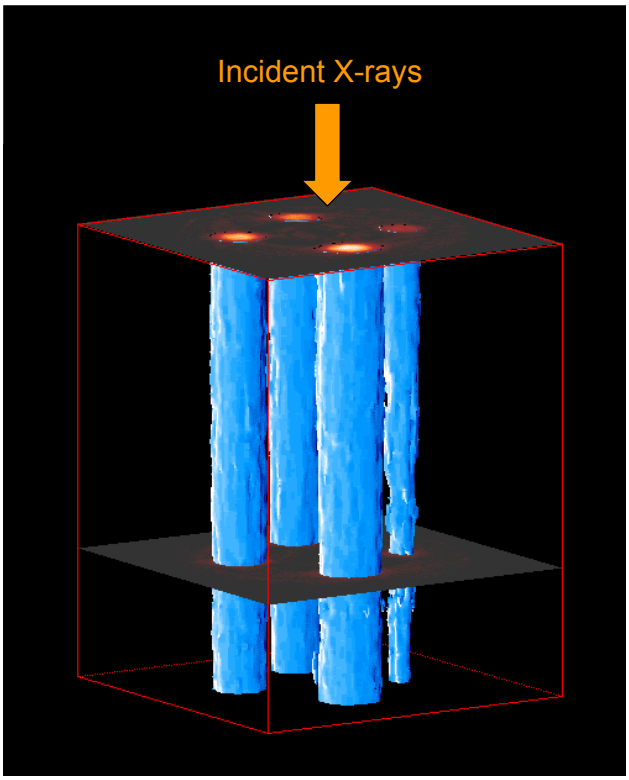

Fig. 2. 3-D reconstruction of the dose map of a phantom irradiated on four separate occasions.

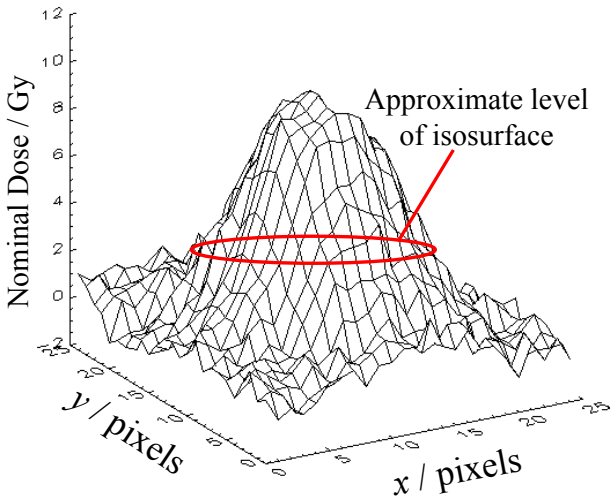

Fig. 3. Surface plot of the profile of the beam depositing the largest dose in the top slice of the dataset. The level chosen for the isosurface influences the apparent width of the column in Fig. 2, where the effect is most pronounced for the low-dose beam.

image artifacts. The most significant of these occur around the surface of the container and are caused by imperfections in the walls of the container that have not been fully corrected for by the data processing. The importance of taking into account reflection and refraction at the container walls is demonstrated by Fig. 1(c), which exhibits major image artifacts. Profiles through the centre of the object show the characteristic "horns", as described in [3]. Figure 2 shows a 3-D rendering of the dose map. Notice how the low-dose beam appears narrower than the others. This is a consequence of the value selected for the isodose surface and the beam profile, as illustrated in Fig. 3.

Experiment 2: From the previous results, it was clear that the measured beam profile was relatively broad and it was suspected that diffusion during the measurement process was significant. However, as the irradiation apparatus was new, it was not certain to what extent the X-ray beam inherently had a "penumbra". The results of a second experiment can be used to estimate the diffusion coefficent of the ferric-xylenol orange complex.

Phantom irradiation was as before, with the X-ray tube voltage again 100 kV and with exposures: beam 1, 900 s @ 10 mA, followed by 900 s @ 20 mA; beam 2, 2000 s @ 20 mA; beam 3, 500 s @ 20 mA. The sample was imaged immediately after irradiation and then again at 1 hour and approximately 16 hours post-irradiation.

The images in Fig. 4 demonstrate graphically how diffusion is one of the major disadvantages of radiochromic Fricke gel dosimetry compared with laser-based optical tomography using a polymer gel such as BANG™.

In order to compare these results with theory and extract a value for the diffusion coefficent, a simulation was performed. Given an initial concentration distribution of the xylenol complex $C(x,y,t_0)$, each element of area $dx\ dy$ contributes an amount dC to the concentration at a later date, where

$$dC(x,y,t_0+t) = \frac{C(x_0,y_0,t_0)}{4\pi Dt}\exp\left[(\Delta x^2+\Delta y^2)/4Dt\right]$$

with $\Delta x = (x-x_0)$ and $\Delta y = (y-y_0)$. Thus, in order to calculate the image at a later date, it is necessary simply to loop over all pixels (x_0, y_0) in the initial image and add up their contributions to the later image. It will be seen that the only free parameter in the simulation is D, the diffusion coefficient of the complex. The calculated image is compared with the measured image for a range of different values of diffusion coefficent and we choose the one associated with the smallest χ^2 as the most likely for our gel. Notice that the image taken immediately after irradiation was used as our initial concentration estimate, $C(x,y,t_0)$ and the second image as the target $C(x,y,t_0+t)$ for comparison with simulation. In practice, some diffusion will have taken place during the

acquisition of each of the images. Nevertheless, good agreement is seen between theory and experiment. The estimated value of D is (0.12 ± 0.02) mm^2 s^{-1}, slightly lower, but of the same order of magnitude as previous measurements [4]. (Temperature was not measured or controlled in this experiment.)

Conclusions

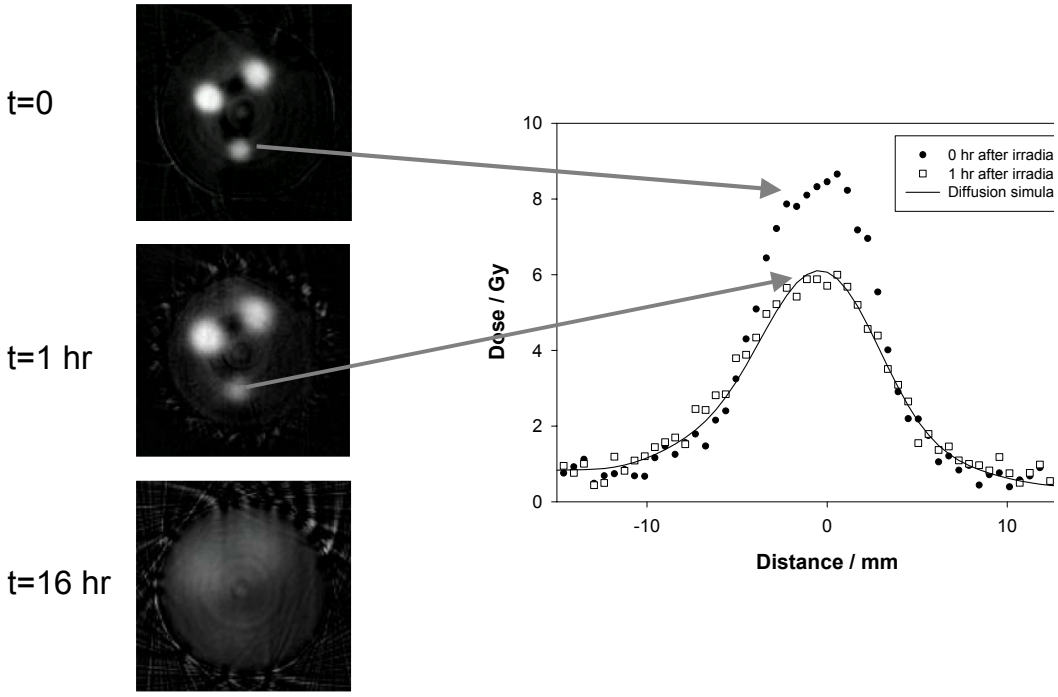

Fig. 4. Three optical computed tomography images of the same sample, acquired at different times after irradiation. A two dimensional diffusion model was fitted to the data from the lowest dose spot in the first two images, where that spot can be considered essentially isolated from the other two. The profiles on the right demonstrate the spatial resolution and signal-to-noise of our initial images.

In this paper, we have presented 3-D gel dosimetry images from a high-resolution optical computed tomography scanner, based around a CCD detector. The problem of diffusion is a significant one when using radiochromic Fricke gels. While the current scanning time is not itself prohibitively long, the diffusion still needs to be overcome when scanning very small objects (e.g., brachytherapy), when the dose delivery itself takes a significant time (e.g., IMRT) or when the imaging experiment cannot be carried out at the same location as the irradiation.

References

1. J. C. Gore, M. Ranade, M. J. Maryañski and R. J. Schulz. Radiation dose distributions in three dimensions from tomographic optical density scanning of polymer gels: I. Development of an optical scanner. *Phys. Med. Biol.*, 41, 2695-2704, 1996
2. M. A. Bero, W. B. Gilboy, P. M. Glover and H. M. El-masri. Tissue-equivalent gel for non-invasive spatial radiation dose measurements. *Nuclear Instruments & Methods in Physics Research Section B- Beam Interactions with Materials and Atoms*, 166, 820-825, 2000
3. K. Jordan. Developmental issues for optical CT and gel dosimetry. DOSGEL '99, 1st International Workshop on Radiation Therapy Gel Dosimetry, Lexington, Kentucky, USA, 1999, pp 91–97
4. S. Å. J. Bäck and L. E. Olsson. Ferrous gels (FeGel) and MRI for absorbed dose measurements; 15 years of development. DOSGEL '99, 1st International Workshop on Radiation Therapy Gel Dosimetry, Lexington, Kentucky, USA, 1999, pp 47–61

TECHNICAL DEVELOPMENT OF A HIGH-RESOLUTION CCD-BASED SCANNER FOR 3-D GEL DOSIMETRY: (III) PROBLEMS ENCOUNTERED

Simon J Doran[1], Koen Klein Koerkamp[2]
[1]Department of Physics, University of Surrey, Guildford, Surrey, UK
[2]Department of Physics, University of Twente, Enschede, The Netherlands

Introduction

With increasing interest in the area of gel dosimetry, it is of great importance to assess the robustness of imaging methods to the presence of artifacts. A considerable body of previous work has been performed in quantifying the accuracy of dosimetry based on Magnetic Resonance Imaging (MRI) (e.g., [1, 2]). However, little similar work has yet been undertaken for the relatively new modality of Optical Computed Tomography (OCT) [3]. In this paper, we describe a number of sources of image artifact in OCT and discuss ways in which we have overcome these in our prototype charge-coupled device (CCD)-based scanner.

Sources of artifact

Computed Tomography imaging can suffer from a number of reconstruction problems when using filtered back-projection. Here, we deal with the two major sources of artifact introduced by the equipment used for our particular OCT scanner. These arise from the signal detection process and from the container in which the gel is stored.

Signal detection: The results below demonstrate that, in attempting to manufacture a scanner cheaply, it is important not to compromise on the quality of the key components. Before undertaking the tomographic imaging experiments, we performed calibration experiments that highlighted a number of issues with the CCD used in this work (~£130, RS Components Ltd., Corby, UK, catalogue number 208-0200). Firstly, the detector response is significantly non-linear with incident light intensity. This was easily corrected for with a suitable calibration curve, but a more serious problem is that the detector pixels do not behave identically. This is most graphically illustrated by Figure 1(a), which shows the "dark-field" image, obtained with the lens cap on the camera. We see a number of isolated "faulty" pixels, for which the values are very different from their surroundings, and also a vertical line pattern, which is clearly a systematic design feature of the chip.

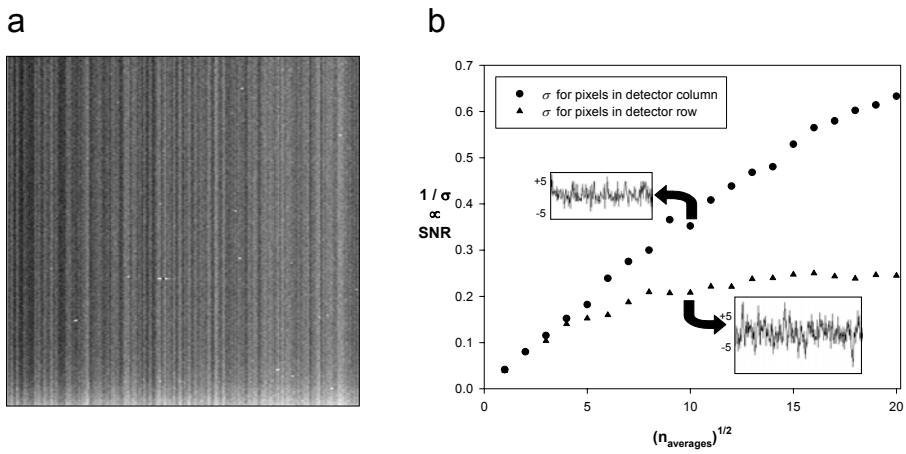

Fig. 1. (a) Image (result of averaging 100 "frames") acquired by PC framegrabber card from CCD detector with no light input (lens cap on); (b) Inverse of pixel-value standard deviation for points in a single column of the dark image (circles) and a single row (triangles) plotted against the square root of the number of frames averaged to create the image.

Figure 1(b) analyses the effect this has on signal averaging. One expects that the signal-to-noise ratio (SNR) of images obtained from a system subject to Gaussian random noise should improve according to the square root of the number of signal averages. However, if one attempts to calculate SNR simply by finding the standard

deviation of pixels in a region of the image, one obtains a result that incorporates the structure of the detector. Two sets of pixels are considered: a vertical line (circles) and a horizontal line (triangles) through the image. It is clear that gains in apparent SNR do not occur simply by signal averaging if one considers horizontal lines. Whilst one might attempt to incorporate this "detector structure" in some calibration, it is not clear that this behaviour is the same at all light levels.

Before the signal reaches the detector, it must first be projected onto a screen (see schematic diagram of the prototype scanner in the accompanying paper). This detector screen should ideally scatter the incident light primarily in a forward direction. Again in quest of a low-cost scanner, our initial material for this screen has been engineering tracing film. This has the disadvantage of being slightly grainy and thus leads to an extra random noise component in the image.

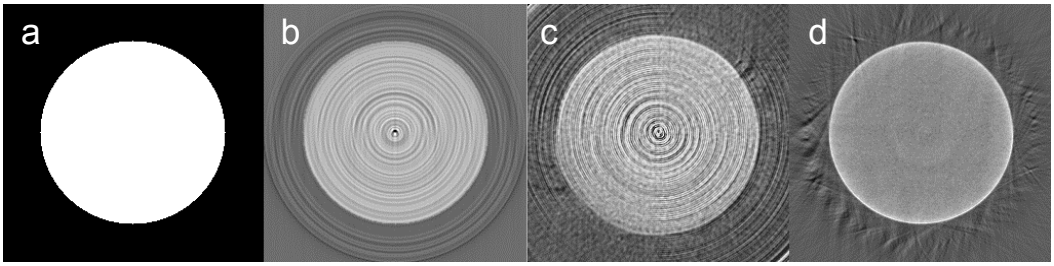

Fig. 2. Illustration of the "ring artifact": (a) simulated back-projection reconstruction of circular object in the absence of "structured noise"; (b) sinogram data from (a) reconstructed after addition of "noise" corresponding to that in one of the rows of Figure 5(a) — the same noise is added to each row of the sinogram; (c) experimental measurement on a uniformly absorbing circular object, showing the same ring artifact as (b); (d) experimental measurement incorporating the "wobble" method described in the main text, showing significant reduction of the ring artifact.

The net effect on the image of the two sources of "structured noise" described above is to introduce a pronounced *ring artifact* into the data. A simulation was performed in which the "noise" measured experimentally was added to the ideal projections of a circular object, Fig. 2(a), in such a way that each projection in the sinogram had the *same* noise. This corresponds to the fact that the CCD properties and the detector granularity do not vary between projections. The modified sinogram was then reconstructed as normal and the result is shown in Figure 2(b). The corresponding experimental image of a uniform circular phantom is shown in Figure 2(c). Ideally, we would hope to correct for these problems with some form of "ratio" or "correction scan" procedure. Suppose that the image intensity in the absence of any sample (i.e., the "open light field") is given by the function $L(x, y)$. Let us denote the attenuation caused by the unirradiated gel in the projection image taken at angle θ by $G_1(x, y, \theta)$. Similarly, the attenuation caused by the irradiated gel is $G_2(x, y, \theta)$. If we take two scans, S_1 before irradiation (the correction scan) and S_2 after irradiation, then

$$\frac{S_2(x,y,\theta)}{S_1(x,y,\theta)} = \frac{L(x,y)\ G_2(x,y,\theta)}{L(x,y)\ G_1(x,y,\theta)} = \frac{G_2(x,y,\theta)}{G_1(x,y,\theta)} \ .$$

The quantity G_2 / G_1 corresponds to the radiation-induced change in optical absorption of the gel, which is what we are trying to find. This technique works well at removing imperfections in our lamp arrangement and in theory, any feature that is constant between the projections, such as a non-uniformity in the projection screen or detector ought to be capable of incorporation into $L(x, y)$. However, in practice, it turns out to be extremely difficult to re-align the sample with sufficient accuracy to acquire the second set of projection data. The "structured" noise that we are trying to eliminate occurs on the length scale of a single pixel and thus repositioning with sub-millimetre precision is needed. This will be incorporated into the next prototype. In the current configuration, the ring artifact has been eliminated by a combination of oscillating the diffuser screen up and down (so that its granularity is to some extent "smeared out") and randomly "wobbling" the detector with respect to the sample, so that in each projection, different detector pixels are used. The resulting improvement in image quality can be seen in Fig. 2(d).

The gel container: An accompanying paper deals with the problem of reflection and refraction at the gel container interfaces and some considerable success has been achieved in correcting for these via simulation and via the ratio technique discussed above. However, during this work, it has proved difficult to obtain adequate containers for the gel samples, with optical properties that are well defined. A brief survey demonstrated that many vessels of the size required present considerable inhomogeneity in refractive index, which degrades the projection data —

many are made by extrusion, which leads to linear features in the projections. In addition, the quality of the projections is very sensitive to surface damage (e.g., scratches during cleaning). The use of glass, which can be polished, may lead to increased problems of refraction and reflection because its refractive index is much greater than that of water.

Fig. 4(a) demonstrates the type of problem that occurs. The container to be used had been pre-selected as the "best in the batch", but nevertheless, superimposed on the desired sinogram are a set of diagonal lines caused by minute imperfections in the container wall. One particularly prominent scratch (which occurred while clamping the container for a previous irradiation) is visualised as a pair of bright diagonal lines. By dividing these data by the correction scan shown in Fig. 4(b), we obtain a sinogram in which the wall effects are substantially reduced. However, it is apparent that they have not been entirely eliminated (Fig. 4(c)) and, again, this may be attributable to poor alignment of the two scans. The final image Fig. 4(d) still displays some residual artifact.

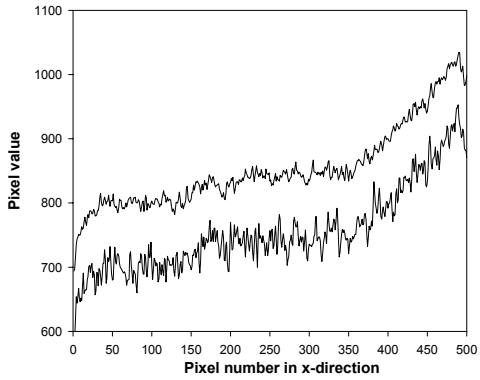

Fig. 3. Profile across the open-field light measurement with (above) and without (below) oscillation of the detector screen. The ratio technique can correct for the large scale non-uniformities, but not the pixel-by-pixel noise.

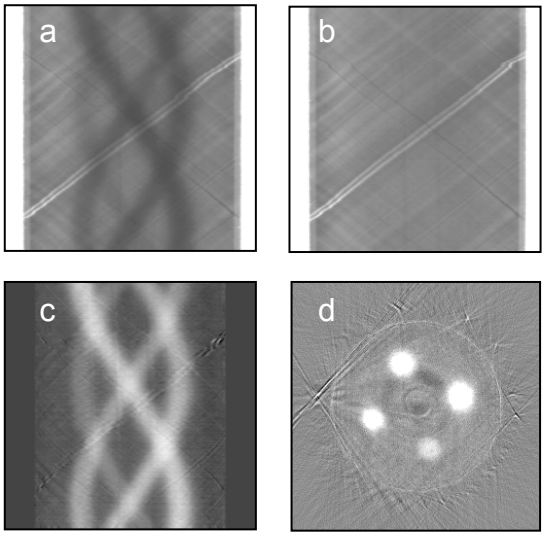

Fig. 4. (a) Raw sinogram data from Experiment 1 — note the presence of numerous diagonal lines corresponding to imperfections in the container walls; (b) the "correction scan"; (c) the processed sinogram data. Notice how the two diagonal "scratch marks" prominent in (a) have been greatly reduced in intensity; (d) reconstructed image showing residual artifacts from the walls.

References

1. I. C. Baustert, M. Oldham, T. A. D. Smith, C. Hayes, S. Webb and M. O. Leach. Optimized MR imaging for polyacrylamide gel dosimetry. *Physics in Medicine and Biology*, 45, 847-858, 2000
2. C. Baldock, P. Murry and T. Kron. Uncertainty analysis in polymer gel dosimetry. *Physics in Medicine and Biology*, 44, N243-N246, 1999
3. J. C. Gore, M. Ranade, M. J. Maryañski and R. J. Schulz. Radiation dose distributions in three dimensions from tomographic optical density scanning of polymer gels: I. Development of an optical scanner. *Phys. Med. Biol.*, 41, 2695-2704, 1996

SIMULATION OF THE EFFECT OF SAMPLE/CONTAINER INTERFACES FOR 3-D GEL DOSIMETRY USING OPTICAL COMPUTED TOMOGRAPHY

Simon J Doran
University of Surrey, Guildford, UK

Introduction

3-D dosimetry using the optical equivalent of X-ray computed tomography (CT) was first suggested in 1996 [1] and was discussed in some detail at the First International Workshop on Radiotherapy Gel Dosimetry [2]. Further work on optical CT has since been published by Wolodzko *et al.* [3] and Jordan *et al.* [4]. A number of these authors have mentioned the use of optical simulation for the characterisation of deviations in light ray paths through the optical scanner, but a detailed account of such a simulation and the results obtained has not yet been presented. In this abstract, the "standard" configuration of a cylindrical sample is analysed. Results of the simulations are very sensitive to the combination of parameters and are sometimes counter-intuitive. The conclusions apply equally to CCD and laser-scanning systems, although the results are validated here only for a CCD-based system.

Method of simulation

Light was initially assumed to be travelling through the matching medium parallel to the *y*-axis, as shown in Fig. 1(a). A given ray is incident on the outer wall of the cylindrical container at horizontal coordinate x_i. As it travels from this point to the projection screen at the other end of the tank, it encounters 6 different interfaces before impinging on the projection screen at x_0. At each of these interfaces, both reflection and refraction can occur. In principle, this makes ray tracing quite complicated as individual rays can reach the screen after multiple reflections and refractions. In practice, the reflection coefficients are such that only a very small error is introduced by ignoring rays that have been multiply reflected. So for this analysis, I take account of rays that hit the screen after being reflected from the container's outer surface, but not those whose first reflection occurs at the gel-container interface.

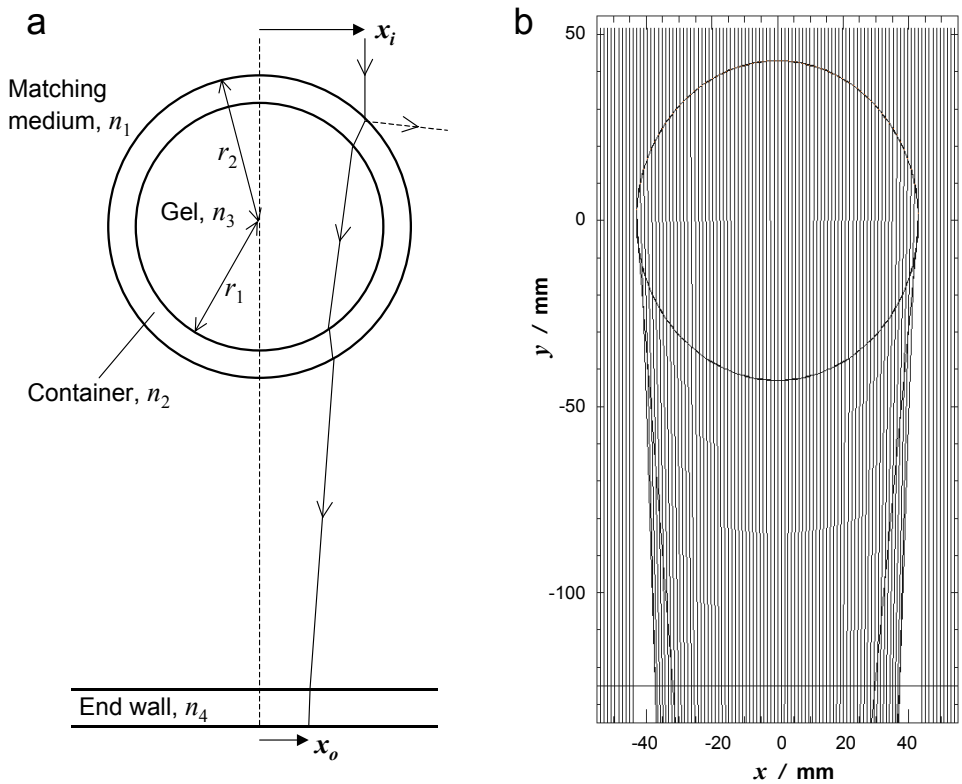

Fig. 1: (a) Geometry of the simulation; (b) simulation result for a system with the following typical characteristics: $n_1 = 1.33$, $n_2 = 1.51$, $n_3 = 1.338$, $n_4 = 1.49$, $r_1 = 42.9$ mm and $r_2 = 43.0$ mm

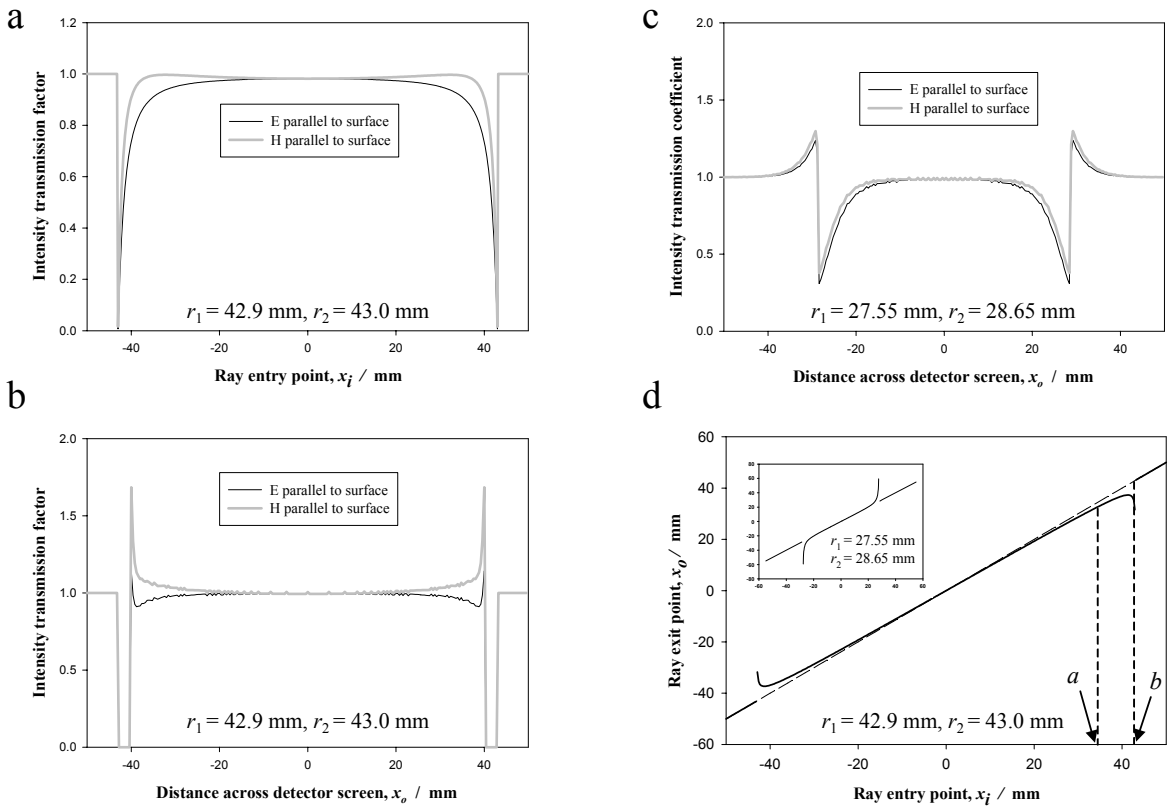

Fig. 2: (a) Transmission coefficients *not* taking into account refraction; (b) transmission coefficients for a thin-walled container taking into account refraction; (c) corresponding results for the container we used in tomography experiments; (d) relationship between input and output positions for light rays.

For a given ray, Snell's Law determines the direction of emergence from an interface, whilst to find its intensity, Fresnel's equations are applied in the following form:

$$T_{\mathrm{E}} = \left(\frac{n_t}{n_i}\right)\left(\frac{2n_i \cos\theta_i}{n_i \cos\theta_t + n_t \cos\theta_i}\right)^2 \quad ; \qquad T_{\mathrm{H}} = \left(\frac{n_t}{n_i}\right)\left(\frac{2n_i \cos\theta_i}{n_i \cos\theta_i + n_t \cos\theta_t}\right)^2$$

where T_{E} and T_{H} are the (intensity) transmission coefficients for light polarised with the E-field and H-field, respectively, parallel to the surface. These expressions are calculated at each interface in turn and the final results, shown in Fig. 2(a) are the products of these terms for all six interfaces. (The final result also includes a factor corresponding to the cosine of the exit angle at the final interface, as this determines the rate of power transfer in the vertical direction. However, this correction is almost negligible for the cases considered; the perspex end wall plays only a very minor role.)

Results

Whilst Fig. 2(a) is largely what one might expect, the results in Figs. 2(b) and 2(c) are perhaps surprising. The figures correspond to two different types of container. Both illustrate the intensity of light along a profile of the measurement screen *once the non-uniform distribution of light rays along the x_o-axis has been taken into account*. Fig. 2(b) corresponds to a piece of overhead projector film, bent into a cylinder and is somewhat similar to a polycarbonate cylinder with 0.2 mm walls described by Jordan *et al*. [4]. Fig. 2(b) is simulated using the same measurement parameters as Fig. 1(b) and the regions of zero signal can clearly be associated with rays close to the edges of the sample that have been strongly refracted. These rays leave an unilluminated void and then bunch together just inside the edge of the container, leading to a bright fringe in the projection images. This simulated effect is reproduced under experimental conditions (Fig. 3). Notice that the effect is substantially different between the two polarisations, but that in both cases, there is a complete loss in the projection data at the edge of the sample.

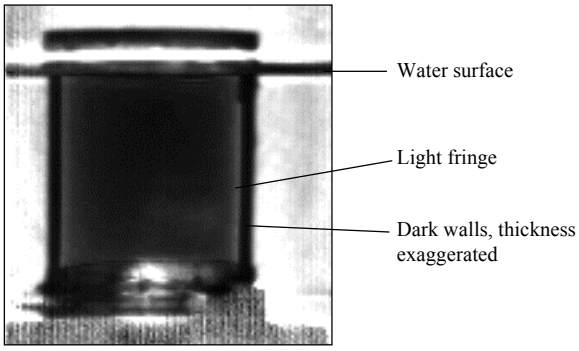

Fig. 3: Experimental demonstration of the effect described in the text. Note that in this case, the matching medium was transparent and so a higher intensity signal is seen outside.

Compare this situation with that in Fig. 2(c), which corresponds to the actual container used in our tomography experiments. Although the signal drops towards zero at the edges, there is no dark void; instead of a bright fringe inside the sample, there is now an extended bright region outside the sample; instead of rays bent inwards at the left and right edges of the sample, as in Fig. 1(b), the rays close to the edge bend outwards and do not cross each other (data not shown). This scenario is potentially more hopeful, as, in principle this light could be recovered.

The results are clearly very sensitive to the exact dimensions of the containers (and also to the exact values of their refractive indices, although this will not be discussed further here.) It is not enough simply to make the container walls as thin as possible, nor to make the matching medium have exactly the same refractive index as the gel. An instructive way of visualising the situation is to consider Fig. 2(d). This shows the relationship between the position x_i at which the light ray enters the sample and x_o where the ray hits the projection screen. The main graph demonstrates the situation for the container discussed earlier with thin film walls, whilst the smaller inset is for the container we used in tomography experiments. For approximately 75% of the field-of-view, the input and output coordinates match well, i.e., the line is straight and has gradient ~1. However, at the edge of the field-of-view, the thin-film graph has a turning point. For ray entry points between *a* and *b*, two rays traversing *different* paths through the sample map onto the *same* point on the projection screen. The problem is underdetermined and hence one loses the whole region of the projection between *a* and *b*, not just the dark region where no signal is seen. This can be up to a quarter of the field-of-view and would cause considerable degradation of the reconstructed images, as described in [2].

The corresponding graph for the other container displays opposite behaviour. Here the graph does not turn over and so we do not have the case where two paths through the sample overlap. Instead, one sees locations *outside* of the sample where rays that have traversed the sample are superimposed on rays that have passed only through the matching medium. In principle, this open field is known and can be subtracted, thus allowing us to recover the *entire* profile. A final point of interest to note is that Figs. 2(b) and 2(c) represent extremes of behaviour. By a judicious choice of container dimensions and refractive indices, it is possible to obtain a relation between x_i and x_o that is straight for its entire length. Since no rays are superimposed, it is in principle possible to recover an arbitrarily large fraction of profile, depending only on the dynamic range and sensitivity of the detector. Both of these scenarios requires further practical investigation.

Conclusions

By a ray-tracing simulation of the light paths through a gel sample in a container, one can obtain useful results that guide the choice of container dimensions and wall thickness. In principle, untruncated projection images may be recovered given suitable equipment, allowing reconstruction of images free of artifacts due to incomplete data

References

1. J. C. Gore, M. Ranade, M. J. Maryañski and R. J. Schulz. Radiation dose distributions in three dimensions from tomographic optical density scanning of polymer gels: I. Development of an optical scanner. *Phys. Med. Biol.*, 41, 2695-2704, 1996
2. K. Jordan. Developmental issues for optical CT and gel dosimetry. DOSGEL '99, 1st International Workshop on Radiation Therapy Gel Dosimetry, Lexington, Kentucky, USA, 1999, pp 91–97
3. J. G. Wolodzko, C. Marsden and A. Appleby. CCD imaging for optical tomography of gel radiation dosimeters. *Medical Physics*, 26, 2508-2513, 1999
4. K. Jordan, G. Garvey and J. Battista. Measuring complete optical CT data sets using thin-walled vessels for 3D gel dosimetry. World Congress on Medical Physics and Biomedical Engineering, Chicago, 2000, E309-06

OPTICAL CONE BEAM TOMOGRAPHY WITH LOW PRESSURE SODIUM LIGHT

Kevin J. Jordan[1,2], Tomasz M. Pajak[1], Collin Piontek[1] and Jerry J. Battista[1,2]
[1]London Regional Cancer Centre, [2]Medical Biophysics, University of Western Ontario
London, Ontario, Canada

Introduction

Two groups have described implementing CCD array detectors for fast optical tomographic scanning of radiosensitive gels[1,2,3]. Array detectors and large effective area light sources are basic technologies for designing fast inexpensive optical CT scanners. Recently, the performance of consumer digital cameras has increased dramatically. We began this project to determine the limitations of such cameras for the construction of educational-grade optical cone beam scanners. Such projects are considered ideal for developing teaching experiments related to CT scanning, imaging, reconstruction algorithms and radiation dosimetry. Our group is developing methods to reduce the optical scatter in radiochromic gels in order to improve the range of absorbances and the ultimate resolution that can be obtained with these systems[4]. While single beam single detector 'first generation' x-ray or optical scanners provide the greatest scatter rejection, it may be possible to combine fast 'area' scanners with low scatter gels to obtain satisfactory data for determining 3D dose distributions at clinically acceptable tolerances. We chose the optical geometry reported by J. Wolodzko, et. al. because of its simplicity and substituted a low pressure sodium lamp to allow direct performance comparisons with our 594nm He-Ne laser scanner. The visible emission of a low- pressure sodium lamp consists to two sharp lines at 589.0 and 589.6 nm which are equivalent to the 594 nm He-Ne laser line. This approach of recording transmission images of the gel in a refractive index matched liquid with a diffuse uniform light source is the inverse of x-ray 'cone beam' CT if you consider only the rays which contribute to image formation. The added feature is that visible rays refract at the wall of the optical aquarium. In this work we present our initial results with parallel re-sorting of rays in allow reconstruction with the filtered backprojection algorithm[5].

Experiment

Transmission images of 9.6 cm inner diameter, thin-walled teflon cylinders located in the centre of a 15x15x15 cm, liquid-filled 'aquarium' were recorded with a digital camera, Olympus C3030Zoom. The light source was a 35 W low pressure sodium lamp, mounted in box with a diffusing plastic sheet located 25 cm from the bulb. The camera was mounted 80 cm from the rotation axis of the cylindrical phantoms. Images were recorded with 0.125 sec exposures, F11 aperture and JPEG file format. A background image taken with a red long wavelength pass filter in front of the camera verified that an internal filter was blocking the near infrared emission of the sodium lamp. The long exposure time effectively dc averaged the lamp intensity which was full-wave modulated at 120 Hz. To quantify optical distortions, a transparent 1 cm grid was positioned perpendicular to the optic axis in the centre of the liquid-filled aquarium coplanar with the cylinder's rotation axis. Examination of the grid image determined that no significant distortions were present and that the effective resolution was 7.0 pixels per mm over the 10x10 cm field of view occupied by the cylinder. A calibrated stepped optical density film was imaged through the aquarium in order to measure the camera linearity. Rotation control was provided by a computer controller motor, connected to the cylinder. CT data sets consisted of 60 or 360 images collected over 360 degrees. Data was collected in a semi-automated sequence at an approximate rate of 20 seconds per image. The 8 bit RGB images were imported into MatLab where the area containing the cylinder and adjacent liquid were cropped and the green pixel values were placed into a 3D array. The natural logarithm of the ratio of pre and post scan array elements were input to the Radon transform for reconstruction, Hann filter with linear interpolation. Only the central slice has been reconstructed for this report. Pixels were averaged to give a spatial resolution of 1 or 0.5 mm^3 for the coloured liquid and 1 mm diameter pin phantoms respectively. The absorption coefficients of the coloured liquid samples were independently measured at 594 nm in 1 cm pathlength cuvettes with a commercial absorption spectrometer. Within the central slice off-axis rays within the cylinder were re-sorted according to the ray's angle relative to the optic axis. For example, in the mth projection a ray with an angle of q degrees relative to the optic axis was shifted into the m+q projection. For this particular experiment, q was less than 3.5 degrees. The net result of resorting was a consistent set of parallel ray projection data for input to the filtered backprojection reconstruction algorithm.

Results

Figure 1a is the reconstructed central slice of a 2 pin phantom, calculated with spatial averaging to generate 0.5 mm^3 voxels. The 7 subsets of projection data were shifted in order to minimize a position discontinuity that occurred while pausing to download groups of images from the camera. No 'wall' correction to smooth the projection data at the walls was made for this example. A better mechanical rotation system will eliminate several of the reconstruction artifacts. Note the distortion of the pin located 42.5 mm from the rotation axis, near the inner cylinder wall at 0.89(radius). Figures 1b and 1c are detailed images of the reconstructed outer pin before and after re-sorting to parallel beam geometry. Re-sorting essentially removes the error caused by ignoring divergence and refraction in the initial images.

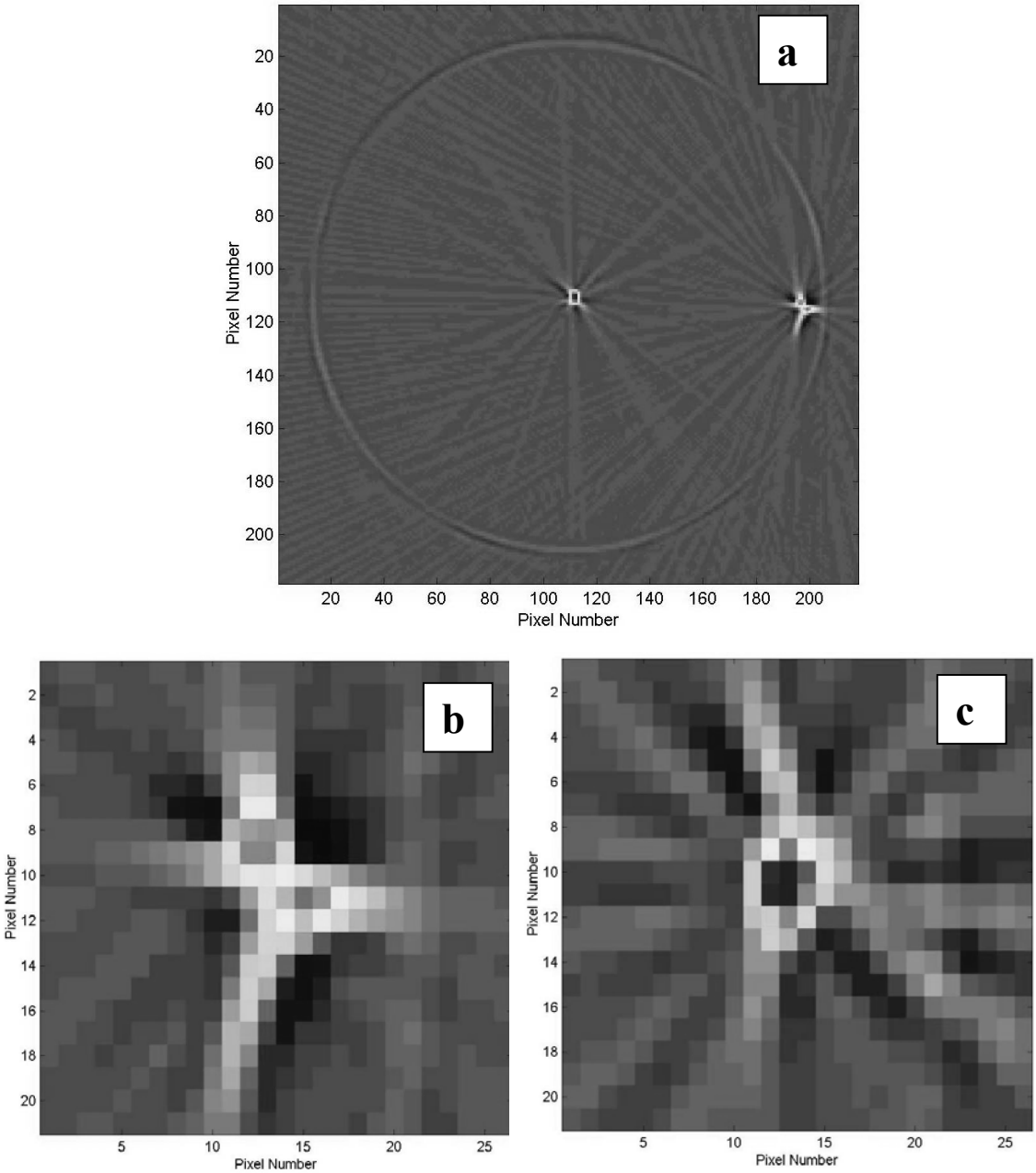

Figure 1. CT reconstruction of 1 mm pin phantom, filtered backprojection, 0.5 mm2 pixels, 360 projections: a) central slice with no wall correction and before re-sorting to parallel projections b) detailed view of outer pin c) detailed view of outer pin after re-sorting.

Optical densities for the calibrated step film as measured with the digital camera were much smaller than the nominal 0.2, measured with a film densitometer, when the pixel values exceeded ~120 (min=0, max=255). For this reason exposures were limited to give maximum green pixel values of <120 for the following CT data sets.
Table 1 lists the absorption coefficients at 594 nm for three coloured liquids as determined from cone beam optic CT data(60 projections) and a commercial spectrometer. The poor agreement at low light levels is likely due to the limited linear range of the camera. It is estimated that the useful dynamic range of camera pixel values may be as low as 20-30, ie max ~120 and min ~5.

Minimum cylinder transmission	Spectrometer absorption coefficient cm^{-1}	Cone beam CT absorption coefficient cm^{-1}
50%	0.066	0.064
10%	0.224	0.18
5%	0.304	0.24

Summary

An optical cone beam scanner with submillimeter resolution has been demonstrated by combining; a low pressure sodium lamp diffuse light source, a consumer grade digital camera, data re-sorting to form parallel beam projection data and filtered backprojection reconstruction algorithms. The major limitation of this device is the small linear response range of the digital camera. Likely the raw CCD intensity values are corrected to closely match human eye response prior to writing to file. The inherent range of optical densities that can be measured with this geometry has yet to be determined. Those measurements will require substitution of a scientific grade CCD camera to this system to enhance the accuracy of the intensity measurements. Reconstructions of all slices to generate a 3D image will experience the same limitations as x-ray cone beam CT. The main feature is the effective slice thickness will evolve into a 'flying saucer' shape as the distance from the optical axis increases. Simple optical cone beam scanners will prove useful as educational instruments for teaching principles of CT imaging and possibly as clinically acceptable devices for 3D gel dosimetry.

Acknowledgements

Ryan Bohnert, participated in the feasibility study as a medical biophysics undergraduate student project at the University of Western Ontario. Robert Tonks designed and constructed the motor controller for this project. This work is fund by a grant from the National Cancer Institute of Canada.

References

1. M.A. Bero, P.M. Jenneson, W.B. Gilboy, P.M. Glover and S.J. Doran. Faster optical tomogaphy with parallel-beam white light for three-dimensional dosimetry, Dosgel99 Proceedings, 136-138, 1999
2. M.A. Bero,W.B. Gilboy, and P.M. Glover. An optical method for three-dimensional dosimetry, J Radiol Prot, **20**, 287-94, 2000
3. John G. Wolodzko, Craig Marsden and Alan Appleby. CCD imaging for optical tomography of gel radiation dosimeters, Med. Phys. **26**, 2508-2513, 1999
4. K. Jordan, L. Coelho, K. Hadley and K. Chu. Glycerine reduces scatter and diffusion in radiochromic gelatin gel for optical CT, manuscript in preparation
5. Avinash Kak and Malcolm Slaney. Principles of computerized tomographic imaging, IEEE Press, pg 92, 1987

OPTICAL SCATTER MEASUREMENTS IN BANG™ AND FX GEL

Mark Oldham, Jeffrey Siewerdsen, Carl Rowbottom, David Jaffray
William Beaumont Hospital, Royal Oak, Michigan, USA

Introduction

The possibility of obtaining accurate and high resolution dosimetric images by optical-CT scanning has recently been proposed and demonstrated [1-3]. The design of these scanning systems has largely been based on that of the first generation x-ray CT scanners, with the x-ray source replaced by a laser in the visible wavelength range. An illustration of a typical 1st generation optical-CT scanner design is shown in **figure 1**. A feature of this type of design is that scanning is restricted to acquiring the transmitted light along a single ray-path through the gel at a time. A single projection is obtained by stepping the scanning ray-path across the extent of the gel-flask, and acquiring the ray-path acquisition at each step. The gel-flask is then rotated by a small increment and the next projection is acquired. A limitation in the scanning design of figure 1 is the length of time that is required to obtain enough projection data to be able to reconstruct a complete 3D data set. To reconstruct a 8x8x8cm volume with 1mm resolution would require 80x180x80=1.15million single ray-path transmission acquisitions, assuming 180 projections are required to reconstruct each slice. If each ray-path acquisition takes 0.1s then the total scanning time would exceed 30 hours! A solution to decrease the scanning time would be to acquire a complete projection at a time (i.e. a line-scan) instead of a single ray-path. This would decrease scanning time to ≈0.4hours in the example case. The principle concern in expanding acquisition to a line-scan approach is the effect of scatter. A line-scan is conceived as a linear array of ray-paths and any scatter contamination between rays will severely degrade the image. Clearly the optical quality, and in particular scattering potential of gel dosimeters will play an important role in determining the quality of dosimetry that is achieveable. In this paper we present a prelimary investigation into the optical scattering properties of two gel-dosimeters that have been used in optical-CT scanning. The two gels are the BANG gel [4] and fricke-xylenol-orange or FX gel.

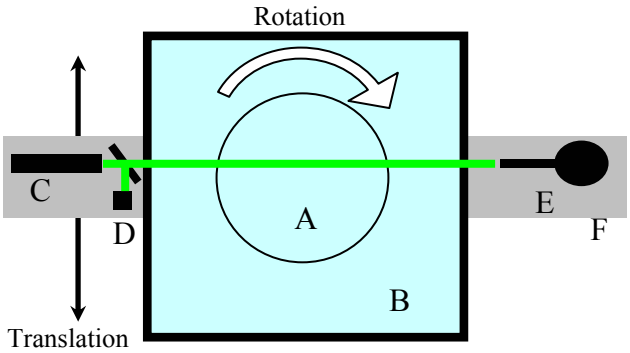

Fig. 1. Schematic view from the top of a 1st generation optical CT scanner [4]. Labels are A=gel-flask, B=optically matched water-bath, C=laser, D=reference photo-diode, E=lab-sphere-field photo-diode assembly, F=base plate. The laser-lab-sphere assembly traverse the flask to acquire a single projection. Then the flask is incremented rotationally before acquiring transmision data of the next projection.

Materials and Methods

The BANG gel was obtained from MGS Research, and the FX gel was made in-house according to the recipe in [2,5] without the addition of benzoic acid. Both the BANG and FX gel were poured and set into 5 identical tissue culture flasks made of polystyrene and of 200ml volume. Each flask was then placed in an antifreeze-bath and scanned prior to irradiation by stepping a laser horizontally across the flask as illustrated in figure 2. The intensity of laser light that transmitted through the flask and anti-freeze bath was measured by a large-area field photodiode. Scanning parameters were set to step the laser by 1mm increments across the flask, and to sample 100 values of the ADC converter on the output of the photodiode. The photodiode was attached to an integrating optical sphere with a 1cm diameter circular aperture, which reduced sensitivity to slight positional variations of the laser light incident into the sphere. The purpose of the dilute green antifreeze was to minimize refraction of laser light incident and exiting the flask. Laser output fluctuations were continuously monitored by a reference photodiode onto which a fraction of the laser was incident from a beam-splitter. The photo-currents from each photodiode were fed into a pre-amplifying electrometer with settings to produce an analogue voltage output of 0-10V for laser illumination from the 1mW HeNe green laser. The output voltage was then fed into the ADC board for acquisition.

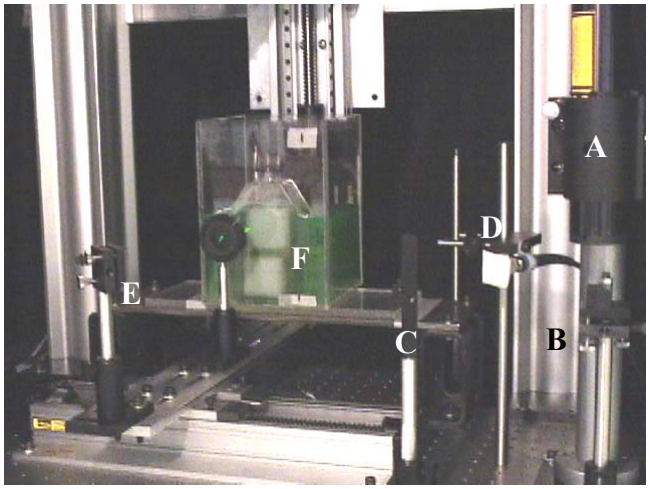

Fig 2. Post irradiation scanning geomtery. A BANG gel flask is shown mounted vertically in the anti-freeze bath. A=laser, B=E=mirror, C=beam-splitter, D=reference diode, F=gel-flask in antifreeze bath.

The pre-irradiation scans were taken to study the uniformity and baseline transmission of laser light through each flask. The laser light measured in these pre-scans consisted of both primary and scattered laser light. Primary laser light was taken to consist of photons that passed straight through the gel and anti-freeze bath without being scattered. The primary is easily distinguishable as an intense and narrow beam, about .75mm in diameter, defining the central axis of the laser path through the optical apparatus. The scattered light forms a greenish halo around the primary, the extent of which depends on the scattering properties of the gel and antifreeze through which the laser passes. To estimate the proportion of scattered light (called the scatter fraction) a further set of pre-irradiation scans were taken where the primary laser light was blocked by the introduction of a steel ball (supported on a metal stick) that was just large enough to block the primary laser light while allowing scattered light to continue on to the collecting field diode. Immediately after pre-scanning, each gel-flask was irradiated twice, in the upper and lower regions of the flask respectively, to known doses by a small 6MV radiation beam. The delivered dose values were selected to span the optical range of the particular gel, and were 0-14Gy for the FX and 0-1.2 Gy for the BANG respectively. The time interval required for stabilization of the polymer reactions in BANG gel and the oxidation reactions in the FX gel have been reported as 20 and 70-90 minutes respectively [3,2]. After stabilization of the respective reactions, post-irradiation scans were taken across all flasks through the centre of each irradiated region in the manner described above for the pre-scans. After irradiation post-scans were obtained of both the primary and scatter-fraction combined and just the scatter fraction by introduction of the steel ball, in the same manner as outlined above. In addition the progress of the FX oxidation reaction was monitored by scanning the gel-flask that received 14Gy immediately post-irradiation and at repeated intervals up to 90 minutes, using the same scanning technique as described above.

Results and Discussion

The amount of primary and scattered, and the scatter fraction of transmitted laser light that reached the field diode for the FX gel is shown in figure 3a,b. An exponential decrease of transmitted light with dose is observed corresponding to the increased absorption due to the increased number of oxidised xylenol orange molecules. No clear trend was observed in the scatter fraction with dose. This observation is consistent with a primarily absorbing gel which produces little scattered light. A scatter fraction of about 0.3% was established from figure 3b over the dose range 0-14Gy. The two anomalous high readings are outliers and probably reflect slight changes in trajectory of the primary beam path relative to the steel ball, and therefore the uncertainty in this measurement. The primary and scattered, and the scatter fraction of transmitted laser light that reached the field diode for the BANG gel is shown in figure 4a,b. A similar exponential decrease of transmitted light with dose is observed corresponding to the increased polymerisation of the gel. The scatter fraction was observed to be between 0.9 and 0.5% (a factor of 2 and 3 times that observed in the FX gel) in the useable region of 0 to 1.2 Gy. Interestingly this preliminary data appears to suggest a slight inversely proportional trend in the scatter fraction with dose. This observation may seem counter-intuitive as an increase in the amount of scattered light is expected with a denser polymer matrix. The effect warrants validation and further investigation.

Conclusions

Preliminary optical scattering measurements have been made to attempt to quantify the scattering properties of two gels currently used in optical-CT gel dosimetry. The fraction of scattered light was estimated to be about 0.2-0.4% for the FX gel, and to be independent of dose to within this noise level. The scatter fraction in the BANG gel was observed to be about 2 to 3 times this value. The preliminary BANG data suggested a slight inversely proportional relationship with dose, an effect which needs further validation and study. The low scatter fraction of the FX gels

appears well suited for the purpose of moving from a 1st generation CT 'ray-path' scanning paradigm to a faster line-scanning approach. The higher scatter fraction in the BANG gels may pose some limitations to the line and broad beam scanning approaches

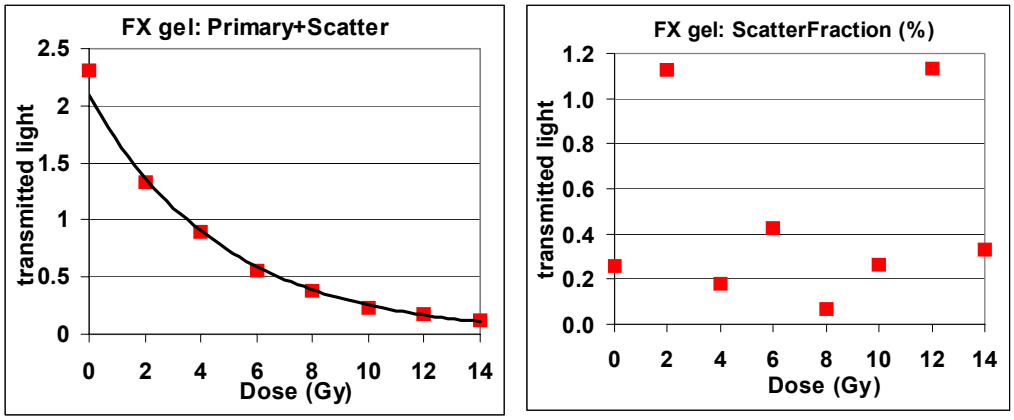

Fig. 3. a) the intensity of transmitted primary and scattered laser light (arbitrary units) through the FX gel-flask and anti-freeze bath. b) The fraction of laser light scattered in the FX gel-flask and anti-freeze bath

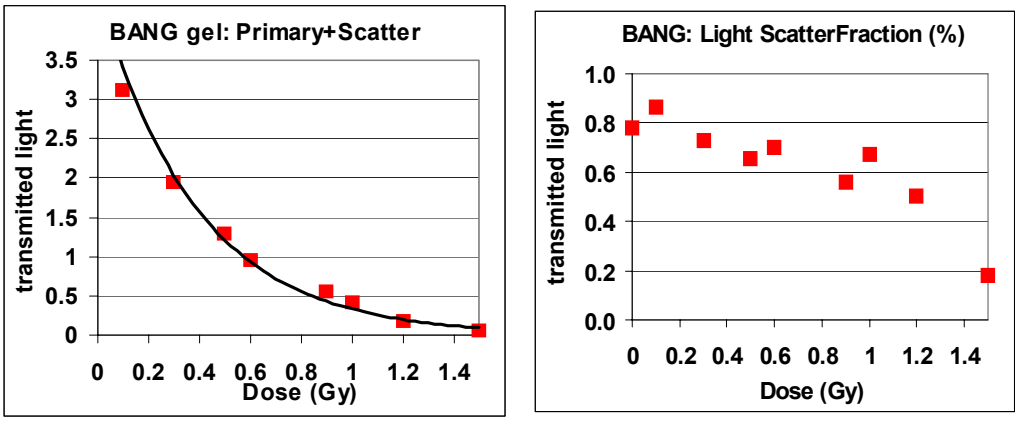

Fig. 4. a) the intensity of transmitted primary and scattered laser light (arbitrary units) through the BANG gel-flask and anti-freeze bath. b) The fraction of laser light scattered in the BANG and anti-freeze bath.

References

1. Gore JC, Ranade M, Maryanski MJ, Schulz RJ, Radiation dose distributions in three dimensions from tomographic optical density scanning of polymer gels: I. Development of an optical scanner. Phys Med Biol 1996 Dec;41(12):2695-704
2. Kelly RG Jordan KJ Batista JJ, Optical CT reconstruction of 3D dose distributions using Ferrous benzoic-xylenol (FBX) gel dosimeter, Med Phys 25, 1741-1750 1998.
3. Oldham M, Siewerdsen JH, Shetty A, Jaffray DA, High resolution gel-dosimetry by optical-CT and MR scanning, In Press, Med Phys 28, (7) 2001
4. MGS Research Inc., P.O. Box 581, Guilford CT-06437
5. Wolodzko JG, Marsden C, Appleby A. CCD imaging for optical tomography of gel radiation dosimeters. Med Phys 1999 Nov;26(11):2508-1

OPTIMIZING THE DOSE RESOLUTION IN POLYMER GEL DOSIMETRY

M. Lepage[1,*], S. Å. J. Bäck[1,2], P. M. Jayasekera[1] and C. Baldock[1,]
[1]Centre for Medical, Health and Environmental Physics
Queensland University of Technology, Brisbane, QLD, Australia
[2]Department of Radiation Physics, Lund University,
Malmö University Hospital, Malmö, Sweden
***Present address: Yale University School of Medicine, Department of Diagnostic Radiology, New Haven, CT, USA**

Introduction

The perception of high levels of uncertainty is a current limitation to the use of polymer gel dosimetry in routine clinical practice. Improvements in every aspect of the dosimetry technique should be achieved in order to approach acceptable level of uncertainties. First, a sound basis for the quantitative comparison of different dosimetry experiments is needed. The R_2-dose sensitivity is often used to compare polymer gel dosimeters evaluated with MRI but this is not a sufficient criteria [1]. Second, optimization of the chemical composition of the dosimeters can be achieved to optimize the quality of a dosimetry experiment [2] and third, improvements in the evaluation of the dosimeters is required [3]. We present the concept of dose resolution which allows a direct comparison between different dosimetry experiments using different gels and different evaluation techniques. Using this concept, we show the role of the chemical composition of polymer gel dosimeters and the importance of optimizing the pulse sequence in a multiple spin-echo (MSE) sequence in an MRI experiment.

Materials and Methods

Polymer gel dosimeters of different chemical compositions were manufactured in an oxygen-free environment. Various monomers (3% w/w) were added to either an aqueous solution of gelatin (5% w/w or agarose 1% w/w) along with another monomer, N,N'-methylene-bis-acrylamide (BIS) (3% w/w). These monomers were acrylamide (AA), acrylic acid (ACA), methacrylic acid (MCA), 1-vinyl-2-pyrrolidinone (VP), 2-hydroxyethyl methacrylate (HEMA) and 2-hydroxyethyl acrylate (HEA). The gels were irradiated up to 50 Gy using γ–rays form ^{60}Co a Gammacell (Atomic Energy Canada Limited). At least two days after irradiation, the gels were imaged with a Siemens Vision (Erlangen, Germany) 1.5T scanner using a customised 32-echoes MSE protocol. The echo spacing (ES) was varied from 12.5 to 50 ms.

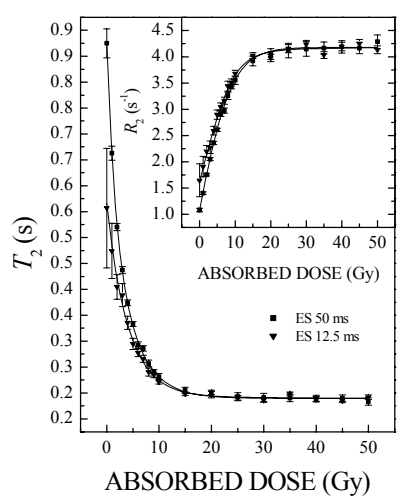

Fig. 1. Typical curves of T_2 (and R_2 in the inset) against absorbed dose for ES set at 12.5 or 50 ms. The polymer gel is composed of AA, BIS and gelatin.

Results and Discussion

Dose resolution: The dose resolution (D_Δ^p) is defined as the minimal difference for which two absorbed dose can be told apart, with a specific level of confidence (p) [1]. For a curve of T_2 against absorbed dose, D_Δ^p is explicitely written as

$$D_\Delta^p = \sqrt{2}k_p \left|\frac{\partial D}{\partial T_2}\right| u(T_2) \qquad (1)$$

where k_p is a coverage factor which enables D_Δ^p to be obtained with the desired p and $u(T_2)$ is an approximation of the experimental standard deviation, taken as the standard deviation around the mean in a region of interest. Eq. 1 outlines that the characteristics of the dosimeter ($|\partial D/\partial T_2|$) and the ability to obtain a low uncertainty in the measurement ($u(T_2)$) both contribute to the value of D_Δ^p. Typical curves for the values of T_2 as a function of the absorbed dose for a gel composed of AA, BIS and gelatin are shown on Fig. 1 for two ES along with $u(T_2)$ shown as error bars. The corresponding curves of R_2 ($R_2 = 1/T_2$) as a function of the absorbed dose are shown in the inset.

Echo spacing: Figure 2 shows $D_{\Delta}^{95\%}$ calculated from the results of Fig. 1 and for additional values of ES. The main result is that a single value of ES does not give an optimal D_{Δ}^{p} over the entire dose range. The higher value of $D_{\Delta}^{95\%}$ for ES = 12.5 ms stems for the higher uncertainty obtained with this ES (see Fig. 1).

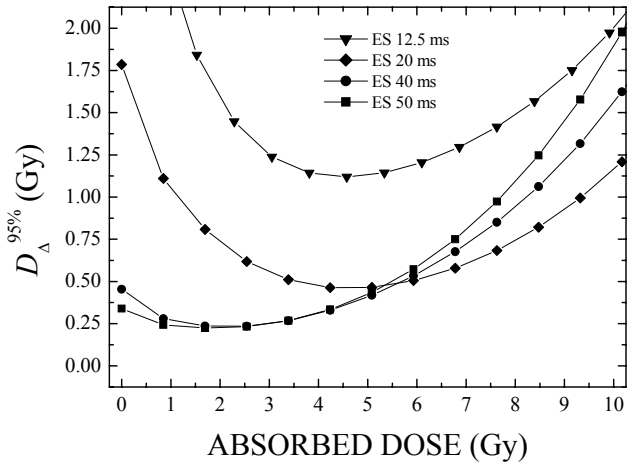

Fig. 2. Dose resolution (p = 0.05) for a gel composed of AA, BIS and gelatin. Note that a single ES does not give an optimal $D_{\Delta}^{95\%}$ over the entire dose range.

Chemical composition: Figure 3 shows $D_{\Delta}^{95\%}$ for different monomers used in the manufacture of the polymer gel dosimeter. In the figure, composite curves obtained from the optimal $D_{\Delta}^{95\%}$ for every ES values used are displayed [4]. It can be seen, for example, that the lowest values of $D_{\Delta}^{95\%}$ are obtained for the MCA-gelatin dosimeter but that for a single ES, the optimal results are obtained only over a narrow range of doses. In general, $D_{\Delta}^{95\%}$ for agarose-based formulations was higher than for their gelatin-based counterpart (not shown). $D_{\Delta}^{95\%}$ for the HEMA dosimeter was higher than 1 Gy over the range of doses presented. By varying the chemical composition of the dosimeter, both the characteristics of the T_2 vs dose curve and the range of T_2 values covered are modified, thus leading to different $D_{\Delta}^{95\%}$ values. Using a model of fast exchange of magnetization between three proton pools [5], parameters were extracted for each polymer gel composition which enable the prediction of the performances of new polymer gel formulations [4].

Conclusions

The concept of dose resolution is useful for the quantitative comparison of different polymer gel dosimetry experiments. In optimizing a polymer gel dosimetry experiment, several aspects must be taken into account. For the specific case when MRI is used for the evaluation of the gels, ES is an important parameter in the scan protocol. Although it was not discussed here, the number of echoes is also important, for obvious reasons. The purpose is to minimize the uncertainty in the determination of the T_2 values covered by the dosimeter used. To this effect, adjusting the chemical composition of new polymer gel dosimeters to match the range of T_2 values that can be determined with a low uncertainty by an MRI scanner is a way to minimize the dose resolution, and hence the overall quality of a polymer gel dosimetry experiment. Considerations of the same type as those made here could provide a useful guideline for the optimization of dosimetry experiments using any type of gel or evaluation technique.

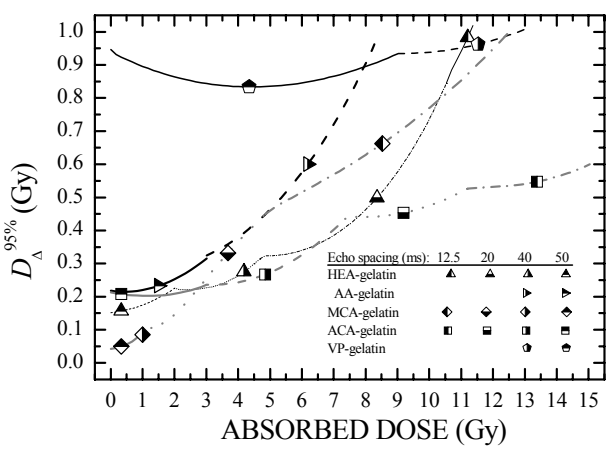

Fig. 3. Dose resolution (p = 0.05) for different gel formulations. A single ES value gives an optimal result only over a narrow range of doses.

Acknowledgements

The contribution of T. Kron, P. J. Murry, D. Porter, L. Rintoul, and A. K. Whittaker at various stages of this work is acknowledged.

References

1. C. Baldock., M. Lepage, S. Å. J. Bäck, P. J. Murry, D. Porter, T. Kron, and C. Baldock, Dose resolution in radiotherapy polymer gel dosimetry: effect of echo spacing in MRI pulse sequence. Phys. Med. Biol. 46, 449, 2001.
2. M. J. Maryanski, C. Audet, and J. C. Gore, Effects of crosslinking and temperature on the dose response of a BANG polymer gel dosimeter, Phys. Med. Biol. 42, 303, 1997.
3. Y. De Deene, C. De Wagter, W. De Neve, and E. Achten, Artefacts in multi-echo T_2 imaging for high-precision gel dosimetry: II. Analysis of B_1-field inhomogeneity, Phys. Med. Biol. 45, 1825, 2000.
4. M. Lepage, , S. Å. J. Bäck, P. M. Jayasekera, and C. Baldock, Dose resolution optimization of polymer gel dosimeters using different monomers. Phys. Med. Biol., accepted for publication.
5. M. Lepage, A. K. Whittaker, L. Rintoul, and C. Baldock, ^{13}C-NMR, ^{1}H-NMR and FT-Raman study of the radiation-induced modifications in radiation dosimetry polymer gels. J. Appl. Polym. Sci. 79, 1572, 2001.

ULTRASOUND – A NEW METHOD FOR EVALUATION OF POLYMER GEL DOSIMETERS

Melissa L. Mather[1], Andrew K. Whittaker[2] and Clive Baldock[1]
[1]Centre for Medical, Health and Environmental Physics
Queensland University of Technology, Brisbane, Queensland Australia
[2]Centre for Magnetic Resonance, The University of Queensland, Australia

Introduction

Radiotherapy treatment plans are becoming increasingly complicated as new technologies and treatment techniques emerge. In response to this, polymer gel dosimeters that can measure absorbed radiation doses in 3D continue to be developed. These dosimeters show great promise and considerable work has gone into their development. For a review of gel dosimetry see Proceedings of DOSGEL '99.

To date, Magnetic Resonance Imaging (MRI) has been used extensively for evaluation of absorbed dose distributions in polymer gel dosimeters. MRI has proven to be a very useful technique as the Nuclear Magnetic Resonance (NMR) relaxation times of polymer gel dosimeters are sensitive to radiation induced chemical changes that occur in the irradiated polymer gel dosimeters [1]. Development of other evaluation techniques has also been undertaken. These include optical tomography techniques based on changes in optical properties [2-4] and x-ray CT techniques based on changes in the linear attenuation coefficient [5,6] of irradiated polymer gel dosimeters.

Despite the considerable amount of research being undertaken in the development of polymer gel dosimeters they are not yet routinely used in the clinical environment. One reason for this may be limitations in the current evaluation techniques. For example, there are a number of technical limitations in the use of MRI in polymer gel dosimetry. These include magnetic field inhomogeneities, temperature inhomogeneities in the dosimeters during scanning and limitations in current pulse sequences [7-9]. Technically simpler and more cost effective systems for evaluation may enable polymer gel dosimeters to become a more viable option in radiotherapy treatment planning.

The present study aims to demonstrate the potential of ultrasound as an evaluation technique for polymer gel dosimeters. Ultrasound is a well-known technique for convenient, non-destructive analysis of materials at relatively low cost. Ultrasound can be successfully applied to characterisation of a wide range of materials [10-12]. In the current work the ultrasonic properties of polymer gel dosimeters exposed to different radiation doses are determined. The usefulness of ultrasound as a technique for evaluation of polymer gel dosimeters is discussed.

Materials and Methods

Polymer Gel Preparation

Polymer gel dosimeters with a formulation of 3% acrylamide, 3% *N,N'* – methylene-bisacrylamide, 5% gelatine and 89% water by mass were prepared in a nitrogen filled glove box. Details of the manufacture process can be found elsewhere [13]. Once prepared the gel was poured into polystyrene spectrophotometer cuvettes and sealed with plastic stoppers. The cuvettes were then placed in specially designed nitrogen filled glass tubes. The tubes were sealed with greased ground glass stoppers to prohibit oxygen from contaminating the samples. Once set, samples were irradiated up to 50 Gy using a Gamma cell 200 Co-60 irradiation facility. Effort was made to ensure all samples were placed in the same position in the Gamma cell during each irradiation. Following irradiation the gels were stored in an air-conditioned environment for four days after which they were removed from the glass tubes. The cuvettes were then placed in a water bath and left for twelve hours to equilibrate to ensure all samples were at the same constant temperature during subsequent ultrasound measurements.

Ultrasound Investigations

A thin-walled, water-filled plastic container was used for ultrasonic measurements. Each cuvette was placed one at a time in the container. The container had a base that held the cuvettes and ensured they were placed in a reproducible position for each measurement. As the acoustic field close to the acoustic source is complicated, the cuvettes were placed approximately 5 cm from the acoustic source, in the far field, where the field is less complicated. The temperature of the water in the container was monitored with a thermocouple throughout the experiment.

Two Panametrics A310S transducers were coupled with commercially available ultrasound transmission gel to opposite sides of the container. One transducer was used as a transmitter and receiver while the other transducer

was used solely as a receiver. The transducers were aligned to produce maximums in the reflected and transmitted signals. Once in place the transducers were not moved. This ensured the coupling of the transducers to the container remained constant for each measurement.

The transmitting transducer was operated at its fundamental frequency (~4 MHz). A short pulse was applied to the transmitting transducer. The signals received by both transducers were displayed on a Tektronics TDS 220 digitising oscilloscope. The signals were digitised and sent to a PC for storage via a GPIB connection. Five acquisitions of each sample were made. Signals were processed and analysed using in house software written in Matlab®. The amplitude of the reflected and transmitted waves was determined as well as the time of flight of the signal through the gel. This information was used to calculate acoustic attenuation in the gel and the speed of propagation of sound through the gel.

Results and Discussion

The inverse of the acoustic speed of propagation of bulk longitudinal waves through the polymer gel dosimeters with absorbed dose is shown in Figure 1. Acoustic speed displays a dependence on absorbed radiation dose and is seen to vary with absorbed dose up to 40 Gy. These results indicate that assessments of received dose with ultrasound will produce a greater dynamic range than using other techniques such as MRI which typically only have a useful dose range up to approximately 20 Gy [14].

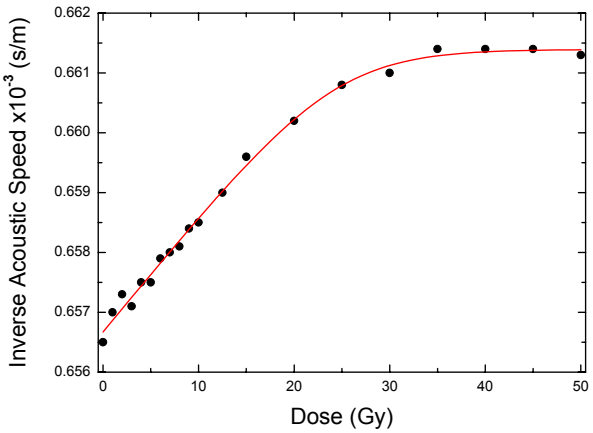

Fig. 1 – Dependence of acoustic speed of propagation on absorbed dose

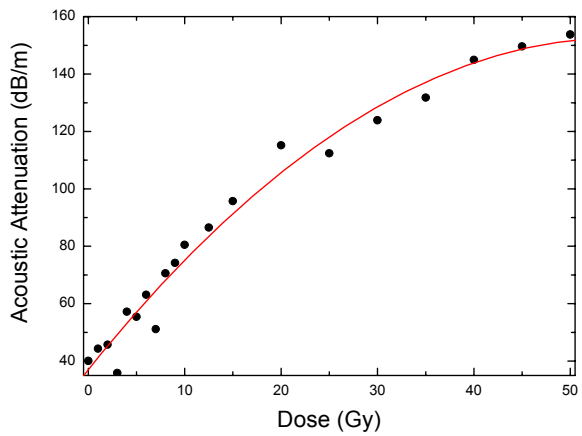

Fig. 2 – Dependence of acoustic attenuation on absorbed dose

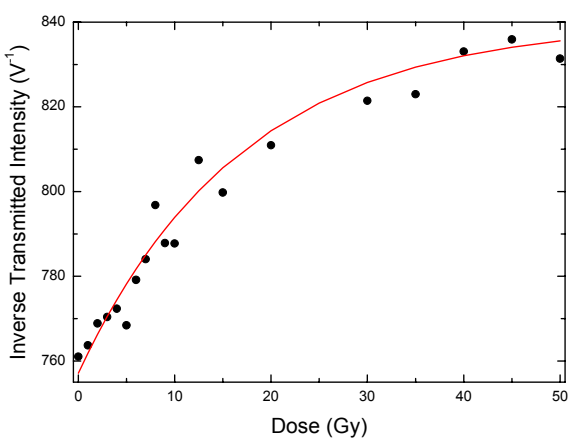

Fig. 3 – Transmitted signal intensity as a function of absorbed dose

The acoustic attenuation in the gels was also measured. Figure 2 displays the dependence of acoustic attenuation on dose. It is clear from this figure that attenuation increases noticeably with increase in radiation dose and continues to change over the full dose range investigated. Acoustic attenuation therefore also appears to have potential as a parameter for determination of absorbed dose.

The intensity of the transmitted signal was recorded for each sample and the results are shown in figure 3. The inverse of the transmitted signal in volts is plotted on the y-axis and the received radiation dose on the x-axis. While this data contains more scatter than results of acoustic speed and attenuation a dependence of transmitted signal intensity with dose can be detected. The observed reduction in the transmitted signal with increase in dose follows from results of acoustic attenuation which indicate as dose increases so too do energy losses from the acoustic wave. The observed reduction in the transmitted signal is therefore expected.

The results from measurement of all three acoustic parameters indicate they are highly absorbed dose dependent. Despite these promising results all figures contain scatter which needs to be reduced if ultrasound is to become a successful technique for assessment of absorbed dose in polymer gel dosimetry. The scatter in these figures can be considered to be due to a combination of uncertainty in determination of the acoustic parameters as well as variation in experimental conditions at the time of measurement for each sample.

Conclusions

Ultrasound shows great potential as a technique for evaluation of polymer gel dosimeters. The acoustic speed of propagation, attenuation coefficient and transmitted intensity were measured as a function of absorbed dose. All parameters display variation with absorbed dose that continued beyond absorbed doses of 15 Gy.

The results from these preliminary experiments indicate ultrasound is a worthwhile technique to pursue for evaluation of polymer gels. Ultrasound techniques have a number of advantages over currently used techniques such as their relatively low cost in implementation and portability. The current ultrasound investigations could be extended further to develop an instrument capable of imaging dose distributions with ultrasound.

References

1. Maryanski, M.J., et al., Magnetic resonance imaging of radiation dose distributions using a polymer-gel dosimeter. *Phys. Med. Biol*, 1994. **39**(9): p. 1437-55.
2. Gore, J.C., et al., Radiation dose distributions in three dimensions from tomographic optical density scanning of polymer gels. I. Development of an optical scanner. *Phys. Med. Biol*, 1996. **41**(12): p. 2695-704.
3. Maryanski, M.J., Y.Z. Zastavker, and J.C. Gore, Radiation dose distributions in three dimensions from tomographic optical density scanning of polymer gels. II. Optical properties of the BANG polymer gel. *Phys. Med. Biol*, 1996. **41**(12): p. 2705-17.
4. Oldham, M., et al., High resolution gel-dosimetry by optical-CT and MR scanning. *Med. Phys*, 2001. **28**(7): p. 1436-45.
5. Hilts, M., et al., Polymer gel dosimetry using X-ray computed tomography: a feasibility study. *Phys. Med. Biol*, 2000. **45**(9): p. 2559-71.
6. Trapp, J.V., et al., An experimental study of the dose response of polymer gel dosimeters imaged with x-ray computed tomography. *Phys. Med. Biol*, 2001. **46**(11): p. 2939-2951
7. De Deene, Y., et al., Artefacts in multi-echo T2 imaging for high-precision gel dosimetry: I. Analysis and compensation of eddy currents. *Phys. Med. Biol*, 2000. **45**(7): p. 1807-23.
8. De Deene, Y., et al., Artefacts in multi-echo T-2 imaging for high-precision gel dosimetry: II. Analysis of B-1-field inhomogeneity. *Phys. Med. Biol*, 2000. **45**(7): p. 1825-1839.
9. Baldock, C., et al., Dose resolution in radiotherapy polymer gel dosimetry: effect of echo spacing in MRI pulse sequence (vol 46, pg 449, 2001). *Phys. Med. Biol*, 2001. **46**(5): p. 1591.
10. Maffezzoli, A., et al., Cure monitoring of epoxy matrices for composites by ultrasonic wave propagation. *J. Appl. Poly. Sci*, 1999. **73**(10): p. 1969-1977.
11. Luprano, V.A.M., et al., Non-destructive characterization of hydrogels. *J. Mat. Sci. Mat. Med*, 1997. **8**(3): p. 175-178.
12. Krstelj, V., Ultrasonic testing of polymer materials. *Insight Non Destructive Testing and Condition Monitoring,* 1996. **38**(9): p. 640-4.
13. Baldock, C., et al., Experimental procedure for the manufacture and calibration of polyacrylamide gel (pag) for magnetic resonance imaging (mri) radiation dosimetry. *Phys. Med. Biol*, 1998. **43**(3): p. 695-702.
14. Lepage, M., et al., The relationship between radiation-induced chemical processes and transverse relaxation times in polymer gel dosimeters. *Phys. Med. Biol*, 2001. **46**(4): p. 1061-1074.

THEORETICAL CONSIDERATIONS OF SCAN PARAMETERS APPROPRIATE FOR CT IMAGING OF POLYMER GEL DOSIMETERS

Jamie Trapp, Greg Michael, and Clive Baldock
Centre for Medical, Health and Environmental Physics,
Queensland University of Technology, Brisbane, Australia

Introduction

A feasibility study has shown that x-ray computed tomography (CT) is a promising method for evaluation of polymer gel dosimeters due to changes in linear attenuation coefficient with increasing dose [1]. A subsequent study showed that the sensitivity of the dosimeter can be varied by changing the concentrations of the chemicals used, and that the change of linear attenuation coefficient is primarily due to a change in physical density [2].

In this paper the authors propose theoretical operating parameters for CT imaging of polymer gel dosimeters by examining spatial resolution and contrast resolution.

Dosimeter Spatial Resolution

A CT image is a map of linear attenuation coefficients in a slice through the object being imaged. As stated in the introduction, the primary cause for the change in linear attenuation coefficient in polymer gel dosimeters is believed to be an increase in physical density of the gel, which in turn is due to a decrease in volume. This poses an interesting problem for polymer gel dosimetry, i.e. as the signal is increased (and presumably dose resolution is improved), spatial distortions due to volume changes occur.

In the Hounsfield scale the CT number *(H)* in the gel dosimeter will be:

$$H = 1000\frac{\mu_g - \mu_w}{\mu_w} \qquad (1)$$

where μ_g and μ_w are the linear attenuation coefficients for gel and water respectively. The change in H (the signal) will be:

$$\Delta H = \frac{1000}{\mu_w}\left(\mu_1 - \mu_0\right) \qquad (2)$$

where μ_0 and μ_1 represent the linear attenuation coefficients of the gel before and after irradiation respectively. The linear attenuation coefficient for each constituent is:

$$\mu = N_e \sigma_e \rho \qquad (3)$$

where N_e is the number of electrons per mass unit, σ_e is the cross sectional area per electron and ρ is the physical density. If it is assumed that N_e and σ_e remains constant with irradiation, then equation 2 becomes:

$$\Delta H = \left(H_0 + 1000\right)\left(\frac{\rho_1}{\rho_0} - 1\right). \qquad (4)$$

In the application of gel dosimetry to radiotherapy, many authors have striven to meet the 2% dose uncertainty and 0.2 cm spatial uncertainty requirements of ICRU42 [3]. To ensure that these requirements are not exceeded, the density change in a polymer gel dosimeter must be within some upper limit depending upon the irradiation field.

For a simple example, consider a uniformly irradiated sphere with a radius of 5 cm and assume that the post-irradiation shrinkage is towards the centre of the sphere. No point can move by more than 0.2 cm without exceeding the uncertainty requirements of ICRU42. However, if the CT scanner itself has a spatial resolution of 0.1 cm the movement in the gel cannot exceed 0.1 cm or addition of the uncertainties will exceed 0.2 cm. If we assume an initial density of 1.021 g.cm^{-3} [2] the maximum change in density allowable is:

$$\Delta\rho = \frac{m}{\frac{4}{3}\pi 5^3 - \frac{4}{3}\pi 4.9^3} = 0.065 g cm^{-3}. \qquad (5)$$

Using equation 4 this equates a maximum range of CT numbers of 63 H.

The above calculation illustrates that in order to meet spatial resolution requirements there is an upper limit to the obtainable signal in a polymer gel dosimeter and is regardless of imaging modality.

CT Scanner Spatial Resolution Considerations

Spatial resolution in a scanner can vary due to many factors including source and detector geometry, reconstruction algorithms and display parameters.

Geometric factors which affect spatial resolution include focal spot size, detector width, sampling interval and source to object distance. Small focal spot size and small aperture width increases spatial resolution [4]. It is recommended that sampling intervals are approximately equal to the detector width, as sampling at intervals much smaller or much larger can cause widening or even distortions of the point spread function of a scanner [4].

Edge enhancement algorithms can cause overshoot in CT numbers and are not recommended for quantitative CT [5], however, in very low contrast situations such as CT of polymer gel dosimeters the overshoot may be much less than 1 H in magnitude and therefore insignificant. Comparison of the line spread function at low contrast of reconstruction algorithms available on the scanner with all other parameters kept constant should reveal the most appropriate mode for polymer gel dosimetry.

To optimise spatial resolution the pixel size corresponding to the best spatial resolution should be chosen. It has been shown that there is a cubic dependence of statistical noise on the pixel width for noise per pixel, and a dependence to the first power for noise per unit area [6], however this noise can be reduced and will be discussed in the next section.

Recommended low contrast resolution tests such as the contrast-detail plot rely on perception by the human observer [5, 7, 8]. It is unlikely that dose information will be extracted from polymer gel dosimeters 'by eye' in the manner a radiologist would normally examine a CT image. Therefore, for consistency and accuracy, to assess the scanner for use in gel dosimetry applications the method of display should be the same as that used to assess the dosimeter. For example, if dose contours are to be used in the assessment of the dosimeter, then this method should be used to examine spatial resolution. Figure 1 is an example of an image of a low dose phantom (Catphan, The Phantom Laboratory, Salem USA) imaged and displayed as contours.

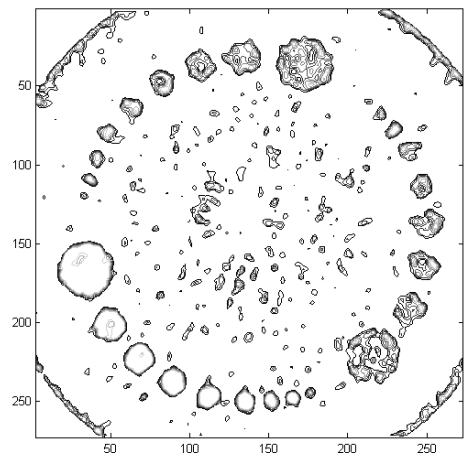

Fig 1 - Catphan® module CTP500 (The Phantom Laboratory) imaged on a Siemens Somaton Plus 4 scanner at 140 kV 360 mAs. The image has been filtered post-acquisition with a 5 × 5 wiener filter using the image processing toolbox in Matlab (The Mathworks Inc). Assessment of low contrast phantom by use of contours.

Contrast Resolution and Noise

As explained above, in order to meet spatial resolution requirements, CT evaluation of polymer gel dosimeters is by necessity a low contrast imaging modality. It is well known that the limiting factor in low contrast imaging is noise [7].

The noise in a CT image is comprised of statistical noise due to photon counting and inherent system noise due to the reconstruction algorithm used, electronic noise and CT number quantization [5, 9]. Due to the relatively low dose of a CT scanner compared to the treatment dose, increasing the total photon count of the scanner can be used to reduce statistical noise without the measurement process adversely affecting the values being measured [9]. Figure 2 shows that 64 images averaged

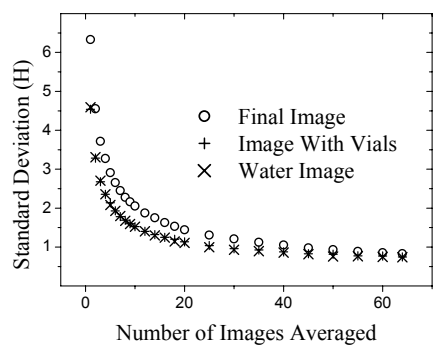

Fig 2 – The standard deviation of pixel values in the centre of a 25 cm diameter phantom after averaging several images together. Scanning was performed on a Picker PQ5000 at 140 kV and each scan was 600 mAs. The phantom used was designed to subtract a water only image from an image of polymer gel dosimeter calibration vials for removal of imaging artifacts [2].

together greatly reduces the noise. A previous study has shown that as the number of averaged images increases the noise remaining will tend asymptotically to approximately 0.6 H [2].

Electronic noise in CT scanners is due to random variations in detector signal which tend to remain constant in magnitude and is practically independent of operating parameters [5]. This type of noise is due to factors such as amplifier noise, noise from junction capacitances, noise from the leakage current of the detector, and analogue to digital conversion [10]. Little can be done about electronic noise in a clinical situation except to ensure that the scanner is operating well and maintained correctly.

Many artifacts such as beam hardening, ring artifacts etc can be reduced by using a phantom which allows subtraction of these artifacts by taking an image of the dosimeter and a separate water image. Subtraction of one image from the other effectively removes most major artifacts as has been shown previously [2]. It can be seen in Figure 2 that the subtraction results in an increase of statistical noise by a factor of $\sqrt{2}$, however if many images are averaged this added statistical component of noise becomes less significant.

Conclusion

An inherent challenge in polymer gel dosimetry (regardless of imaging modality) will be to find the balance between increasing signal-to-noise ratio (hence decreasing dose uncertainty) without exceeding the 0.2 cm spatial uncertainty of ICRU42. This necessarily implies that extraction of dose distribution information from polymer gel dosimeters will be a problem of low contrast, high spatial resolution imaging. As such, one of the most important areas of improvement in this field will be the reduction of image noise.

It has been shown that noise in CT images can be reduced significantly, however the non-statistical noise of CT will become the limiting factor for this imaging mode. Post-acquisition image processing will be required if acceptable uncertainty levels are to be reached.

References

1. Hilts, H., et al., *Polymer Gel Dosimetry Using X-ray Computed Tomography: A Feasibility Study.* Phys. Med. Biol, 2000. **54**: p. 2559-2571.
2. Trapp, J.V., et al., *An experimental study of the dose response of polymer gel dosimeters imaged with x-ray computed tomography.* Phys. Med. Biol., 2001. **46**(11): p. 2939-2951.
3. ICRU, *ICRU Report No 42: Use of Computers in External Beam Radiotherapy Procedures with High-Energy Photons and Electrons*. 1987, ICRU Publications: Betesda, MD.
4. Blumenfeld, S.M. and G. Glover, *Radiology of the skull and brain: Chapter 112 - Spatial resolution in computed tomography*, in *Radiology of the skull and brain*, T.H. Newton and D.G. Potts, Editors. 1981, The C.V. Mosby Company: St Louis, USA. p. 3918-3940.
5. AAPM, *AAPM Report No 39. Specification and acceptance testing of computed tomography scanners*. 1993, American Association of Physicists in Medicine: New York.
6. Goodenough, D.J., *Chapter 8 - Tomographic Imaging*, in *Handbook of Medical Imaging*, J. Beutel, H.L. Kundel, and R.L. Van Metter, Editors. 2000, SPIE Press: Bellingham, USA. p. 511-554.
7. Cohen, G. and F.A. DiBianca, *The Use of Contrast - Detail - Dose Evaluation of Image Quality in a Computed Tomographic Scanner.* J. Comp. Asst. Tomo., 1979. **3**(2): p. 189-195.
8. HPA, *Measurement of the Performance Characteristics of Diagnostic X-Ray Systems Used in Medicine: Part III The Physical Specification of Computed Tomography X-Ray Scanners: Measurement and Use of the Associated Performance Parameters*. 1981, The Hospital Physicists Association: London, UK.
9. Faulkner, K. and B.M. Moores, *Noise and contrast detection in computed tomography images.* Phys. Med. Biol., 1984. **29**(4): p. 329-339.
10. Miyai, H., et al., *Response of Silicon Detector for High Energy X-Ray Computed Tomography.* IEEE Transactions on Nuclear Science, 1994. **41**(4): p. 999-1003.

OPTICAL CT SCANNING: FROM 2D TO 3D WHILE MEETING THE RTAP CRITERIA

Mark Oldham, Jeffrey Siewerdsen, David Jaffray
William Beaumont Hospital, Royal Oak, Michigan, USA

Introduction

In a previous paper [1] we reported a prototype optical-CT gel-dosimetry scanning system constructed at William Beaumont Hospital based on a first-generation model [2,3]. 2D images were obtained through selected planes of a gel-dosimeter, designed and constructed in collaboration with MGS Research, for use in a radiosurgery head-phantom verification system. The aim of the work was to evaluate, with the resources available in our institution, the performance of both optical-CT scanning and conventional MR scanning with regards to high resolution gel-dosimetry. Comparisons were made of image-noise, sensitivity, and accuracy of calibration. The key underlying concept for the comparison is that imaging parameters were selected to meet as closely as possible an ideal Resolution-Time-Accuracy-Precision (RTAP) criteria. The RTAP criteria was defined as the minimum required for dosimetric verification of a radiosurgery delivery, namely spatial resolution <1mm^3, imaging time <1hour, accuracy within 3% and precision per pixel within 1%.

Although gel dosimetry is inherently 3D, a limitation in the preliminary work in [1] was that the scanner was essentially of 2D design. Although scans at different planes through the flasks were possible, manual intervention was required to physically alter the mounting of the flask such that the scanning plane coincided with the desired imaging plane in the flask. Recently the scanner has been re-designed and re-built to include the functionality for convenient 3D scanning. In this presentation we review details of the new scanner, and the issues associated with going from 2D to 3D.

Materials and Methods

The new scanner design is illustrated in figures a) and b). The wide view (figure a) illustrates the X95(NEWPORT CORPORATION, 1791 Deere Avenue, Irvine, CA 92606) scaffolding rail used as a secure supporting structure for the vertical mounted translation and rotation assembly which provides the third scanning dimension. The X95 rails are cylindrical aluminium extrusions with four longitudinal re-inforcing ribs. The 10mm thick ribs provide four symmetrical dovetail clamping surfaces, two of which were used for attachment of the rotation-translation assembly. Half-inch steel plates were used to couple the rail ends directly to the optical bench. The entire structure is stable and robust with negligible response to vibrations and sag associated to moving the gel flask in the vertical dimension. The laser light was monitored by two large area photo-diodes (reference and field)(UDT Sensers Inc, 12525 Chadron Av, Hawthorne CA 90250) each with a stationary mount to the optical bench. The photocurrents were fed to a pre-amplifying electrometer (from Welhofer water tank scanning system) producing 0-10V output corresponding to maximum signal range. This voltage was then fed as input to a NI-DAQ PC-LPM-16 (National Instruments Coorporation, 6504 Bridge Point Parkway, Austin, TX 78730) ADC board mounted into the 16bit expansion slot on standard PC.

Laser light from a stationary HeNe green laser (536nm, 3mW) is reflected to transect a water-bath containing the gel-dosimeter to be scanned at near normal incidence (figure b). A slight offset angle is introduced to discard reflected rays. The water-bath contained optically matched fluid to minimise interface refractions. The laser beam is translated across the length of the gel-flask by means of a linear translation stage which moves mirrors on either side of the water-bath. Both mirrors are mounted on a 1/2inch aluminium bar which is attached to the translation stage. The laser light is reflected from the downstream mirror onto a stationary, collimated, integrating optical lab-sphere assembly. Careful alignment is required to ensure the laser hits centrally in the lab-sphere at all translation positions.

Results and Discussion

The new scanner design enables either spiral or sequential slice 3D optical scanning. In sequential mode individual slices are scanned by translating the laser line across the flask and then incrementally rotating the gel-flask about the central axis. Typically a 100 such projections are acquired at 1.8 degree intervals. Each slice is reconstructed using

the MATLAB Iradon transform. After each slice has been acquired the whole flask is incrementally shifted vertically in preparation for acquisition of the net slice. A typical increment would be 1mm. In spiral mode the gel-flask is incremented both rotationally and vertically after each projection. In this mode the vertical increment is considerably less (e.g. 1/180 = .0055mm per projection).

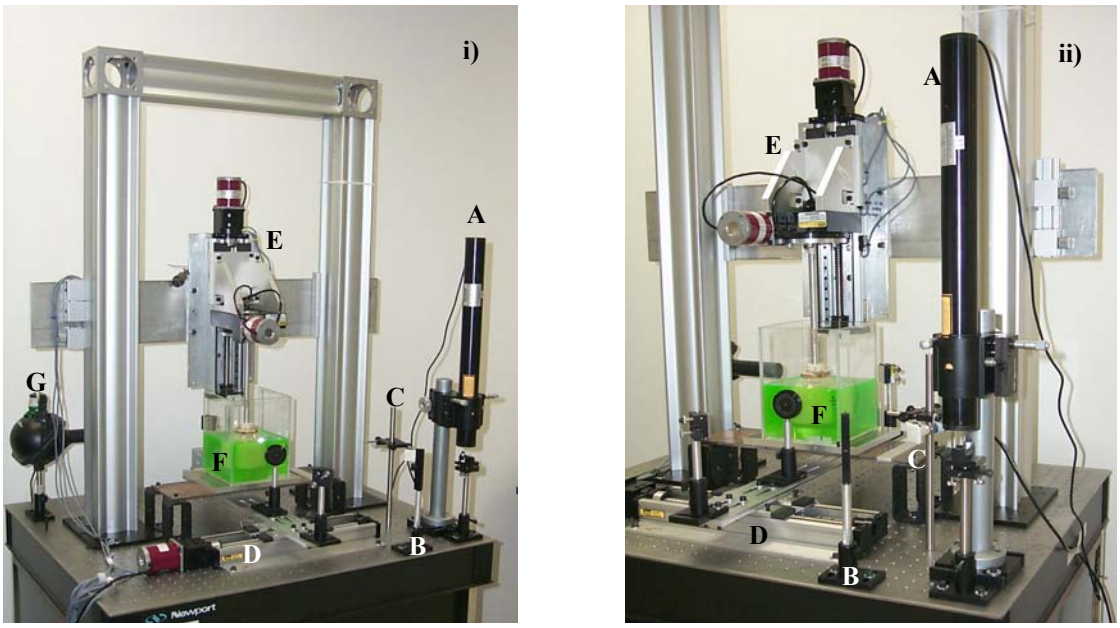

Fig. 1. Two views of the optical-CT scanner. i) expanded view illustrating the X95 support structure, and ii) close-in view. The labels correspond to A=HeNe laser, B=beam-splitter, C=reference photodiode, D=linear translation stage, E=vertically mounted rotation-translation stages (the gel flask is shown suspended in the optical bath on an Aluminum rod hanging vertically down from the rotation stage), F=gel-flask in optically-matched water bath, G=field photodiode.

Conclusions

A laser based optical CT scanner is presented which has the capability for convenient 3D acquisition. Our aim is to approach a long-standing goal of radiation dosimetry by achieving a dosimetry technique that approaches the RTAP criteria. The benefits of the present system include high spatial resolution and low noise. The most difficult aspect of RTAP to achieve with the present system is that of scanning a sizeable 3D volume (e.g. 80x80x80mm^3) within the one-hour time restriction. This stringent requirement is not feasible with the current scanning paradigm, and will require a shift to broader beam scanning approaches as has been illustrated by Wolodzko et al [4].

References

1. M Oldham, JH Siewerdsen, A Shetty, and DA. Jaffray, High resolution gel-dosimetry by optical-CT and MR scanning Medical Physics, July Volume 28, Issue 7 pp. 1436-1445, 2001
2. Gore JC, Ranade M, Maryanski MJ, Schulz RJ, Radiation dose distributions in three dimensions from tomographic optical density scanning of polymer gels: I. Development of an optical scanner. Phys Med Biol Dec;41(12):2695-704 1996
3. Kelly RG Jordan KJ Batista JJ, Optical CT reconstruction of 3D dose distributions using Ferrous benzoic-xylenol (FBX) gel dosimeter, Med Phys 25, 1741-1750 1998.
4. Wolodzko JG, Marsden C, Appleby A., CCD imaging for optical tomography of gel radiation dosimeters. Med Phys Nov;26(11):2508-13, 1999

DOSIMETER GELS AND ^{129}Xe NMR

James M. Joers, Peter M. Fong, John C. Gore
Yale University School of Medicine, New Haven, CT, USA

Introduction

Due to the large polarisability of the xenon atom, the chemical shift of xenon is sensitive to the environment in which it resides, giving rise to a chemical shift range over 200 ppm. This makes it a suitable probe for morphology and surface studies of polymeric and porous materials, including zeolites, polymer blends and biopolymers.

In order for xenon to be a viable probe, it must be able to diffuse into the sample of interest. Additionally, if a multi-component system is to be probed, it is also requisite that the ^{129}Xe chemical shift in each of the pure components be different. If exchange between the two solid domains is faster than that of the NMR time scale, a single resonance (apart from the free gas peak) will be observed, with the chemical shift of the single peak described [1] as:

$$\sigma_{avg} = ((1-w_b)\rho_a\sigma_a + w_b\rho_b\sigma_b)/((1-w_b)\rho_a + w_b\rho_b) \qquad (1)$$

where σ_a and σ_b are the ^{129}Xe chemical shifts of the two components, a and b, in the blend, ρ_a and ρ_b are the relative solubilities of ^{129}Xe in each of the two components in the blend. w_b is the mass fraction of component b in the blend.

If the domains become large enough so that xenon is no longer in rapid exchange during the NMR time scale, then two distinct ^{129}Xe NMR resonances will be observed. In the case of two miscible solids, one xenon resonance will be observed.

Polymer dosimeter gels have been developed to monitor radiation dose levels and to investigate local effects of radiation. These gels consist of a gelatin matrix and differing cocktails (acrylamide/bis-acrylamide or agarose/bis-acrylamide, for example) which form polymerised microparticles upon exposure to radiation. The degree of end linking, and hence, the size and number of the particles, is an indication of the absorbed radiation dose [3]. Traditionally, proton T_2 measurements [2,3,4] have been used as a probe of absorbed dose.

The work described here uses xenon NMR as a probe for dosimeter gels. While the use of conventional xenon NMR precludes the ability to image local effects of radiation, it allows us to investigate the microstructure of the polymer network as the degree of polymerisation changes. It was recently demonstrated that the degree of crosslinking in a polymeric dendrimer could be monitored by the chemical shift in Xe NMR and free volume changes due to polymerisation can be calculated if the polymerising reaction is well-understood [5].

Methods

6% MAGIC (*M*ethacrylic and *A*scorbic acid in *G*elatin *I*nitiated by *C*opper) dosimeter gels recently developed in our lab were prepared and irradiated (^{137}Cs source) to different doses (0, 10, 20, 30, 40 and 50 Gy) and placed in a vial which was subsequently pressurised to 170 psi with natural abundance xenon. Gels were held at pressure for 30 minutes to allow the gas to diffuse into the gel matrix before the vials were sealed.

NMR measurements were made on a Bruker Avance system at 4.7T at room temperature. The pulsed RF frequency was centered between the free xenon peak and the xenon in the gel matrix. A repetition rate of 15 seconds was used, and 256 scans were obtained using a sweep width of 20 kHz.

Results and Discussion

Pure components (gelatin and poly(methacrylic acid), Aldrich (Milwaukee, WI)) of the dosimeter were placed in a sample chamber and pressurised with Xenon. A ^{129}Xe NMR spectrum (figure 1) of the two pure components of the dosimeter acquired at 4.7T reveals three peaks: one associated with the free xenon gas (referenced to 0 ppm), one associated with Xenon in the gelatin matrix (188 ppm) and a third peak from xenon in the poly(methacrylic acid) phase (195 ppm). A ^{129}Xe spectrum of a prepared, but non-irradiated gel revealed two peaks: that of the free xenon gas, and one for the dosimeter cocktail (188ppm).

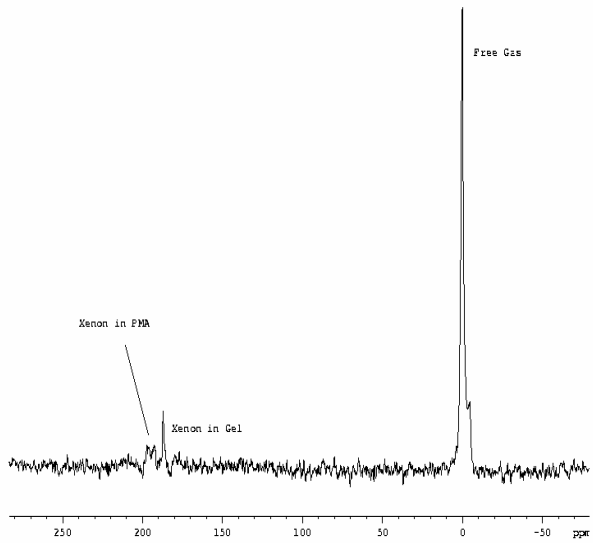

Figure 1. ^{129}Xe spectrum of the two pure components, placed atop each other in the pressurised sample chamber.

Preliminary results we have obtained indicate that the chemical shift of the xenon residing in the dosimeter cocktail is sensitive to the radiation dose applied. The effect is small but readily measurable in the 6% gels. Figure 2 shows the linear relationship between absorbed dose and the xenon chemical shift for various levels of radiation exposure .

Similar experiments are being carried out with 9% monomer gels at 11.74T. The higher density of the polymers is expected to achieve higher signal to noise. While it appears that xenon NMR may be used as a novel dosimeter for this particular system, the main purpose of this work is to probe size and characteristics of the solid pools of the dosimeter.

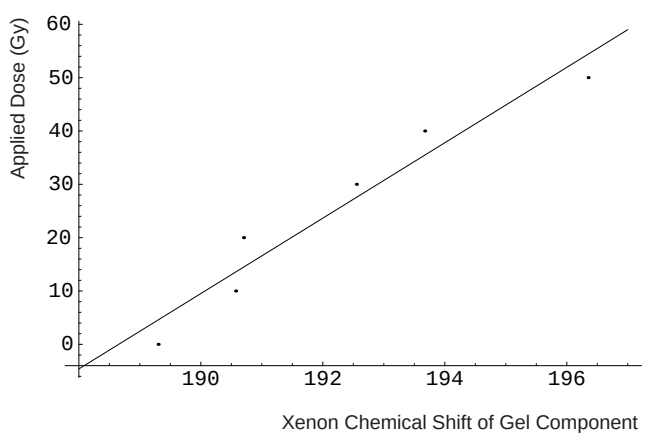

Figure 2. Plot of applied dose versus the xenon chemical shift of the xenon in the gel cocktail.

References

1. J.H. Walton, J.B. Miller, C.M. Roland 129 Xe as a Probe for Polymer Blends *J Polym Sci Pol Phys* **30**: (6) 527-532 (1992).
2. M.J. Maryanski, J.C. Gore, R.P.Kennan, R.J.Schultz *Magnetic Resonance Imaging*,**11**, 253-258 (1993).
3. M.J.Maryanski, R.J.Schultz, G.S.Ibbot, J.C. Gatenby, J.Xie, D.Horton and J.C.Gore *Phys Med Biol.*,**39**, 1437-1455 (1994).
4. M.J.Maryanski, G.S.Ibbot, P.Eastman, R.J. Schultz and J.C Gore *Med Phys.*,**23**,(5), 699-705 (1996).
5. D.R. Morgan and E.O. Stejskal *Macromolecules*,**32**, 1897-1903 (1999).

6a. P.M. Fong, D.C. Keil, M.D. Does, J.C. Gore *Physics in Medicine and Biology* ,**46**, (12), 3105 - 3113 (2001).

6b. P.M. Fong, D.C. Keil, J.C. Gore Radiation Dosimetry using MRI of Normoxic Polymer Gels, poster 901 presented at the International Society of Magnetic Resonance in Medicine Conference, Glasgow, Scotland, UK 2001.

A STUDY OF REPRODUCIBILITY AND POSSIBLE SOURCES OF ERROR IN GEL DOSIMETRY

A.R Farajollahi* and D.E Bonnett**
***Tabriz University of Medical Sciences, Iran**
****Department of Medical Physics, Kent Oncology Centre**
Maidstone Hospital, Kent, UK

Introduction

Since the initial work on polymer gel dosimetry in 1994 (Maryanski et al) there has been increasing interest in application of the gel in radiotherapy. Although the main properties of the polymer gel have been the subject of several studies, there are still some questions that remain to be answered, particularly relating to the measurement of absolute absorbed dose. The aim of this paper is to address some of the practical aspects of the polymer gel dosimeter including reproducibility, possible sources of error and gel calibration particularly as they relate to absolute dosimetry. The areas considered include reproducibility of relaxation time measurement, effects of RF inhomogeneity, sensitivity to positioning lights, effects of multiple irradiations and calibration methods. All of which may effect the measurement of absorbed dose and account for differences between delivered and measured dose.

Methods and Materials

The gels were manufactured in a nitrogen-filled glove box using a method that has been reported in the literature (Farajollahi, et al 1999). The reproducibility of relaxation time measurements was investigated by measuring the performance of MRI scanner in order to determine how constant the scanner performance was from one measurement to another and to identify any variations that may be caused by possible inhomogenities in the gel. The reproducibility of R_2 was assessed by repeatedly scanning both an irradiated gel in a rectangular phantom (20 x 12 x4.8 cm) and 1 L of the un-irradiated gel in a similar phantom. The irradiated gel was divided into 6 areas and irradiated from opposing sides to give uniform doses of 2,5, 8, 10 and 15 Gy. The sixth area was used for a background measurement. The irradiated samples were scanned six times and the non-irradiated gel three times. The effect of any RF inhomogeniety was assessed by imaging four irradiated gel vials inside and outside of a 2.5-liter gel phantom of 15 cm diameter and by measuring 9 unirradiated vials at different positions within the head coil. The possible effects of field defining lights, multiple exposures and the method of gel calibration on absolute measurement of dose were also determined. To assess the sensitivity of the gel to short exposures to positioning lights, five irradiated gel vials and an un-irradiated gel phantom were exposed to the Linac field defining light for a maximum of 10 min. It was also possible that the gel response may be altered by the number of consecutive irradiations i.e. successively sensitized. Therefore a gel phantom of 3-litre capacity was irradiated with two radiation fields (3 x 3cm). One was given an absorbed dose of 6 Gy to the isocentre but the other the 6 Gy was given in 4 fractions of 1.5 Gy with five minutes delay between them. This measurement was also repeated using 3 glass vials giving 6 Gy in one, two, and four fractions. To verify any differences between the methods of calibration a comparison was made between the calibration curves obtained by using multiple irradiations in a single large container and several small glass vials irradiated to different doses. In all the above investigations the gel was imaged at room temperature.

Results

Dose (Gy)	Mean R_2 values (s^{-1})
0	0.94 ± 0.03
2	1.21 ± 0.05
5	1.72 ± 0.04
8	2.19 ± 0.05
10	2.50 ± 0.04
15	2.97 ± 0.09

Table 1. Reproducibility of R_2 measurements (uncertainties 1 SD)

Location	R_2 values (s^{-1})
Top left	1.14 ± 0.02
Top right	1.13 ± 0.02
Middle left	1.13 ±0.02
Middle right	1.14 ± 0.02
Bottom right	1.16 ± 0.01
Mean	1.14 ± 0.01

Table 2. R_2 values in an un-irradiated gel (uncertainties 1 SD)

The results for the reproducibility studies are given in tables 1 and 2. It was found that the R_2 values measured in the irradiated gel are reproducible to within a maximum ± 4 % of each mean value. R_2 values in the un-irradiated gel were found to be uniform throughout the phantom with a mean R_2 value of 1.14 s^{-1} with a SD of ± 0.01.

Dose (Gy)	R_2 measured in the gel phantom	R_2 measured in a polystyrene box
4	2.43 ± 0.03	2.48 ± 0.1
6	2.83 ± 0.01	2.83 ± 0.1
8	3.37 ± 0.06	3.36 ± 0.16
10	3.54 ± 0.1	3.57 ± 0.08

Table 3. R_2 values measured inside a gel phantom compared with those measured in polystyrene

The irradiated vials inside and outside of the gel phantom (Table 3) show no evidence of any effects due to inhomogeneity in the RF. The nine R_2 values measured at different positions in the polystyrene box showed no significant difference with a mean of 1.20 s^{-1} and SD of± 0.02.

The R_2 values measured in the area exposed to light was 1.59 ± 0.02 s^{-1} which compared with 1.60± 0.03 s^{-1} in the shielded area. The irradiated vials also showed no significant difference when exposed to light for periods of up to 10 minutes. From the results it is clear that the gel is not affected by short exposures to the beam alignment lights.

	No. of Exposures		
	1	2	4
Vials	3.66 ± 0.02	3.74± 0.03	3.71± 0.02
Phantoms	3.37± 0.08		3.43 ± 0.09

Table 4. Variation in gel response with multiple exposures.

Table 4 shows that there was no significant difference in gel response with multiple exposures compared with that for a single exposure ($P<0.05$).

Figure 1 shows the calibration curves that obtained using phantom and small glass vials. The gel calibration using a large phantom gave a different slope (0.33 ± 0.003 s^{-1} Gy^{-1}) to that of the vials 0.24 ± 0.01 s^{-1} Gy^{-1}.

Conclusions

Of the variables studied which included reproducibility of relaxation time measurement, effects of RF inhomogeneity, sensitivity to positioning lights, effects of multiple irradiations and calibration methods it was found that only the calibration method would have any significant effect on dose measurement. It is concluded that a calibration curve using small vials should not be used to calibrate a larger phantom if a measurement of absolute dose is required. The reasons for this require further investigation but could include thermal history and uniformity of temperature within the lager phantom.

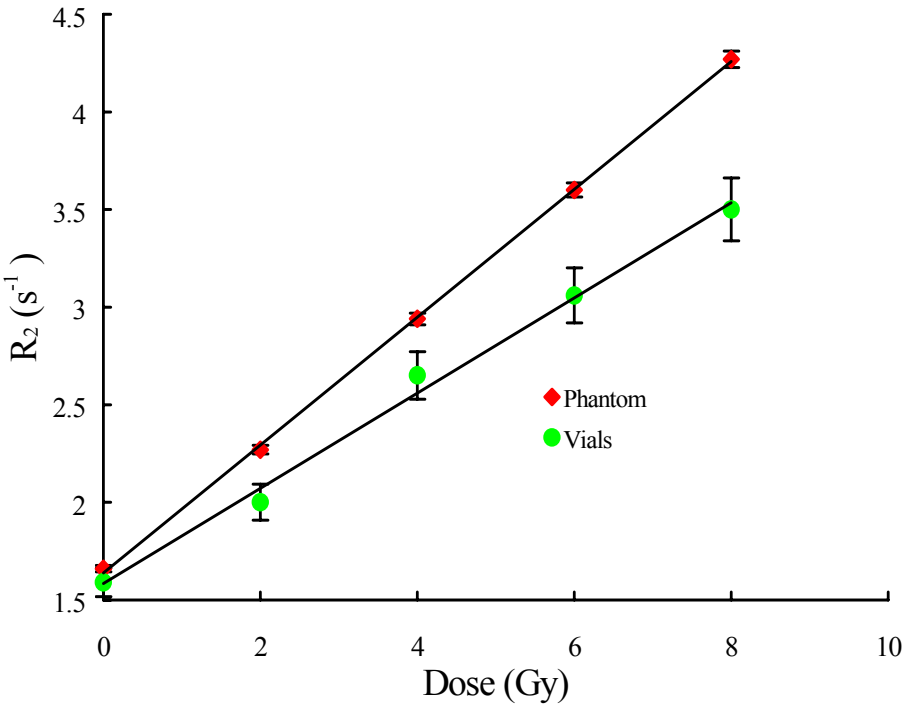

Figure 1. Comparison of the different method of calibration

References

A R Farajollahi, D E Bonnett, A J Ratcliffe, R J Aukett and J A Mills, Br J Radiol, 72,1085-1092, 1999
M J Maryanski, et al., Phys. Med. Biol. 39,1437-1455, 1994

3D MRI DOISMETRY BASED ON IMAGE INTENSITY

S. Akhlaghpour, M.H. Zahmatkash, H. Pourbeigi
Novin Medical Radiation Institute, Tehran, Iran

Introduction

Three-dimensional dosimetry is possible only with spatial combinations of films. With introducing gel as a dosimeter, a new revolution in 3D dosimetry is happening. Since the gels used for dosimetry contain more than 99% of water therefore it is tissue equivalent. Application of the gel to make different phantoms is easily feasible. It is also possible to measure dose up to 15 Gy, which means the response of the gel dosimeter is linear up to 15 Gy without dependent to the type of radiation or energy. Two types of gel dosimeters have been used, Fricke and polymer gels. In Fricke gel the Fe^{2+} ions oxidize to Fe^{+3} ions due to ionization [6,10,11].

In the polymer gels the construction of polymer changes due to irradiation. One difficulty with Fricke gel dosimeter is diffusion of Fe^{3+}ions with time. This problem has been investigated by several researchers [1] and diffusion rate of Fricke gel dosimeters with different ingredients have been measured. Obtaining a faster technique results in reduction of measurement time, which in turn reduces the diffusion effect.

If the time between irradiation and final scanning is kept below an hour the diffusion effect is unimportant, which enables the user to avoid complicated calculation.

So far dosimetry with Fricke gel had been performed either with optical scanning techniques or with magnetic resonance imaging (MRI), in which spin lattice relaxation rate was measured. Application of signal intensity in MRI has been rear and only one work was found in the literature by[4] who used signal intensity for dose calculation in gel dosimeter.

In this study, it has been tried to measure dose in Frick gel dosimeter via image intensity for R_1 measurement.

Material and Method

Gel dosimeter contains 0.4mM ferrous sulphate, 1mM sodium chloride, 50mM sulphuric acid, and 1% by weight agarose. In this research Perspex phantoms with dimensions of 15 x 10 x 1cm^3 and vial shaped plastic phantoms with inner diameter of 27 mm and height of 115 mm were used. The wall thickness of the Perspex phantoms was 6mm.

A Cobalt 60 unit (Theratron 780C) was used for irradiation. To verify the variation of signal intensity with absorbed dose; vial shaped phantoms were fixed in a plastic water tank with dimensions of 22 x 12 x11cm^3 in vertical positions. The tank was filled up to the level of the gels to produce a homogenous environment and reduce the scatter effect. SSD and field size were fixed to 80 cm and 15x10 cm^2 respectively. In cases that wider phantoms were necessary to use, a 10 x 10 x 1cm^3 Perspex phantom with 6mm wall thickness was used. In these cases SSD and field size were fixed to 80cm and 10 x10 cm^2 respectively.

For imaging purposes a 0.5T commercial MR imaging system (Gyroscan T5/Philips) was used. A special wooden mold was constructed to be fixed in the head coil. The water tank also was stuck to this wooden mold to prevent dislocation of the phantom in the head coil. The scanning protocols were also identical for before and after irradiation. For each image an average region of interest (ROI) was obtained and the value of noise was subtracted from this ROI. The data of the signal intensity for after irradiation was subtracted from before irradiation data to obtain the variation of signal intensity (ΔI) due to irradiation for each region. Two imaging protocols named spin echo (SE) and gradient echo (GRE) were used. In SE technique scanning parameters are: TE = 11ms, TR = 100, 120, 150, 200, 250, 350, 500, 1000, 2000, 4000ms, slice thickness = 10mm, gap thickness = 0 mm , NSA = 2, while in GRE technique imaging parameters are: TE =11ms, TR = 500ms, flip angles = 30,60,75,90^o, slice thickness = 10mm, gap thickness = 0 mm, NSA = 2.

Total time for this kind of two stages GRE technique was 4 minutes.

Results

In order to evaluate the effect of non-uniformity, Perspex phantom was placed in the head coil at X = 40, X = 0 and X = - 40 positions and was imaged with SE technique with TE = 11 and TR =500.

Results of non-uniformity in profiles perpendicular to Z axis (axis along with head coil inward) is shown in figure(1-a). Non-uniformity of the field is also shown in profile perpendicular to Y axis (axis perpendicular to treatment coach and upward) in figure(1-b). Non-uniformity profiles in figure(1-b) are comparable to the variation of signal intensity produced due to phantom irradiation. However, when the images of irradiated and unirradiated gel was subtracted, for a certain position the related non-uniformity was cancelled out and had no effect in the final results. This is a sign of good reproducibility for this technique.

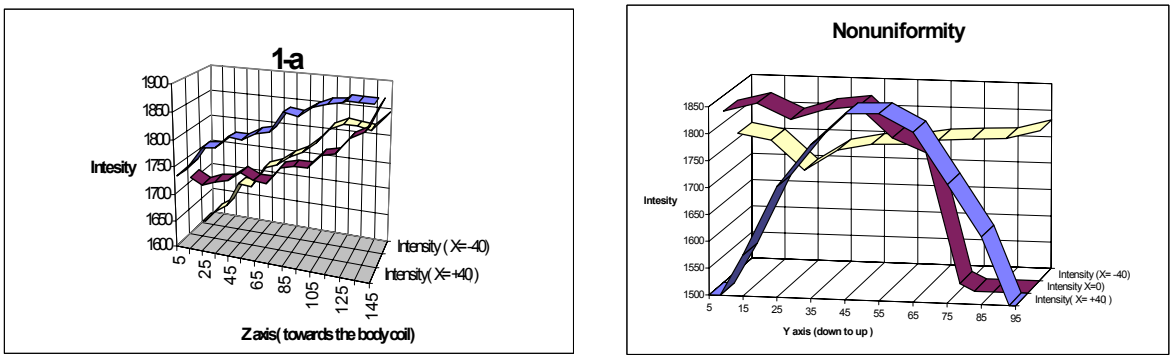

Figure1. a)non-uniformity in magnetic field in head coil for image profile perpendicular to Z axis, b) non-uniformity in magnetic field in head coil in image profile perpendicular to Y axis.

To find a proper SE protocol, it was assumed that TE<<TR and TE = 11 ms, for TR = 100, 120, 200, 250, 500, 2000 and 4000 ms, values of ΔI versus dose (D) was graphed in figure(2). An optimum TR must be selected so that these conditions are met: TE<<TR, images are T_1 weighted and have good variation of ΔI for unit of irradiation (ΔD). It was found that TR = 500ms have those three requirements and were accepted as spin echo imaging protocol. The slopes of the lines fitted to the curves correspond to TR= 100, 500 and 2000 are. 36.478, 39 616 and 8.998 respectively.

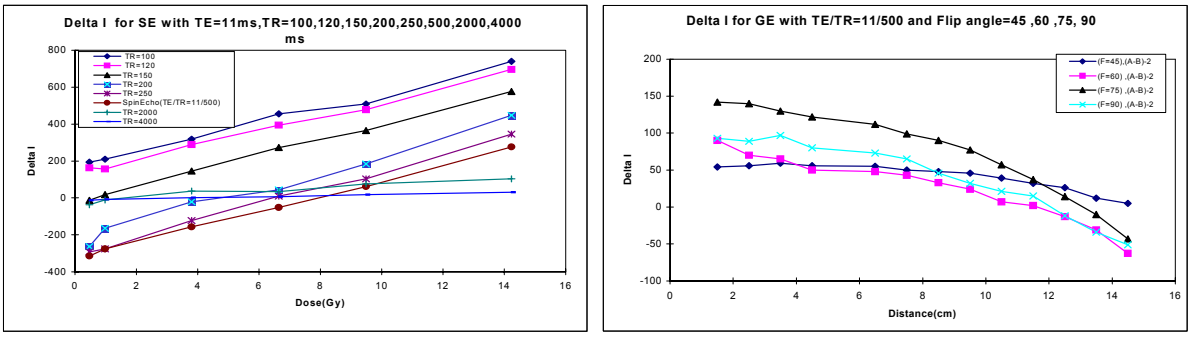

Figure 2. a) variation of signal intensity (ΔI), for different doses (0.47 Gy and 14.23Gy) with SE technique, b) Curves obtained with GRE technique for TE = 11ms, TR = 500ms with flip angles of 45°, 60°, 75°, and 90°. Results obtained for ΔI due to different angles inicate that flip angle = 75° has higher sensitivity.

Results for ΔI versus D were graphed for both SE and GRE techniques and their sensitivity are compared (figure3-a). Results indicate that both graphs in dose interval of 0.9 to 14.23 Gy are linear and relative sensitivity of SE to GRE is 1.5.

To determine reproducibility with SE technique, vial shaped phantoms were imaged for four times and ΔI versus D were graphed in figure 3 -b.

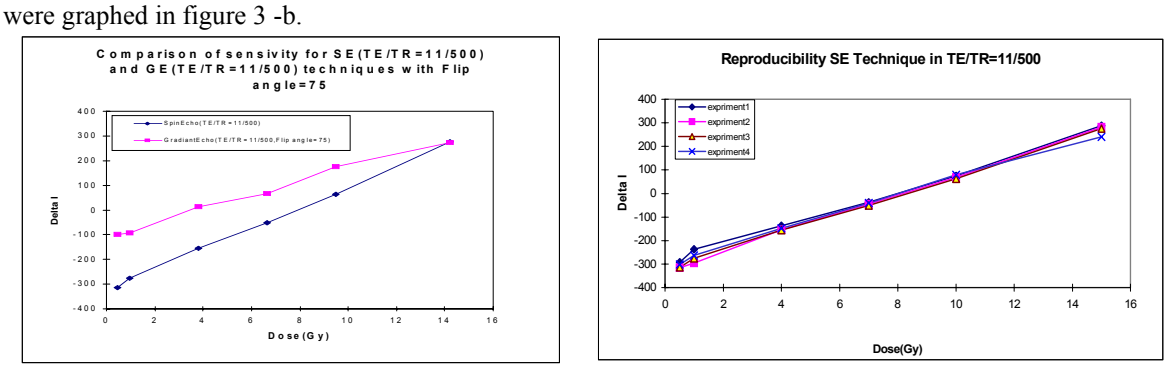

Figure3. a) ΔI profiles for dose range of o.47 to 14.23 Gy, 1) SE technique with TE = 11, TR = 500, 2) GRE technique with TE = 11, TR = 500 and flip angle75. The sensitivity in (1) is 39.9 Gy^{-1} while for (2) is 26.9 Gy^{-1} ,b) Reproducibility in SE imaging technique for gel dosimeter.

Discussion

Figure2-a , prove that for T_1 weighted SE image, if TE<<TR and doses lower than 15 Gy, signal intensity due to irradiation (ΔI) is increasing linearly with absorbed dose (D). Maximum sensitivity happens for TR = 500ms. For TRs higher than 2000ms and up to 4000ms,sensitivity is reduced rapidly. This reduction in sensitivity is a sign of T_1 weighted area, and image is going towards a proton density weighted image. Therefore, ΔI does not increase significantly and is independent of dose (D).

In equation $\Delta I = C.N(H) \exp.(-TE/T_2) [(1/T_1' - 1/T_1) (TR-TE)]$which is taken from reference [4], from one side in very short TRs, (TR<100ms), Mcloren expansion can be used to obtain a linear relation between ΔI and various R_1 and in the other side the T_1 weighted condition will be on force, however for low signal to noise condition, the dose would be reduced. In dose evaluation, signal intensity is used directly in such a way that signal to noise ratio will increase which in turn will increase the sensitivity of the dose response. To achieve a higher SNR , a scanner with stronger field, more averaged number and gel with more ferrous ion can be used. One drawback for increasing the number of averaging, is the growth of the ferric ion diffusion. Error fraction due toT_2 variation in ΔI calculation is similar to R_1calculation [1,9,8] and for TE = 11ms it has been estimated to be 3%.

In ΔI calculation only one image of irradiated gel is needed, therefore in compare to R_1 calculation that two or more irradiated gel is required, imaging time is reduced from one hour to 5 minutes. The reduction of imaging time will minimize the ferric ion diffusion and a three dimensional (3D) dosimetry is achievable.

In R_1 calculation also an error exists which is considerable in compare to the error in the image intensity calculation. In GRE technique, because the $\alpha < 90°$ and in contrast to SE technique, the 180° pulse was not present, the imaging time shows 2 minutes reduction in compare to SE technique when TR <<TR. This reduction of time makes the ferric ion diffusion more unimportant. As it was shown in figure 2-b, as α angle is smaller, the sensitivity also is reduced. The reason is that in smaller α, images are leaving T_1 weighted state and go towards proton density (T_2 weighted). Of course the TR should be high enough to be able to have a T_1 weighted image in larger α. In this regard, the optimum values of TR and α were selected to be 500 ms and 75° respectively as shown in figure2-b. Although, in GRE technique, the variation of sensitivity of signal intensity to dose is 1.5 times less than SE, but for increase in imaging speed and also for 3D imaging, the GRE can be used as a proper imaging technique. In ΔI technique, with changing the field power of MRI system, recalibration should be performed. This is also true for R_1 calculation technique, as with change of the field, T_1 also would be different. Therefore from this point of view, these two techniques have no advantage to each other. In R_1 calculation technique, sensitivity (variation of R_1 in the unit of absorbed dose) is mentioned to be $.0129 s^{-1} Gy^{-1}$ [12] which is much lower than the sensitivity found in ΔI technique which is in the order of 10^{-3}.

References

1. Balcom B.J., Lees T.J., Sharp A.R., Kulkarni N.S. and Wagner G.S.; Phys. Med. Biol.40, pp. 1665-1676, (1997)
2. Bengtsson Magnus, Furie TorbjQrn, Dal Jon R.Q., Skretting Arne and Olson Dog R.; Phys. Med. Biol. 41, pp. 269-244(1994)
3. Knutsen Bjorn H., Skretting Arne, Hellebust Taran P., Olson Dag R.; Radio therapy and Oncology vol. 43, pp. 219-224, (1994)
4. Chu W.C., Guo W.Y., Wa M.C. Chung W.Y. and Pan D.H.C; Med. Phys. 25, pp. 2326-2332, Dec. 1988,
5. Gambarini G., Arrigoni S., Contone M.C., Molho N. , Facchielli L. and Sichirollo A.E.; Phys. Med. Biol. 39 pp.703-717, (1994)
6. Gore J.C., Kang Y.S. and Schulz R. J.; Phys. Med. Biol. 29, pp. 1189-1197 (1984)
7. Kron T., Metcalfe P., and Pope J.M.; Phys. Med. Biol. 38 pp.139-150, (1993)
8. Maryaanski M.J., Ibbott G.S., Eastmen P., Schulz R.J., Gore J.C.; Med. Phys. 23 (5), (May 1996)
9. Oldham M., McJury M., Bauster I. B., Webb S. and Leach M.O.; Phys. Med. Biol. 43 pp. 2709-2720,(1998)
10. Olsson L.E., Fronsson A., Erucssib A., and Mattson S.; phys. Med. Biol., 35 pp.1923–1631(1990)
11. Olsson L.E., Petersson S., Ahlgren L. and Mattsson S.; Phys., Med. Biol. 34. pp. 43-52(1989)
12. Rae William I.D., Willemes Casper A. And Swarts J. Annio C.; Med. Phys. 23 (1), (January1996)

UNCERTAINTY CALCULATIONS DETERMINED FROM CALIBRATION DATA FOR CT IMAGING OF POLYMER GEL DOSIMETERS

Jamie Trapp, Greg Michael, and Clive Baldock
Centre for Medical Health and Environmental Physics
Queensland University of Technology, Brisbane, Australia

Introduction

Uncertainty in dose in gel dosimetry determined with calibration graphs has had several methods of treatment. Oldham *et al* 1998a and Oldham *et al* 1998b used magnetic resonance imaging (MRI) to measure transverse relaxation time (R_2) and assumed a linear response with increasing dose, D, to a maximum of 10 Gy, as described by:

$$D = \alpha R_2 + R_2(0) \quad (1)$$

where the values of α and D_0 are determined by least-squares fit to experimentally measured values for D and R_2. For a pixel in the gel image with a measured R_2 value of ($R_2 \pm \sigma_{R2}$), the uncertainty in the dose, σ_D, is given by:

$$\sigma_D = \sqrt{R_2^2 \sigma_\alpha{}^2 + \alpha^2 \sigma_{R_2}{}^2 + \sigma_{R_2(0)}{}^2}\ . \quad (2)$$

The work of Oldham *et al* was later revisited by Baldock *et al* 1999 who suggested that potential reductions in σ_{R_2} will have more effect on the overall uncertainty than improvements in σ_α and σ_{D_0}. Equation 2 was later expanded [4] to include a covariance term:

$$\sigma_D = \sqrt{R_2^2 \sigma_\alpha{}^2 + \alpha^2 \sigma_{R_2}{}^2 + \sigma_{D_o}{}^2 + 2R_2 \sigma_{\alpha D_0}} \quad (4)$$

however the covariance term can be neglected if R_o and α are independent variables.

An alternative treatment of uncertainty [5] has combined the uncertainty in the measurement of R_2 and the statistical fluctuations in the calibration curve where equation 1 has been inverted to $R_2 = R_{2,0} + \gamma D$:

$$\sigma_D = \sqrt{\frac{\sigma_{R_2}^2}{\gamma^2} + \frac{\sigma_{cal}^2}{\gamma^2 N_{ROI}} CCF^2} \quad (3)$$

where CCF is a calibration contribution factor, N_{ROI} is the number of pixels in a region of interest and σ_{cal} is the standard deviation of R_2 values in the region of interest.

The requirement for linearity was later removed and the concept of a coverage factor k_p was introduced [6]. The coverage factor is a multiplier to be used to determine uncertainty to a specific level of confidence, p [7]:

$$U_p(D) = k_p u_c(D) \quad (5)$$

where $U_p(D)$ is the expanded uncertainty to the required level of confidence $u_c(D)$ is the combined standard uncertainty [7] and is defined as the product of the squares of the uncertainty in pixel value σ_{T2} and the partial derivative (slope) of the calibration curve [6]:

$$u_c^2(D) = \frac{\partial D}{\partial T_2}^2 \sigma_{T2}{}^2\ . \quad (6)$$

The concept of dose resolution, D_Δ^p, was introduced. D_Δ^p is the minimal separation of the dose distributions at which their most probable values are different (i.e. the difference is greater than zero) to a level of confidence given by p [6]:

$$D_\Delta^p = k_p \sqrt{2} \sigma_D \quad (7)$$

where the $\sqrt{2}$ multiplier is due to an assumption that neighbouring dose distributions are equal.

The above methods each treat various aspects of uncertainty in gel dosimetry calibration, however, a truer evaluation would be to combine all of the above. For example, deviation from linearity has been reported [2, 8-11] so treatment of the response as linear, or selecting an inappropriate function to fit the data would introduce further uncertainty into dose measurements. Alternately, neglecting assumed uncertainty in the fit parameters will cause an under-estimation of uncertainty.

This paper aims to demonstrate that a first order Taylor expansion of all parameters of the function fitted to the data results in an improved estimation of uncertainty in calibration graphs of gel dosimeters. The data in this paper is obtained from x-ray computed tomography (CT) measurements, however the principles can be applied to any other imaging modality such as optical tomography and MRI where a calibration curve is utilised.

Methods

The data used in this paper is based on dose response curves for CT imaging of polymer gel dosimeters previously published [12]. Curve fitting and analysis of the results was achieved with Origin® software (Microcal™) and data was manipulated using Excel (Microsoft®) and Matlab (The Mathworks Inc). It was found that an empirical function which fitted the data was of the form:

$$H = y + A\exp\left(\frac{-D}{t}\right) \tag{8}$$

where H is the dose response in Hounsfield Units, D is the dose (Gy), and y, A, t are the fit parameters of the function. Solving for D allows the uncertainty in D to be calculated from the uncertainty in H:

$$D = t\ln(A) - t\ln(H - y). \tag{9}$$

The first order Taylor expansion of equation 9 gives a combined standard uncertainty, u_c of [7]:

$$u_c(D) = \sqrt{\sigma_y^2\left(\frac{\partial D}{\partial y}\right)^2 + \sigma_H^2\left(\frac{\partial D}{\partial H}\right)^2 + \sigma_A^2\left(\frac{\partial D}{\partial A}\right)^2 + \sigma_t^2\left(\frac{\partial D}{\partial t}\right)^2} \tag{10}$$

For a level of confidence of 95%, and assuming an infinite number of degrees of freedom due to a large number of pixel values in the region of interest (230) for each measurement, a multiplier of 1.96 must be applied [7] to give an expanded uncertainty, U of:

$$U(D) = 1.96 \times \sqrt{\sigma_y^2\left(\frac{\partial D}{\partial y}\right)^2 + \sigma_H^2\left(\frac{\partial D}{\partial H}\right)^2 + \sigma_A^2\left(\frac{\partial D}{\partial A}\right)^2 + \sigma_t^2\left(\frac{\partial D}{\partial t}\right)^2} \tag{11}$$

As the data points for the calibration curve are taken from ROIs containing 230 pixels and not single points, the best estimate of the uncertainty in pixel values within the region of interest is given by the experimental standard deviation of the mean, σ_H [7]:

$$\sigma_H = \frac{s_H}{\sqrt{n}} \tag{12}$$

where: s_H is the experimental standard deviation of pixel value within the ROI, and n is the number of pixels within the ROI.

Results

Figure 1 is a plot of the data with two calibration curves fitted, one good fit and one poor fit. It can be seen that by using the Taylor expansion the goodness of fit of the calibration curve is a significant factor in determining uncertainty. Although the poorly fit calibration curve would appear to indicate a greater sensitivity in the low dose region due to a steeper gradient, the uncertainty introduced by the poor fit negates the initial false indication that the greater sensitivity will produce a lower uncertainty.

A consideration in determining uncertainty in polymer gel dosimetry is the noise in the dose map. This is represented by the experimental standard deviation of the mean as determined by equation 12 and can be seen as the uncertainty of each individual data point of the calibration curve. Figure 2 is a plot of the expanded uncertainty for increased σ_H and for σ_H reduced to zero. Increasing σ_H will increase the expanded uncertainty as expected and reducing this term to zero does not reduce the expanded uncertainty to zero.

Figure 3 shows the original data and also the same data with the scatter of points artificially increased with a random number generator. This figure demonstrates the need for good experimental method. Even small changes in the scatter of data points can greatly affect the uncertainty of a measurement.

Figure 4 shows a systematic error has be introduced into the region 3-7 Gy. Calculations using the Taylor expansion show that a systematic error causes a marked increase in uncertainty.

The above examples examine expanded uncertainty. This work also applies to dose resolution which can be determined by multiplying U by a factor of $\sqrt{2}$ [6]. These examples apply specifically to one set of data and the results will obviously be altered if different data is used due to the several parameters of equation 11.

Conclusion

It has been demonstrated that a first order Taylor expansion shows that goodness of fit of the calibration curve is an important consideration when determining uncertainty. This method allows for errors in the fit of the calibration function and experimental technique, and systematic errors.

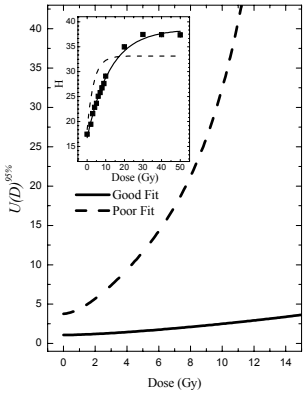

Fig 1 – Expanded uncertainty for calibration curves which fit well and a poor fit as shown in the insert.

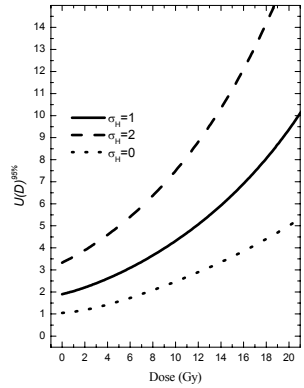

Fig 2 – Expanded uncertainty of the data in Figure 1 when σ_H is artificially

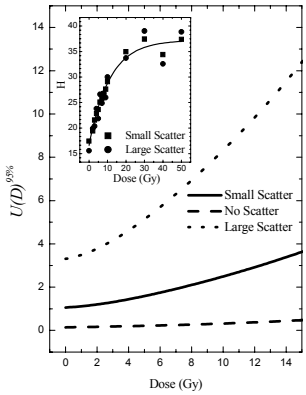

Fig 3 - Expanded uncertainty for small, large and zero scatter of data points about the fitted line.

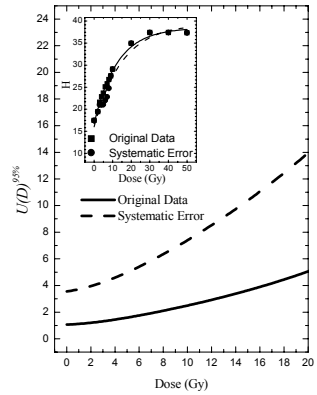

Fig 4 – Expanded uncertainty when a systematic error has been introduced into the calibration graph.

References

1. Oldham, M., et al., An investigation into the dosimetry of a nine-field tomotherapy irradiation using BANG-gel dosimetry. *Phys. Med. Biol*, 1998. **43**: p. 1113-1132.
2. Oldham, M., et al., Improving calibration accuracy in gel dosimetry. *Phys. Med. Biol*, 1998. **43**: p. 2709-2720.
3. Baldock, C., P. Murry, and T. Kron, Uncertainty analysis in polymer gel dosimetry. *Phys. Med. Biol*, 1999. **44**: p. N243-N246.
4. Low, D.A., et al., Noise in Polymer Gel Measurements using MRI. Med. Phys., 2000. **27**(8): p. 1814-1817.
5. De Deene, Y., et al., Mathematical analysis and experimental investigation of noise in quantitative magnetic resonance imaging applied in polymer gel dosimetry. *Signal Processing*, 1998. **70**: p. 85-101.
6. Baldock, C., et al., Dose Resolution in Radiotherapy Polymer Gel Dosimetry: Effect of Echo Spacing in MRI Pulse Sequence. *Phys. Med. Biol*, 2001. **46**(2): p. 449-460.
7. ISO. Guide to the Expression of Uncertainty in Measurement. 1995. Geneva: International Organization for Standardization: International Organization for Standardization.
8. Ibbott, G.S., et al., Three-Dimensional Visualization and Measurement of Conformal Dose Distributions Using Magnetic Resonance Imaging of BANG Polymer Gel Dosimeters. *Int. J. Radiation Oncology Biol. Phys*, 1997. **38**(5): p. 1097-1103.
9. De Deene, Y., et al., An investigation of the chemical stability of a monomer/polymer gel dosimeter. *Phys. Med. Biol*, 2000. **45**: p. 859-878.
10. Lepage, M., et al., ^{13}C-NMR, ^{1}H-NMR, and FT-Raman Study of Radiation-Induced Modifications in Radiation Dosimetry Polymer Gels. *J. Appl. Poly. Sci.*, 2000. **79**: p. 1572-1581.
11. Murphy, P.S., et al., Proton spectroscopic imaging of polyacrylamide gel dosimeters for absolute radiation dosimetry. *Phys. Med. Biol*, 2000. **45**: p. 835-845.
12. Trapp, J.V., et al., An experimental study of the dose response of polymer gel dosimeters imaged with x-ray computed tomography. *Phys. Med. Biol*, 2001. **46**(11): p. 2939-2951.

PRELIMINARY MEASUREMENTS OF DEPTH DOSES IN POLYMER GEL DOSIMETERS USING RAMAN MICROSCOPY

Clive Baldock[1], Llew Rintoul[2], Martin Lepage[1] and Brendan Healy[1]
[1]Centre for Medical, Health and Environmental Physics, [2]Centre for Instrumental and [2]Developmental Chemistry, Queensland University of Technology, Brisbane, Australia

Introduction

Vibrational spectroscopy has been utilised to provide direct measurements of the concentration of monomers and polymer, post-irradiation, as a function of absorbed radiation dose in polymer gel dosimeters (1-3). Adapting this work to Raman microscopy (4) is an attractive proposition as it has the potential to enable dose to be measured to spatial resolutions down to one micron.

Materials and Methods

Manufacture

Polymer gel dosimeters were manufactured according to a previously published methodology (5) and of composition 3% acrylamide, 3% N,N'-methylene-bis-acrylamide, 5% gelatin and 89% water by weight. After manufacture the polymer gel was transferred to SUPRASIL® quartz cuvettes (Sigma Aldrich, Sydney) under a nitrogen atmosphere.

Irradiation

Each polymer gel dosimeter filled cuvette was positioned in a tank of water with the base of the cuvette pointing upwards and level with the surface of the water. Each cuvette was irradiated from the base end using either photons or electrons from a 6 MV linear accelerator to a maximum dose of 8 Gy. The size of the radiation field at the surface of the water was 10 cm x 10 cm. The samples (Figure 1) were left seven days post-irradiation before evaluation.

Figure 1. Cuvettes irradiated with electons (left) and photons (right).

Raman Spectroscopy

Raman spectra were acquired using a Renishaw System 1000 Raman microprobe spectrometer (Renishaw plc, Wotton-under-edge, UK) equipped with a helium neon laser operating at 632.8 nm. An Olympus MDPlan long working distance 50 x objective with a 0.55 numerical aperture was used to focus the laser to a focal spot of nominal spatial resolution of 1 µm. The operating power of the laser at the sample was 8 mW. Raman spectra were collected in static mode for 240 s in the range 2800 – 3800 cm^{-1}. Each cuvette was placed securely on the sample stage which could be computer controlled in the *x*, *y* and *z* directions. The sample was aligned using the graticule of the

microscope and subsequently translated in a linear-positive direction at 500 μm step intervals from the origin until the entire sample had been evaluated.

Data manipulation, including principle component regression (1) was undertaken using GRAMS software (Galactic Industries Corp., New Hampshire).

Results and Discussion

Figure 2 illustrates the relative depth dose measurement of photons and electrons using the Raman microscopy technique.

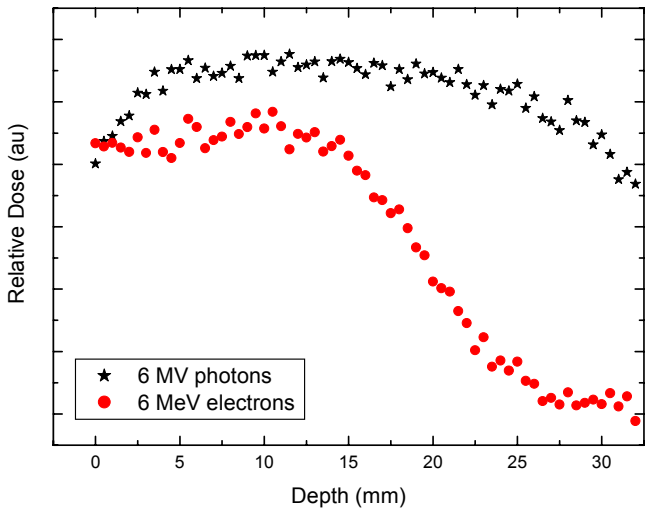

Figure 2. Relative depth dose measurement of photons and electrons.

This preliminary study indicates that Raman microscopy has the potential for measuring depth doses for both electrons and photons. It is apparent from figure 2 however, that the change in depth dose with for 6 MV photons is very small, as expected. Also, for electrons it is possible to see a significant change in depth dose with distance, again as expected.

Conclusion

Raman microscopy of polymer gel dosimeters shows great potential in determining dose distributions with high spatial resolution and may have potential in areas such as cardiovascular brachytherapy where there is a significant change in absorbed dose with distance from the source of radiation.

Acknowledgements

The authors acknowledge Melissa Mather for manufacturing the polymer gel. Discussions with Sven Å. J. Bäck and Yves De Deene are also acknowledged.

References

1. Baldock C, Rintoul L, Keevil S F, Pope J M and George G A. Fourier transform Raman spectroscopy of polyacrylamide gels (PAGs) for radiation dosimetry. *Phys. Med. Biol.* **43**, 3617-27 (1998).
2. Lepage L, Whittaker A K, Rintoul L and Baldock C. ^{13}C-NMR, ^{1}H-NMR and FT-Raman study of the radiation-induced modifications in radiation dosimetry polymer gels. *J. Appl. Polym. Sci.* **79**, 1572-81 (2001).
3. Jirasek A I, Duzenli C, Audet C and Eldridge J. Characterization of monomer/crosslinker consumption and polymer formation observed in FT Raman spectra of irradiated polyacrylamide gels. *Phys. Med. Biol.* **46**, 151-65 (2001).

4. Baldock C, Rintoul L, Lepage M and Bäck S Å J. Radiation dosimetry of polymer gel dosimeters using Raman microscopy. *Med. Phys.* **28** 1291 (2001).
5. Baldock C, Burford R P, Billingham N, Wagner G S, Patval S, Badawi R D and Keevil S F Experimental procedure for the manufacture and calibration of polyacrylamide gel (PAG) for magnetic resonance imaging (MRI) radiation dosimetry *Phys. Med. Biol.* **43** 695-702 (1998)

INDEX

Akhlaghpour	S	189
Amin	MN	127
Ayyangar	KM	80,121
Bäck	SÅJ	89,101,113,136 172
Baldock	C	89,113,136,172 175,178,192,195
Battista	JJ	95,166
Beavis	AW	107
Bero	MA	77,154,157
Bonnett	DE	40,119,127,148 186
Brindha	S	80,121
Burnham	KJ	148
Chu	KC	86
Claus	F	133
Cross	A	83
De Deene	Y	49,133,136,139 142,145
De Gersem	W	133
De Wagter	C	133,139,142,145
Does	MD	98
Doran	SJ	77,154,157,160 163
Dunn	M	127
Duzenli	C	124
Farajollahi	AR	119,186
Fong	PM	98,183
Galloway	GJ	136
Gambarini	G	92,151
Gianolini	S	130
Gilboy	WB	77,154,157
Goodby	JW	107
Gore	JC	73,98,183
Gustavsson	H	101,113
Haas	OCL	148
Hall	AW	107
Harding	PJ	127,148
Hill	B	89
Horsfield	MA	127
Jaffray	D	169,181
Jayasekera	PM	172
Jenner	AG	107
Jenneson	P	154,157
Jirasek	A	124
Joers	JM	183
Jordan	K	66,86,95,166
Keil	DC	98
Koerkamp	KK	154,157,160
Kron	T	2
Lazaridis	E	130
Lepage	M	31,89,113,136 172,195
Liney	GP	107
MacDonald	DJ	95
Mariani	M	151
Mather	ML	175
McAuley	KB	116
McMahon	K	136
Meyer	J	148
Michael	G	178,192
Mills	JA	148
Morton	EJ	154,157
Nkongchu	K	83
Oldham	M	169,181
Olsson	LE	101
Pajak	TM	95,166
Park	YS	104,110
Piontek	C	166
Pirola	L	151
Pompilio	E	151
Pourbeigi	H	189
Prestini	P	151
Rintoul	L	113,195
Rowbottom	C	169
Salomons	G	116
Santyr	G	83
Saw	CB	80, 121
Scheib	SG	130
Schreiner	LJ	15,104,110,116
Schulz	RJ	73

Sella	M	151
Shen	B	80,121
Shortt	K	10,83
Sia	S	107
Siewerdsen	J	169,181
Simpson	J	89
Tomatis	S	151
Trapp	J	178,192
Van Duyse	B	133
Vergote	K	133
Wallace	J	83
Whittaker	A	23,175
Wolff,	T	148
Zahmatkash	MH	189
Zhang	Q	116